HIGH MOLECULAR SIEVE LOADING MIXED MATRIX MEMBRANES FOR GAS SEPARATIONS

A Thesis
Presented to
The Academic Faculty

By

Ryan Thomas Adams

In Partial Fulfillment
Of the Requirements for the Degree
Doctor of Philosophy in the School of
Chemical and Biomolecular Engineering

Georgia Institute of Technology

May 2010

HIGH MOLECULAR SIEVE LOADING
MIXED MATRIX MEMBRANES
FOR GAS SEPARATIONS

Approved by:

Dr. William Koros, Advisor
School of Chemical &
Biomolecular Engineering
Georgia Institute of Technology

Dr. Carson Meredith
School of Chemical &
Biomolecular Engineering
Georgia Institute of Technology

Dr. Victor Breedveld
School of Chemical &
Biomolecular Engineering
Georgia Institute of Technology

Dr. John Muzzy
School of Chemical &
Biomolecular Engineering
Georgia Institute of Technology

Dr. David Bucknall
School of Polymer, Textile, and
Fiber Engineering
Georgia Institute of Technology

Date Approved: January 5, 2010

This thesis is dedicated to

My loving parents,
James & Susan, and

My high school chemistry teacher,
David Vernon.

Without my parents,
I would not be the well-balanced,
Happy person that I am.

Without Mr. Vernon,
I would be doing something
Much less useful!

ACKNOWLEDGEMENTS

My time in the Koros Research Group at Georgia Tech has been truly special. I worked with many kind, intelligent, and passionate people. This section of my thesis is all about these people…except this part: I would like to acknowledge the NSF-STC, Center for Environmentally Responsible Solvents and Processes, under agreement CHE-9876674 for funding.

Firstly, I would like to thank Dr. Bill Koros. Dr. Koros has an impeccable reputation, and positions in his group are highly coveted, but I waltzed into his office the day before advisor choices were due to express interest in his group. I was not always the easiest guy to get along with, but he always supported me. He is kind-hearted, hard-working, and intelligent person with a great sense of humor. While I doubt I will ever have the focus and patience to achieve what he has, I will do my best to make him proud and help better the world as he has done his entire career.

I hate the idea of acknowledging some of my colleagues and friends more than others, but there were a few people that had an especially significant impact on me during my Ph.D. work. It was an extraordinary pleasure to meet and work with my office mate, and close friend, Jason Ward. Work was a lot of fun (and a lot easier) with him around, and I hope to continue to be his colleague and friend beyond the Koros Group. Ryan Lively is another close friend and colleague that has made working in the Koros Group special. He is an unflappably optimistic, warm-hearted, and intelligent person that was always more than eager to help out. Tae-Hyun Bae made the best zeolite 4A I used, and I would not have succeeded without him. If I highlight every friend and colleague in

detail, I'll never finish so I'll round-up a few in one shot—Imona Omole, Madhava Kosuri, Jong-Suk Lee, and Cantwell Carson are all great friends and bright researchers that I admire and have helped me so much in my studies. I certainly hope to remain close friends and colleagues with them all.

I genuinely acknowledge and admire all of the Koros group members that I have had the pleasure of working with. Alexis McKittrick spent a lot of time showing me the ropes when I joined the group and was very patient and friendly. John Perry is another senior student that helped me a lot with advice and friendship. I would also like to acknowledge those we often take for granted—our infinitely patient administrative assistant, Michelle, our incredible building manager, Rod, and our hard-working, friendly janitorial staff.

Although she has not been in Atlanta with me my entire time in the Koros Group, I must acknowledge my wonderful, loving partner, Esther. Sometimes she did not like my working hours (or my inability to come home on time), but it was a lot easier coming home knowing that I had a caring, hilarious, and fun-loving person there to remind me there is more to life than a career. I almost forgot our special little Kitty. Everyone should have a cat—they do not care how successful you are…they just want to be petted.

I bet someone thinks I forgot him! JR Johnson was my first friend here in Atlanta, and is one of the most impressive people I have ever known. My time living with JR—especially that second year with our dear friend Ronnie—will always be cherished. It would be silly to try to enumerate the favors he has done and sacrifices he has made for me and all of his many friends. JR will always be a great friend and colleague.

TABLE OF CONTENTS

LIST OF TABLES

LIST OF FIGURES

NOMENCLATURE

MMM(s)	Mixed matrix membrane(s)
PVAc	Poly(vinyl acetate)
Permeate	The gas or gases that exit a membrane.
Retentate	The gas or gases that flow past a membrane but not through it.
T_g	The glass transition temperature of a polymer.
φ_s	Solvent concentration where polymer-solvent $T_g = T_{ambient}$.
Upper-bound	Maximum efficiency-productivity boundary for a gas pair.
Permeability	Pressure and thickness normalized flux of a membrane.
Permselectivity	Ratio of fast gas permeability to slow gas permeability.
Time lag	Initial period of permeation test where little permeate accumulates.
Barrer	Conventional unit of permeability named after RM Barrer.
4A	Zeolite NaA or zeolite 4A.
NaY	Zeolite NaY
MOF(s)	Metal organic framework(s)
CuTPA	A MOF of copper and terephthalic acid.
TGA	Thermal gravimetric analysis
XRD	X-ray diffraction (or diffractogram)
SEM	Scanning electron microscopy (or micrograph)
DSC	Differential scanning calorimetry
ICP	Inductively coupled plasma
EDS	Energy dispersive spectroscopy

SUMMARY

Traditional gas separation technologies are thermally-driven and can have adverse environmental and economic impacts. Gas separation membrane processes are not thermally-driven and have low capital and operational costs which make them attractive alternatives to traditional technologies. Polymers are easily processed into large, defect-free membrane modules which have made polymeric membranes the industrial standard; however, polymers show separation efficiency-productivity trade-offs and are often not thermally or chemically robust. Molecular sieves, such as zeolites, have gas separation properties that exceed polymeric materials and are more thermally and chemically robust. Unfortunately, formation of large, defect-free molecular sieve membranes is not economically feasible. Mixed matrix membranes (MMMs) combine the ease of processing polymeric materials with the superior transport properties of molecular sieves by dispersing molecular sieve particles in polymer matrices to enhance the performance of the polymers.

MMMs with high molecular sieve loadings were made using polyvinyl acetate (PVAc) and various molecular sieves. Successful formation of these MMMs required substantial modifications to low loading MMM formation techniques. The gas separation properties of these MMMs show significant improvements over PVAc properties, especially for high pressure mixed carbon dioxide-methane feeds that are of great industrial relevance.

CHAPTER 1

INTRODUCTION

1.1 Gas Separations Overview

Gas separation processes are key but costly components of many chemical industries. In 2009 the global market for industrial gas was estimated at $59 billion/year and expected to grow to $76 billion/year by 2014 [1]. Many technologies are used to meet the global demand for purified gas streams and most of them are thermally driven. For instance, cryogenic distillation is the primary means for oxygen and nitrogen enrichment of air, and purification of natural gas uses liquid amine scrubbing towers with large thermal regeneration requirements. While these technologies are effective, they have drawbacks that newer alternative methods avoid. [2]

For instance, large columns and towers are not attractive for off-shore platforms where acid gases (like CO_2, H_2S, and H_2O) must be removed to acceptable levels to allow piping to shore with traditional, low cost materials of construction. Even on shore, compact footprints are desirable. Figure 1.1 displays the size of a membrane unit relative to the amine scrubbing towers it replaced.

Figure 1.1: Footprint of membrane unit (circled in green) versus 2 large amine scrubbers it replaced. Photo courtesy of Medal Inc.

Although the capital, operational, and maintenance costs of these traditional technologies are high, their proven track record has promoted the status quo. Recently, the ever increasing cost of energy to drive these traditional technologies has caused the status quo to be reconsidered. Overall, 40 – 50 % of the energy use in major commodity producing industries can be attributed to such thermally driven separations. Coupling this massive energy consumption with an expected global population growth from 6 billion to 10 billion people by 2040, it is simple to see that the alternatives to thermally driven separations are attractive. [2]

Aside from the economic drawbacks of traditional gas separations technologies, environmental drawbacks are also related to wasteful energy consumption, since most of the energy comes from the burning of fossil fuels. The burning of fossil fuels emits atmospheric pollutants such as carbon dioxide so a direct way to ease the environmental impact of gas separations is to shift towards more energy efficient processes such as this thesis considers.

1.2 Alternative Gas Separation Technology: Gas Separation Membranes

Gas separation membranes are emerging as the leading alternative to economically and environmentally costly traditional technologies. As of 2002, membrane gas separations were a $150 million/year business with a predicted growth to $760 million/year by 2020 [3]. Membrane-based processes for gas separations are non-thermal in nature, and with proper engineering, can significantly reduce the carbon footprint of large-scale, energy intensive processes such as natural gas purification.

Gas separation membranes separate a relatively high pressure feed from a relatively low pressure product stream. This pressure differential results in a chemical potential gradient across the membrane, which is the driving force for gas transport. Differences in the sizes, shapes, and thermodynamic partitioning properties of the gas molecules result in different rates of transport through the membrane, thus, mixed feeds can be separated into purified product effluents. A schematic of a membrane gas separation is provided in Figure 1.2.

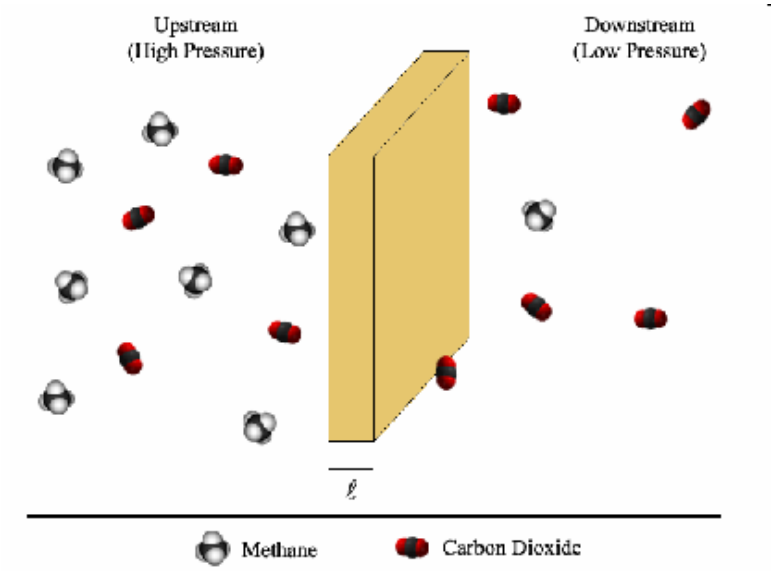

Figure 1.2: Schematic of a membrane separating carbon dioxide from natural gas.

Unlike absorption and adsorption technologies that require heat input to release the desired product, or cryogenic distillation technologies that rely on temperature differentials from top to bottom of columns, there is no inherent need for additional heat input in a membrane-based gas separation process.

Some compression of the feed and/or effluent may be needed in a membrane separation to deliver the desired products at the required conditions; however, naturally occurring feed pressures in cases such as natural gas wells can eliminate these costs. In any case, the energy consumed in a membrane-based separation process can be substantially lower than a thermally driven separation. As traditional energy sources (fossil fuels) become more scarce and expensive and concerns about carbon emissions grow, membrane separations become increasingly attractive.

1.3 Gas Separation Membrane Materials

Two basic types of membrane materials are generally considered to separate gases: polymeric and molecular sieving materials. Although some separations can be done with metallic and ceramic membranes, their application is small, and likely to remain small, so these materials will not be discussed further. Polymeric and molecular sieving membrane materials have opposing advantages and disadvantages with regards to potential performance and practical implementation of devices. The following subsections will describe the pros and cons of these 2 materials for use in membrane applications.

1.3.1 Polymeric Membranes

Polymers are the most common materials for creation of gas separation membranes. This is largely due to the ease of processing polymer solutions into useful

membrane morphologies. An additional benefit is that polymers can be made into the industry-preferred asymmetric hollow fiber morphology which has thin, large areas resulting in high productivity (i.e., high gas fluxes). Hollow fibers are subsequently bundled into cylindrical modules as shown in Figure 1.3 which boast high separation surface areas per volume of module thereby further enhancing productivity.

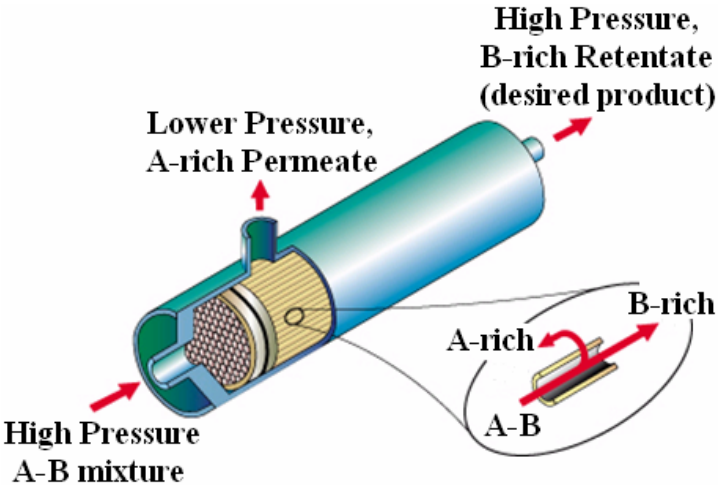

Figure 1.3: Membrane module schematic showing separation of A from A-B mixture. Image courtesy of Medal Inc.

The unique thermodynamic and mechanical properties of polymers impart interesting gas transport properties to polymeric membranes. Depending on the nature of the polymer and the feed conditions, the polymer can be in the rubbery state where the polymer chains can undergo large scale segmental movements, or in the glassy state where polymer chain segments are restricted to vibrational and small scale rotational movements only.

Rubbery polymers behave similarly to liquids; thus, gas transport tends to be fast and separation efficiency is dominated by thermodynamic partitioning into the polymer.

Glassy polymers are rigid in nature, have relatively low gas transport rates compared to rubbery polymers, and behave like loose molecular sieves, i.e. separation efficiency is dominated by differences in the sizes and shapes of molecules in the feed. Most large scale, industrial gas separations of interest do not exhibit adequately high thermodynamic partitioning for rubbery polymers to be useful. Glassy polymers have been shown to be far more useful for gas separations in general. For the sake of brevity, rubbery polymers will be mostly ignored, and gas transport in glassy polymers will be discussed in depth in Chapter 2.

1.3.2 Molecular Sieving Membranes

Many different material types fall into the category of molecular sieving membranes. The two of greatest interest are zeolitic and carbon-based materials. Zeolites are typically comprised of alumina and/or silica tetrahedra which form high specific surface area, microporous crystals. The microporosity imparts a molecular sponge-like quality to zeolites while the well-defined, atomic scale pore entries allow zeolites to reject entities on the size scale of a molecule; hence the term molecular sieve.

Carbon molecular sieves (CMS) are the product of thermal degradation of polymeric materials. This thermal degradation, often called pyrrolysis, converts the relatively flexible hydrocarbon-based polymer into a relatively rigid network of carbon. Both the starting polymeric materials and pyrrolysis conditions affect the gas transport properties of the resulting carbon molecular sieve. Like zeolites, CMS have high specific surface areas, are microporous (although not crystalline), and have pore entries on the molecular scale. [4]

1.3.3 Overcoming Membrane Materials' Limitations

Gas separation membranes must be highly productive, highly efficient, be easily constructed, and installed as large separation area modules in order for membrane processes to become serious competitors with traditional gas separation technologies. Glassy polymer membranes handily meet one of these criteria: large scale production of highly productive membranes can be easily achieved and installed for use in the field. The gas transport properties of polymeric membranes are the limiting parameters for widespread use in gas separations. Figure 1.4 on the next page is a schematic representation of Robeson's upper-bound trade-off for polymeric membranes.

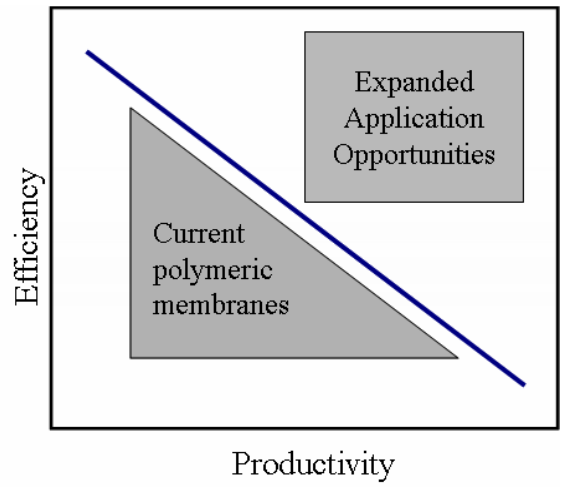

Figure 1.4: Schematic of Robeson's upper-bound trade-off. Log-log scale.

Robeson first identified and compiled the necessary data to create upper-bound plots for gas separations of interest [5], and other researchers later provided a fundamental basis for the relationship [6]. Although advances in polymer synthesis and controlling polymer morphology and chain dynamics have resulted in small favorable movement of upper-

bound plots over the last few decades [7], there is great demand for membranes that far exceed the upper-bounds [8].

Molecular sieving membrane materials have potential transport properties that far exceed those of polymeric membranes' upper-bounds for various gas pairs. The major drawback of these molecular sieving materials is the difficulty of forming large, defect-free membrane areas into useful modules.

1.4 Mixed Matrix Membranes

The mixed matrix membrane (MMM) concept is simple: combine the processing advantages of polymeric materials with the superior transport properties of molecular sieving materials. This is done by dispersing small, defect-free molecular sieve particles in a polymer matrix. As early as the late 1960, researchers aimed to enhance polymeric transport properties with use of filler particles [9], but the term "mixed matrix membrane" was not introduced until the 1980s [10]. Throughout Chapter 2, many MMM research highlights will be introduced so the remainder of this subsection will simply introduce the parameters needed to understand gas separation MMMs in general.

1.4.1 Designing the Ideal MMM

When designing the ideal MMM, selecting a polymer near Robeson's upper-bound (as shown in Figure 1.4) for the gas separation of interest is a good starting point. Next the appropriate molecular sieve filler must be chosen. The ideal molecular sieve would be one that allows unrestricted, rapid transport (as rapid or more than through the polymer matrix) of the faster gas while totally rejecting transport of the slower gas as shown schematically in Figure 1.5.

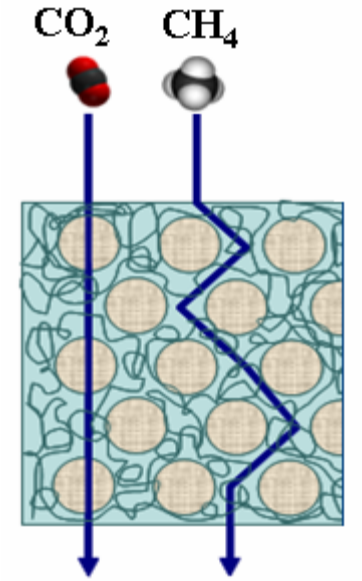

Figure 1.5: Ideal MMM showing unrestricted CO_2 path and CH_4 rejection.

Unfortunately finding such an ideal sieve is a difficult task as accurate prediction and even direct determination of the gas transport properties of the small molecular sieving particles used in MMMs is currently not feasible and is expected to remain a significant problem in the coming decades [11]. If such a successful pairing of polymer and molecular sieve is achieved, the expectation is that the transport properties of the resulting MMM will move towards the region of "expanded application opportunities" as shown schematically in Figure 1.4 provided the loading of molecular sieve particles is sufficiently high.

1.4.2 Non-idealities in MMMs

Aside from the difficulty of designing an ideal matching of polymer and molecular sieving particles, there are many common non-idealities in MMMs that are not witnessed in pure polymeric membranes. Not surprisingly, most of these non-idealities are related to polymer-filler interfacial phenomena. [12]

1.4.2.1 Interfacial Voids

The most commonly witnessed and easily diagnosed non-ideality is the presence of voids at polymer-filler particle interfaces as shown in Figure 1.6.

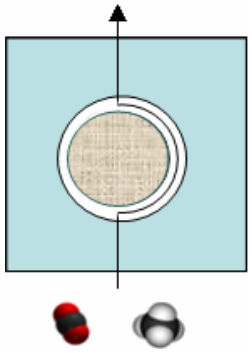

Figure 1.6: Void defect at polymer-particle interface. The CO_2 and CH_4 shown bypass the particle at roughly the same, high speed.

Interfacial voids occur for 2 primary reasons: 1) polymer-filler incompatibility and 2) destructive stress relief during MMM formation [13]. Most MMMs with voids at polymer-filler interfaces will result in increased membrane productivity with no change in gas separation efficiency. Voids on the order of a few nanometers can actually result in slightly better or worse separation efficiencies depending on the molecular weights of the gas molecules due to the contribution of Knudsen diffusivity [12]; however, the overriding effect is still increased productivity. While increased productivity is certainly a desired effect, a MMM with void defects do not capitalize on the superb gas separation efficiencies of molecular sieving materials.

Fortunately, there are ways to improve polymer-filler adhesion. Many researchers have found that physical and chemical filler surface treatments can improve adhesion [14-17]. There are also many ways of reducing stress accumulation during MMM

formation that decreases the likelihood of destructive stress relief mechanisms [14]. Although such methods can improve adhesion, they may also influence gas transport through the molecular sieves in undesired and unpredictable ways.

1.4.2.2 Partially and Totally Blocked/Clogged Molecular Sieves

Ideal matching of polymer and molecular sieve is no guarantee of a successful MMM even in the absence of void defects. There are a variety of ways in which access to the molecular sieving materials may be partially or totally restricted including the physical and chemical surface treatments on molecular sieving particles as discussed in Section 1.4.2.1 above. Such surface treatments can effectively shrink the size of molecular sieve pores and channels resulting in slower gas transport, or worse yet, can totally block the access or completely clog the pores. The effect of a totally blocked molecular sieve in a MMM is illustrated in Figure 1.7.

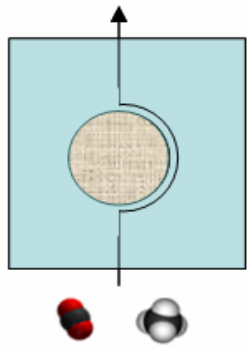

Figure 1.7: Clogged/blocked molecular sieve defect in a MMM. The CO_2 and CH_4 shown bypass the sieve at the same speed they go through the polymer matrix.

Examples of blocking/clogging agents include strongly adsorbed or covalently bound polymer chains that have reduced mobility compared to bulk polymer chains and may be oriented in ways that cover the otherwise open pore windows [18]. Similarly, chemical

treatments of molecular sieve surfaces, such as the Grignard treatment procedure [19] or silanation procudeures [20, 21] may retard access to the molecular sieves in some cases.

Other possible clogging agents are the organic solvents typically used to process polymeric and mixed matrix membranes. While most organic solvent molecules are considered too large to enter molecular sieve pores and channels of sizes on the order of gas molecules (2 – 6 Å), certain MMM preparation conditions may allow for organic solvent molecules to enter and clog the molecular sieve porosity. For example, ultrasonic mixing is typically utilized to break up molecular sieve crystal aggregates and disperse single crystals evenly in the polymer matrix. High speed interparticle collisions that occur during ultrasonic processing can generate local effective temperature spikes as high as 3400 °C [22]. The potential for these large temperature spikes may result in molecular sieve pore and channel window expansions that allow large solutes to penetrate and clog the pores. Furthermore, molecular sieving materials like zeolites are known to be catalytically active. The chemical activity of zeolite surfaces can result in strongly chemisorbed species that may restrict gas access to pores.

1.4.2.3 Interfacial "Zones of Influence"

There is one more class of interfacial defects sometimes referred to as "zones of influence". This term encompasses two different interfacial polymer chain conformations that are distinct from the equilibrium polymer chain conformation seen in the bulk of the polymer matrix. Unrestrained, bulk polymer chains adopt an equilibrium conformation, i.e. there is a specific polymer chain density and maximum entropy associated with the chain conformation. Adsorbed polymer chains exhibit a variety of conformations. When a polymer chain has neutral affinity to adsorb the adsorbed chain

bears the same equilibrium chain conformation and only differs from a bulk polymer chain in that it is slightly less mobile by virtue of being adsorbed. Polymer chains can also adsorb such that the chain density is either higher or lower than at equilibrium.

When polymer chains are relatively flexible and have strong affinity for adsorbing to the surfaces of filler particles in a MMM, the chains may be inclined to stretch out and adsorb strongly in a conformation that resembles trains. This type of adsorption results in relatively high chain density and thereby could create an effective partial barrier for gas transport. Conversely, relatively immobile chains with poor affinity for adsorbing to filler particles may have few points of contact with the filler particles. This type of adsorption leaves a polymer-lean interface, or depletion layer, that displays faster gas transport than equilibrium, or "normal", polymer chains. Figure 1.8 provides a cartoon depiction of the various adsorbed polymer chain conformations. [23-25]

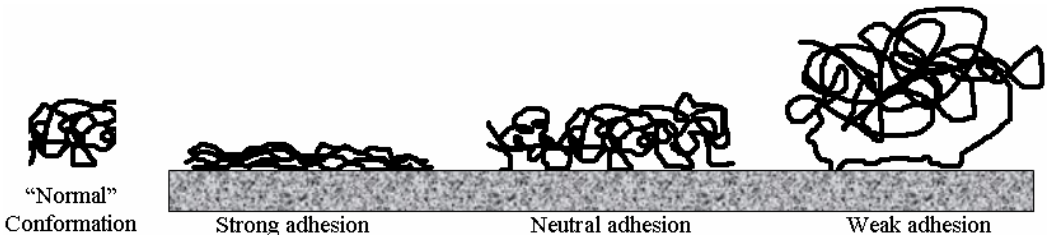

Figure 1.8: Bulk and adhered polymer chain conformations.

1.4.3 Real MMM Optimization

While a straightforward, ideal MMM may not be feasible, engineering strategies can be implemented to work around the documented non-idealities. A general strategy for real MMM optimization is provided:

1. *Address interfacial void defects*. Many researchers have and are actively pursuing molecular sieve surface treatments to achieve this goal. Another well studied method for doing so is by minimizing stress accumulation during processing.
2. *Work around the other MMM non-idealities*. For example, if preventing a solvent molecule or polymer chain from partially blocking a pore is impossible, then the next best thing is to engineer around these phenomena. By understanding the effect of molecular sieve pore/channel sizes on MMM transport properties as well as understanding how processing conditions impact partial/total blocking of molecular sieve pores/channels, membranologists can design better MMMs.
3. *Maximize molecular sieve loadings*. The main driving force for MMM development is to utilize the superior transport properties of molecular sieves, but there have been few reports of MMM success at high molecular sieve loadings. It is critical that the MMM community attains a better understanding of the factors that lead to defect-free high loading MMMs.

1.5 Research Objectives

This research project has 3 primary objectives related to major issues for the practical implementation of MMMs for industrial gas separations:

1. *Create void-free, high molecular sieve loading (≥ 50 vol.%) MMMs*. This objective is achieved creating MMMs with various molecular sieves in a poly(vinyl acetate) (PVAc) matrix from low to high loadings. These MMMs are primarily characterized with pure gas permeation experiments.
2. *Investigate the effects of molecular sieve pore size on MMM performance*. By using PVAc (a polymer that is known to adhere strongly to a variety of surfaces),

a survey of MMM performance will be conducted using molecular sieves of different pore/channel window sizes to create low loading MMMs. Attempts will also be made to alter the pore/channel sizes of certain molecular sieves.

3. *Understand the effects of processing conditions on MMM performance*. There are many aspects of MMM processing and formation such as molecular sieve preparation, MMM solution preparation, and MMM annealing conditions that may result in undesirable MMM performance.

1.6 Thesis Organization

The remainder of this thesis addresses the 3 objectives described in Section 1.6 by providing the relevant background and theoretical tools, describing the experimental methods and analysis, discussing the results of the 3 objectives in 3 separate body chapters, and offering global conclusions and recommendations for future work. Four appendices close out the thesis. The following list summarizes the thesis chapter organization.

- Chapter 2: Theory and Background
- Chapter 3: Materials and Methods
- Chapter 4: Effects of Processing Conditions on MMM Materials and MMM Transport Properties
- Chapter 5: Effects of High Molecular Sieve Loading on MMM Properties
- Chapter 6: Effects of Molecular Sieve Pore Size on MMM Permeation Properties
- Chapter 7: Conclusions and Recommendations
- Appendix A: Gas Adsorption Isotherms of Molecular Sieves

- Appendix B: Pure Gas Permeability in 50 vol.% Zeolite 4A MMMs
- Appendix C: Pure Gas Permeability in CuTPA MMMs
- Appendix D: Pure Gas Permeability in Partial K^+ Zeolite A MMMs

1.7 References

[1] Mcwilliams, A. *The global industrial gas business*. 2009; Available from: http://www.bccresearch.com/report/CHM041C.html.

[2] Koros, W.J. and R. Mahajan, *Pushing the limits on possibilities for large scale gas separation: Which strategies?* Journal of Membrane Science, 2000. **175**(2): p. 181-196.

[3] Baker, R.W., *Future directions of membrane gas separation technology.* Industrial & Engineering Chemistry Research, 2002. **41**(6): p. 1393-1411.

[4] Williams, P.J., *Analysis of factors influencing the performance of cms for gas separations*. 2006, Georgia Institute of Technology, Ph.D. Thesis.

[5] Robeson, L.M., *Correlation of separation factor versus permeability for polymeric membranes.* Journal of Membrane Science, 1991. **62**(2): p. 165-185.

[6] Freeman, B.D., *Basis of permeability/selectivity tradeoff relations in polymeric gas separation membranes.* Macromolecules, 1999. **32**(2): p. 375-380.

[7] Robeson, L.M., *The upper bound revisited.* Journal of Membrane Science, 2008. **320**(1-2): p. 390-400.

[8] Zimmerman, C.M., A. Singh, and W.J. Koros, *Tailoring mixed matrix composite membranes for gas separations.* Journal of Membrane Science, 1997. **137**(1-2): p. 145-154.

[9] Higuchi, W.I. and T. Higuchi, *Theoretical analysis of diffusional movement through heterogeneous barriers.* Journal of the American Pharmaceutical Association, 1960. **49**(9): p. 598-606.

[10] Kulprathipanja, S., *Separation of fluids by means of mixed matrix membranes*, U.S.P. Office, Editor. 1988.

[11] Karger, J. *Measurement of diffusion in zeolites - a never ending challenge?* 2003.

[12] Moore, T.T. and W.J. Koros, *Non-ideal effects in organic-inorganic materials for gas separation membranes.* Journal of Molecular Structure, 2005. **739**(1-3): p. 87-98.

[13] Mahajan, R. and W.J. Koros, *Factors controlling successful formation of mixed-matrix gas separation materials.* Industrial & Engineering Chemistry Research, 2000. **39**(8): p. 2692-2696.

[14] Mahajan, R., *Formation, characterization, and modeling of mixed matrix membrane materials*. 2000, The University of Texas at Austin, Ph.D. Thesis.

[15] Moore, T.T., *Effects of materials, processing, and operating conditions on the morphology and gas transport properties of mixed matrix membranes*. 2004, The University of Texas at Austin, Ph.D. Thesis.

[16] Hillock-Mckittrick, A.M.W., *Crosslinkable polyimide mixed matrix membranes for natural gas purification*. 2005, Georgia Institute of Technology, Ph.D. Thesis.

[17] Shu, S., *Engineering the performance of mixed matrix membranes for gas separations*. 2007, Georgia Institute of Technology, Ph.D. Thesis.

[18] Li, Y., T.S. Chung, C. Cao, and S. Kulprathipanja, *The effects of polymer chain rigidification, zeolite pore size and pore blockage on polyethersulfone (pes)-zeolite a mixed matrix membranes.* Journal of Membrane Science, 2005. **260**(1-2): p. 45-55.

[19] Shu, S., S. Husain, and W.J. Koros, *Formation of nanostructured zeolite particle surfaces via a halide/grignard route.* Chemistry of Materials, 2007. **19**(16): p. 4000-4006.

[20] Li, Y., H.M. Guan, T.S. Chung, and S. Kulprathipanja, *Effects of novel silane modification of zeolite surface on polymer chain rigidification and partial pore blockage in polyethersulfone (pes)-zeolite a mixed matrix membranes.* Journal of Membrane Science, 2006. **275**(1-2): p. 17-28.

[21] Moore, T.T. and W.J. Koros, *Sorption in zeolites modified for use in organic anorganic hybrid membranes.* Industrial & Engineering Chemistry Research, 2008. **47**(3): p. 591-598.

[22] Doktycz, S.J. and K.S. Suslick, *Interparticle collisions driven by ultrasound.* Science, 1990. **247**(4946): p. 1067-1069.

[23] Fontana, B.J. and J.R. Thomas, *Configuration of adsorbed alkyl methacrylate polymers by infrared and sedimentation studies.* Journal of Physical Chemistry, 1961. **65**(3): p. 480-&.

[24] Stuart, M.A.C., G.J. Fleer, and B.H. Bijsterbosch, *Adsorption of polyvinyl pyrrolidone) on silica .2. The fraction of bound segments, measured by a variety of techniques.* Journal of Colloid and Interface Science, 1982. **90**(2): p. 321-334.

[25] Degennes, P.G., *Polymers at an interface - a simplified view.* Advances in Colloid and Interface Science, 1987. **27**(3-4): p. 189-209.

CHAPTER 2

THEORY AND BACKGROUND

2.1 Polymers—A Unique Class of Materials

Polymers are large molecules, or macromolecules, that are made of smaller parts, or monomers. Depending on the monomers used and the synthetic conditions, an essentially limitless number of polymers can be made. The simplest and most common synthetic polymers are long chains of hydrocarbons that bend, twist, and entangle with each other to form spaghetti-like structures. Polymers display a wide array of physical and chemical properties which depend on the physical and chemical properties of individual monomers as well as the size, shape, and properties of higher order structures, i.e. the geometry and properties of multiple monomers in concert. [1, 2]

One of the most unique properties of polymers is the presence of a 2^{nd} order phase transition known as the glass transition temperature, or T_g. Above T_g, polymers are considered "rubbery" whereas below T_g, polymers are considered "glassy". The rubbery state of polymers can be likened to the liquid state of small molecules. In the rubbery state there is enough thermal energy in the system that the polymer chains can undergo bulk translational movements, i.e. whole chains or large segments of a chain slide past other chains or segments due to random thermal fluctuations. [1, 2]

The glassy state of polymers is similar to the solid state of small molecules in that the polymer chains are effectively locked in place and only undergo vibrational and rotational movements due to random thermal fluctuations. Strictly speaking, however, a glassy polymer is not a solid—rather a super-cooled liquid that will never crystallize as

small molecules do when cooled below melting temperature. Some polymers show degrees of crystallinity among fractions of chains and chain segments, but not the molecular level, homogeneous crystallinity of small molecules. [1, 2]

Many variables control the value of T_g for a polymer including the composition of the monomers, the size and shape of the polymer chains, the degree of bond saturation of the backbones of the chains, the size and shape of chain side groups, and inter/intra-chain interactions. A detailed understanding of the variable space that controls T_g is beyond the scope of this work, but an understanding of how the molar volume of a polymer changes with temperature (especially in the vicinity of T_g) is critical to understanding polymeric membrane formation, gas transport in polymeric materials, and the effect of thermal history on the temporal stability of polymer properties. Figure 2.1 illustrates the impact of temperature on the molar volume of a polymer. [1, 2]

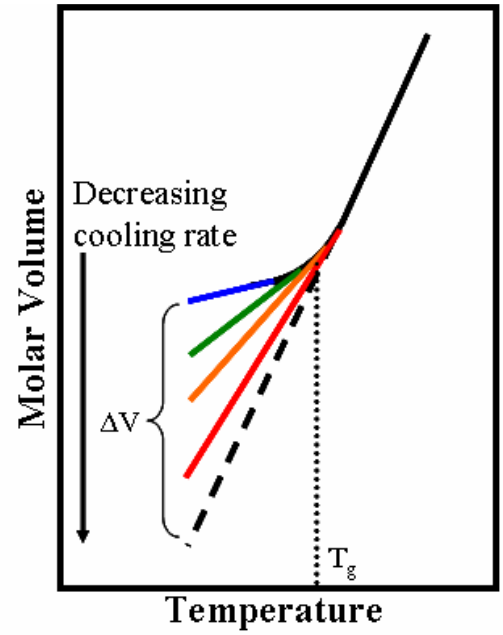

Figure 2.1: Polymer molar volume vs. temperature with respect to cooling rate.

Figure 2.1 shows several important traits of polymeric systems. The solid black line represents the change in molar volume of a rubbery polymer as it is cooled towards its T_g. This behavior is also seen for most small molecule liquids decreasing in temperature [3]. The dashed black line that follows the trajectory of the solid black line continuation how a small molecule liquid's molar volume decreases with temperature; this is also where polymeric materials deviate from normal liquids. The colored lines that bend away from the dashed line at T_g illustrate both the glassy nature of a polymer and the effect of cooling rate on polymer molar volume. As a polymer is cooled below T_g chain mobility is restricted and the bulky macromolecules and even segments of the macromolecules can no longer move around each other leaving packets of excess free volume behind. The blue, green, orange, and red lines depict decreasing cooling rates, respectively. In other words, the blue line represents a polymer that is rapidly cooled through its T_g while the red line shows a polymer that is slowly cooled through its T_g. The excess free volume that is left behind, ΔV, in a thermally quenched polymer can be expressed:

$$\Delta V = V_{actual} - V_{equilibrium} \qquad \text{(Equation 2.1)}$$

Values of V_{actual} appear on the colored lines in Figure 2.1 with corresponding $V_{equilibrium}$ values on the dashed black line representing what the molar volume would be if the macromolecules of a polymer achieved thermodynamic equilibrium. [1, 2]

The effect of solvent evaporation rate on resulting polymer molar volume for polymer-solvent systems is analogous to the effect of cooling a polymer through T_g. When a polymer is dissolved in a solvent, the chains move freely, even if the temperature of the system is below the T_g of the pure polymer. As solvent evaporates the chains

become less mobile and denser—just like a rubbery polymer cooling towards its T_g. At a certain, critical solvent volume fraction, φ_s, the chains cease bulk translational motion and the polymer-solvent system is at T_g [4]. Further evaporation results in the molar volume of the polymer to follow one of the colored lines in Figure 2.1 depending on the rate of evaporation. Rapid evaporation is depicted with the blue line whereas slow evaporation may follow the red line. The way a polymer is processed from solution can affect the resulting polymer properties. It should also be noted that the rate of thermal quenching or solvent evaporation can also have undesired effects on membrane morphology as will be discussed later in this chapter.

2.2 Gas Transport in Polymers

Polymeric materials exhibit a rich variety of gas transport properties due to dependence upon many variables. Some of the pure polymeric properties that influence gas transport are polymer molecular weight and molecular weight distribution, temperature, thermal history of the polymer, polymer glass transition temperature (T_g), intra/inter-polymer chain spacing, polymer morphology, and fractional free volume. The size and shape of a gas molecule have an enormous impact on gas transport through polymers as the molecules must navigate through a tangled web of polymer chains. Pure gas compressibilities as well as the thermodynamic properties of gas mixtures also play important roles in overall transport. Finally, there are polymer-gas parameters and phenomena that influence transport, such as a thermodynamic affinity parameters, plasticization, and anti-plasticization. [5, 6]

A detailed review that encompasses all aspects of gas transport through polymeric materials is beyond the scope of this thesis. Furthermore, such a review is redundant as

there are many useful texts that cover the complexity of gas transport in polymers in great detail [5, 6]. Instead, the following sections will focus on the aspects of gas transport in polymers that are directly related to my thesis work.

2.2.1 Gas Sorption in Rubbery Polymers

When the surrounding atmosphere of a material at thermodynamic equilibrium with the atmosphere is suddenly changed, i.e. the temperature or composition of the atmosphere changes, a shift from equilibrium occurs, and thermodynamics demands re-establishing a new equilibrium. In the case of polymer-gas systems, changes in the composition and pressure of the gas result in gas absorption or desorption.

The simplest case is that of a rubbery polymer-single gas system at isothermal conditions. Equation 2.2 describes the relationship between the amount of a gas absorbed in a rubbery polymer as a function of external gas pressure.

$$C_{abs} = kp \qquad \text{(Equation 2.2)}$$

In Equation 2.2, C_{abs}, k, and p, represent the amount of gas absorbed in the polymer, the Henry's affinity constant, and external gas partial pressure, respectively. Note that the solubility coefficient of a material for a given gas, i, is defined as the sorbed concentration divided by the external gas partial pressure as shown in Equation 2.3.

$$S = C_{ads} / p \qquad \text{(Equation 2.3)}$$

This simple linear relationship is the result of the molecular homogeneity of rubbery polymers and liquids. In other words, any random control volume of a rubbery polymer or liquid, regardless of size of or position of the control volume, is equivalent to all other control volumes.

2.2.2 Gas Sorption in Glassy Polymers

Gas absorption into glassy polymers is substantially more complicated than absorption in rubbery polymers due to molecular-scale heterogeneity [1, 2, 6]. As described in Section 2.1, when a polymer is cooled below T_g, excess free volume is trapped due to the mismatch between chain mobility below T_g and relatively rapid heat transfer. In gas absorption, these excess free volume packets act as site specific, or Langmuir, absorption sites. Basically, Langmuir absorption is a fixed space-filling absorption mechanism where sorbed concentration plateaus at a certain point as external pressure increases because all sites become occupied. Equation 2.4 and Figure 2.2 describe Langmuir absorption.

$$C_{abs} = \frac{C_H' bp}{1 + bp} \qquad \text{(Equation 2.4)}$$

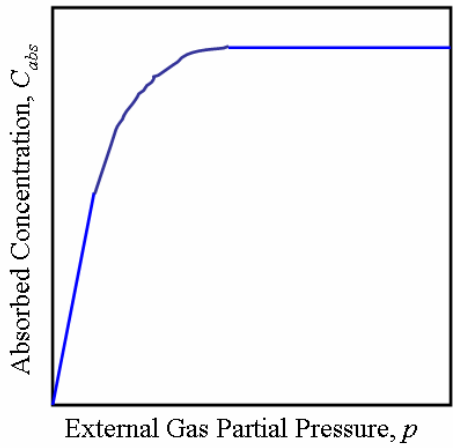

Figure 2.2: Langmuir type absorption response.

Note that C_H' = saturation constant; b = affinity parameter. Although glassy polymers have excess free volume Langmuir sites dispersed throughout, much of the

polymer consists of polymer chains that exhibit a Henry's absorption response as described in Section 2.2.1. This heterogeneous absorption behavior is known as "dual-mode" absorption and is described in great detail elsewhere [7-11]. Equation 2.5 and Figure 2.3 provide a basic description of dual-mode absorption.

$$C_{abs} = k_d\, p + \frac{C_H' b p}{1 + b p} \qquad \text{(Equation 2.5)}$$

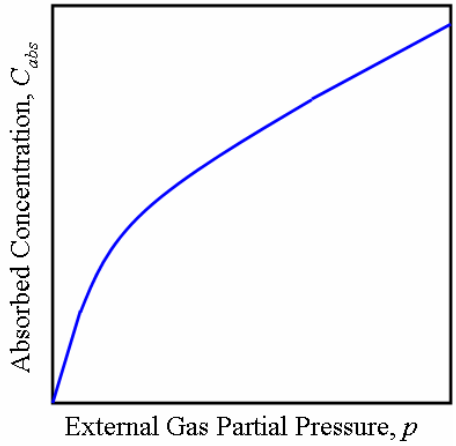

Figure 2.3: Dual-mode absorption response.

Since glassy polymer membrane separate mixtures of gases, it is important to understand mixed gas sorption. A single component of a gas mixture will appear to sorb less in mixed gas sorption due to competition in the absence of complicating phenomena like plasticization and swelling. The dual-mode sorption model discussed in the preceding section can be modified to account for competitive effects as shown in Equation 2.6 below for a penetrant, *A*.

$$C_{abs,A} = k_{d,A}\, p_A + \frac{C_{H,A}' b_A p_A}{1 + \sum_i^N b_i p_i} \qquad \text{(Equation 2.6)}$$

The concept of mixed gas absorption competition is critical for the understanding of polymeric membrane productivity and efficiency in real feeds.

2.2.3 Gas Diffusivity in Polymers

Diffusivity is a measure of how fast a molecule can undergo a translational jump through a medium. Gas diffusion in polymers occurs via an activated process which can be characterized by a diffusion coefficient, D_i:

$$D_i = D_{i,o} e^{-E_a/RT} \qquad \text{(Equation 2.7)}$$

D_i is the average diffusion coefficient of a penetrant, i, in a polymer (usually expressed in cm^2/s). The remaining parameters, $D_{i,o}$, E_a, R, and T, are the exponential prefactor, the activation energy for a diffusion jump, the universal gas constant, and thermodynamic temperature, respectively. The value of E_a is affected by the nature of the polymer, the diffusing gas, and even polymer-gas interactions. [12]

The activated process by which a gas molecule diffuses through a polymer is a function of molecular-scale processes: the opening and closing of "transient gaps". The cartoon in Figure 2.4 represents this process.

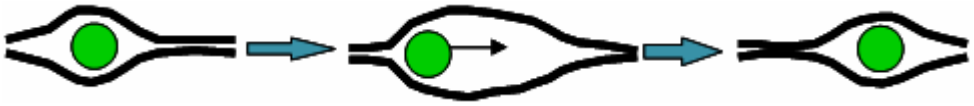

Figure 2.4: Cartoon of the transient gap diffusion mechanism in polymers.

Through random, thermally-driven polymer segmental motions, these transient gaps open and close. The frequency and size of these gaps is a function of polymer chain mobility which in turn is affected by the overall temperature and the proximity to the polymer's T_g, i.e. a polymer well above its T_g has transient gaps that open and close with relatively

high frequency and display a greater size compared to the same polymer well below its T_g. [5]

The size and shape of these transient gaps is also important. Small gas molecules, such as helium, hydrogen, and oxygen, can access a much broader range of transient gap sizes than larger gas molecules, such as alkanes; thus, the smaller gas molecules have relatively high diffusivities in polymers than the larger molecules. As noted above, rubbery polymers are able to form larger transient gaps compared to their glassy counterparts; thus, gas diffusion in a rubbery polymer is relatively high compared to a glassy polymer. [5]

The nature of gas diffusivity through polymers is the major reason that most commercial membrane units contain glassy polymer membranes. Due to the relatively large sizes of transient gaps, rubbery polymers have poor gas size and shape selectivity. Since most gas separations of interest are for light gases that do not exhibit large thermodynamic partitioning in polymers, glassy polymers dominate membrane-based gas separations. [5, 6, 13]

As with gas absorption in glassy polymers, gas diffusivity is governed by a dual-mode process. Since a glassy membrane is heterogeneous on a molecular level, containing both Henry's and Langmuir sites, gas diffusion is multi-modal. Barrer provides an easily understood model for dual-mode mobility in glassy polymers [14]. Four unique diffusion coefficients are defined: 1) translational jumps between Henry's sites denoted as D_{dd} in cm^2/s; 2) translational jumps between Langmuir sites denoted as D_{hh} in cm^2/s; 3) translational jumps from Henry's sites to Langmuir sites denoted as D_{dh} in cm^2/s; 4) translational jumps from Langmuir sites to Henry's sites denoted as D_{hd} in

cm^2/s. All of these 4 types of diffusional jumps are associated with their own spatial, energetic and statistical parameters and can be combined into a single apparent diffusivity.

2.2.4 Gas Permeability in Polymers

The first scientific observation of gas permeability through dense media was made by Sir Thomas Graham [15]. Graham's breakthrough observation was that animal bladders inflated with different gases deflated at different rates. Permeability of penetrant *A*, P_A, can be expressed with the following phenomenological expression:

$$P_A = \frac{n_A \times l}{\Delta p_A} \qquad \text{(Equation 2.8)}$$

In Equation 2.8, n_A is the molar flux of penetrant *A*, *l* is the thickness of the dense film, and Δp_A is the partial pressure difference of penetrant *A* across the dense film. Permeability is a pressure and thickness normalized flux, thus enables researchers to directly compare materials irrespective of sample thickness and gradient imposed.

Observed permeabilities in dense polymeric films is governed by a solution-diffusion mechanism whereby a penetrant first adsorbs to the dense film from a high activity upstream feed, diffuses through the film thickness along a chemical potential gradient, and finally desorbs into a low activity downstream feed. Equation 2.8 is the expression used to determine permeability in isochoric permeation experiments as conducted in this work, and through Fick's 1st law Equation 2.8 can be rearranged so that permeability is expressed as a product of the diffusivity, D_A, and solubility, S_A, of penetrant, *A*:

$$P_A = D_A \times S_A \qquad \text{(Equation 2.9)}$$

Equation 2.9 provides a concise, general thermokinetic representation of gas permeability in dense media. Since permeability is a function of diffusivity and solubility, all of the variables that influence gas diffusivity and sorption in a polymer also influence gas permeability.

The efficiency of a membrane separation can be described by the ideal permselectivity of a gas pair, $\alpha_{A/B}$. Ideal permselectivity is expressed as the ratio of pure gas permeabilities:

$$\alpha_{A/B} = P_A \Big/ P_B \qquad \text{(Equation 2.10)}$$

Typically, the fast penetrant is denoted with an *A* and the slow penetrant with a *B* so that selectivities are greater than one. When Equation 2.9 is substituted into Equation 2.10 the efficiency of a polymeric membrane can be treated as the product of diffusive and sorptive selectivities.

$$\alpha_{A/B} = \frac{D_A}{D_B} \times \frac{S_A}{S_B} \qquad \text{(Equation 2.11)}$$

In an isochoric permeation experiment where the membrane separates a high pressure feed volume from a low pressure permeate volume, steady-state flux is preceded by a time lag, θ, where there is little or no accumulation of penetrant in the permeate volume. For the case of single penetrant permeation through a structurally and compositionally homogeneous film of uniform thickness, l, for which Fickian kinetics apply, the time lag is related to the average diffusivity of penetrant *A*, D_A, through the film as shown in Equation 2.12:

$$D_A = \frac{l^2}{6\theta} \qquad \text{(Equation 2.12)}$$

For the case of zero initial permeate pressure, the time lag is simply the time-intercept of a linear fit of the steady-state permeate pressure rise. Aside from being averaged along the chemical potential gradient of a dense film in a permeation experiment, D_A in Equation 2.12 assumes a single apparent diffusivity that embodies the multi-modal diffusion mechanism in glassy polymers that was described above in Section 2.2.3. [12]

Mixed gas permeation through a polymer film is conceptually similar to pure gas permeation. The primary difference is the effect of sorption competition on overall permeation properties. All of the components of a mixed feed must permeate through the same space so competition occurs for the unrelaxed, fixed Langmuir gaps, $C_H^{'}$ in Equation 2.4, for glassy polymers. This competition means the mixed gas permeability of any given penetrant will be lower than the pure gas permeability for the same partial pressure in a glassy polymer (in the absence of complicating phenomena such as plasticization). Furthermore, depending on the shape and magnitude of the sorption isotherms of the individual components in a mixed gas feed as well as the partial pressures of each component, mixed gas selectivities can be lower or higher than their pure gas counterparts. [5, 6]

2.2.5 Plasticization in Polymers

Plasticization is a sorption induced phenomenon where gas molecules that sorb strongly in polymers increase segmental mobility. This phenomenon is common for high partial pressures of highly condensable gas molecules and gases with strong thermodynamic affinity for sorption—examples include carbon dioxide and propylene. The impact of plasticization on permeation properties can be seriously detrimental to

permselectivity. Figure 2.5 illustrates the effect of plasticization on carbon dioxide permeability and the selectivity of carbon dioxide over methane in a polymer membrane.

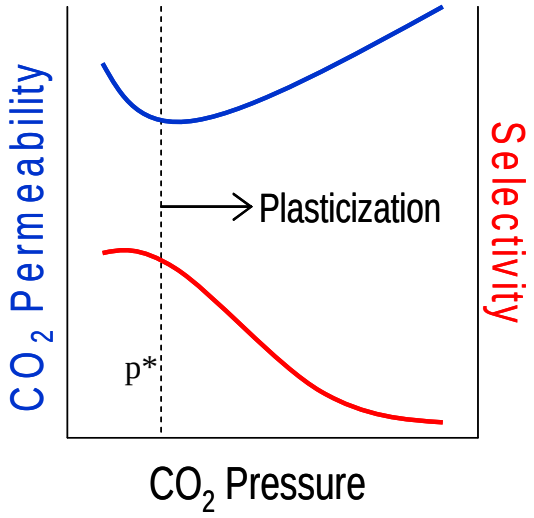

Figure 2.5: Effects of carbon dioxide plasticization on gas transport in polymers.

At the carbon dioxide plasticization pressure, p^*, the enhancement in chain mobility increases the frequency and size of chain fluctuations that give rise to the transient gap transport mechanism through the polymer. This results in higher carbon dioxide permeability and higher methane permeability. The boost in methane permeability is large relative to carbon dioxide due to its larger size; thus, selectivity drops. [5]

The carbon dioxide plasticization phenomenon is a serious problem for polymeric membranes for natural gas separations. Researchers have addressed this issue by developing crosslinked polymer membranes. The chains in a crosslinked polymer are largely immobilized by intra- and inter- chain covalent bonds known as crosslinks. Preventing swelling can reduce or eliminate the effects of plasticization. [16]

2.3 Gas Transport in Molecular Sieves

Microporous molecular sieving materials have transport properties that are highly desired for gas separations. For example, zeolites are rigid, microporous, crystalline materials that typically have high specific surface areas (surface area per mass or volume). The high specific surface areas provide plentiful sites for gas adsorption (note that adsorption is used to describe sorption in zeolites versus absorption for rubbery polymers since sorption occurs on specific sites in a zeolite whereas sorption in a polymer dilates and fills intersegmental spaces between and within chains). Along with high sorption capacities, the rigid, crystalline nature of zeolites results in small molecular scale "windows" through which gas molecules must pass in order to access the internal microporosity. These pore windows impart excellent size selective (or diffusive) selectivities to zeolites and related materials. In fact, many zeolites have pore window sizes that allow a smaller molecule easy access to the internal micropores while outright rejecting larger molecules. This molecular sieving mechanism is shown schematically in Figure 2.6. [17, 18]

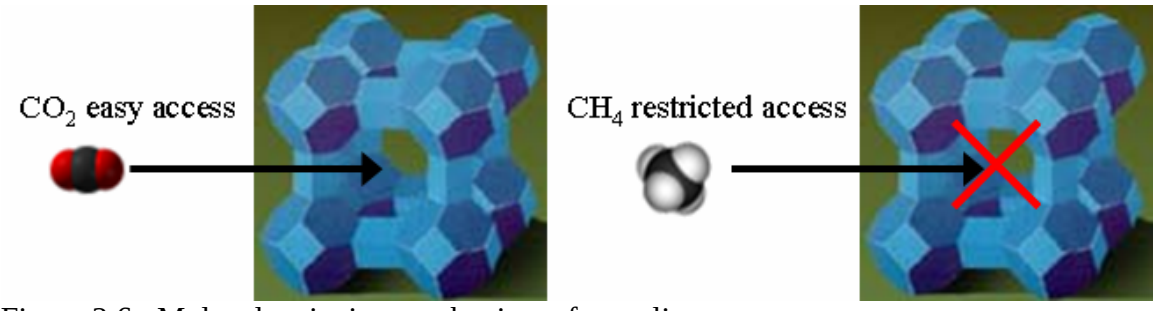

Figure 2.6: Molecular sieving mechanism of a zeolite.

2.3.1 Gas Sorption in Molecular Sieves

Gas sorption in rigid microporous materials is a pore filling process where molecules adsorb at fixed surface sites. Unlike glassy polymers, rigid microporous materials do not swell with increasing pressure; thus they follow the Langmuir isotherm described in Section 2.2.2. The sorption capacities of zeolites and other microporous materials depend on specific surface area, pore volumes and sizes, and chemical composition. The surfaces of microporous materials are usually energetically heterogeneous, and gas molecules can physically or chemically adsorb to these surfaces and fill the volumes between the surfaces. At low temperatures (< 100 °C or so for light gases) physical adsorption is generally much greater than chemical adsorption. Materials like zeolites typically have much higher sorption capacities than polymers. [19]

2.3.2 Gas Diffusion in Molecular Sieves

As with diffusivity in polymers, diffusion in materials such as zeolites is an activated process that can be described by Equation 2.17 in Section 2.2.2. However, the diffusion mechanism is different due to the rigidity of crystalline zeolite structure. A pore "window" moderated mechanism controls diffusion into microporous materials. This concept was briefly described in Section 2.3, but the window moderated mechanism has implications beyond the extreme cases of easy penetrant access and penetrant rejection. Even with pore windows large enough to permit all gaseous penetrants, the rigid pore windows can provide significant size and shape diffusive selectivities in materials like zeolites. [17, 18, 20]

Unfortunately, precisely measuring the diffusion coefficient of zeolites and related microporous materials can be extraordinarily difficult. In 2003, Karger—a

pioneer in the field of gas transport in zeolites—reported that determining diffusion coefficients in zeolites will continue to be a problem in the coming decades [21]. The difficulty of measuring accurate gas diffusion coefficients for zeolites is multi-faceted. Gas adsorption on zeolite surfaces is often highly exothermic and the heat released obscures kinetic measurements [22]. Since the measurements are often made on small crystals (micron scale or less) equilibrium can be reached within fractions of a second [18, 21]. Use of large crystals can lengthen the time to reach equilibrium, but it is also more difficult to maintain isothermal conditions for large crystals [23]. Furthermore, it can be quite difficult to synthesize defect-free large crystal zeolites making diffusivities determined from large crystals questionable [24]. The difficulty in making large crystal zeolites also makes permeation measurements quite difficult [25, 26].

2.3.3 Gas Permeability in Molecular Sieves

In principle, gas permeability in a dense film of a microporous material is similar to permeability in polymers (i.e. with equations 2.8 and 2.9). In practice, however, it is extremely difficult to experimentally determine permeabilities and permselectivities in zeolites due to the difficulty in making large, self-supported zeolite dense films [25, 26]. Typically, large area, thin zeolite films are grown on porous supports that can provide transport resistance, and the films themselves usually contain low resistance, void-defects around grain boundaries [25, 26]. These challenges also explain why pure zeolite membranes are unlikely to ever be applied to large scale gas separations without some unforeseen breakthrough.

2.4 Gas Transport in MMMs

As discussed in Chapter 1, the goal of a MMM is to combine the superior transport properties of microporous materials with the ease of processing polymers. Overall gas transport through a dense film of microporous filler particles in a polymer matrix should be some combination of the properties of each phase in an ideal case where there are no void defects or unusual interfacial phenomena. In the following sections, MMM gas transport will be explained. First gas solubility and diffusivity in MMMs will be discussed. Finally gas permeability and permselectivity will be discussed and MMM transport models will be introduced.

2.4.1 Gas Solubility in MMMs

Gas sorption in MMMs is quite simple in ideal cases free of void defects and interfacial phenomena. The expected solubility of a MMM is simply the volume weighted average of the 2 phases as described in the following equation [27, 28].

$$S_{MMM} = \varphi_d S_d + \varphi_p S_p \qquad \text{(Equation 2.13)}$$

In Equation 2.13, S_{MMM} is solubility coefficient of gas sorbed in a MMM. S_d and S_p are solubility coefficients for the dispersed phase and the polymer matrix, respectively. The volume fractions of the dispersed phase and polymer matrix are φ_d and φ_p, respectively.

Actual solubility in a real MMM may deviate from the expectations of Equation 2.13 due to void defects, dilated or rigidified polymer chains at particle interfaces, or dispersed phase pore obstruction [29]. These potential defect morphologies were discussed in Chapter 1 and will be discussed as necessary in Chapters 4 – 6.

2.4.2 Gas Diffusivity in MMMs

Gas diffusivity in MMMs is conceptually similar to gas diffusivity in the constituent parts of the MMM—only much more complex. A glassy polymer can have up to 4 important diffusion coefficients (see Section 2.2.3) and understanding gas diffusivity and permeability in materials like zeolites has been a source of confusion for at least 50 years and counting. Add in the prospect of interfacial zones of influence [27, 29, 30] in MMMs with their own unique gas mobilities, and the number of potentially significant gas diffusion coefficients grow. Extending Barrer's analysis of dual-mode mobility in glassy polymers to the case of a glassy polymer-zeolite MMM with interfacial zones of influence with their own unique properties helps illustrate the complexity of penetrant mobility in MMMs. Figure 2.7 will be used to guide the discussion.

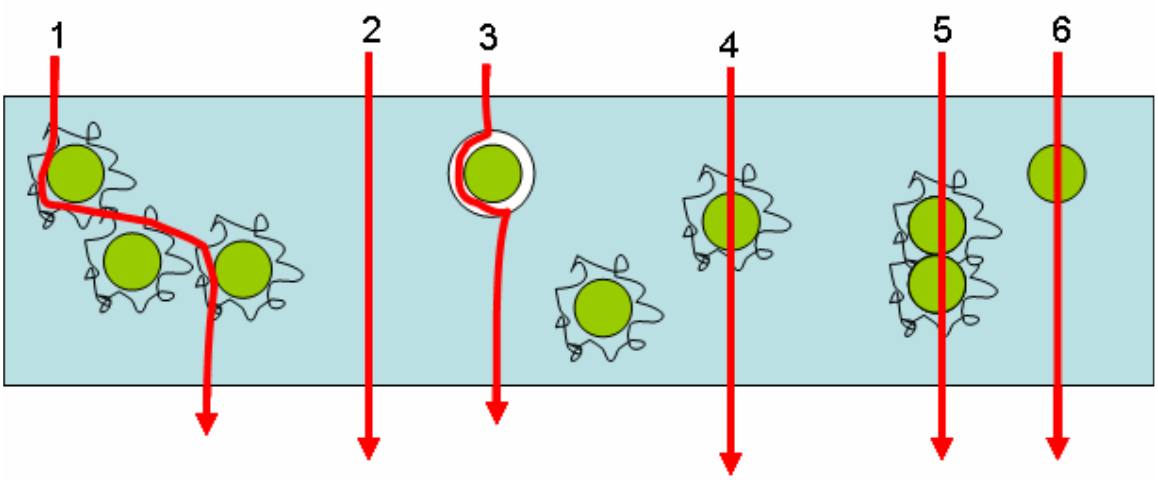

Figure 2.7: Cartoon of some of the unique diffusional pathways in MMMs.

The continuous glassy polymer matrix is shown in light blue while interfacial zones of influence are represented by polymer chains as squiggly black lines. The green circles represent filler particles (zeolites) and the white circle shows a void defect at a

particle-polymer interface. The six arrows in Figure 2.8 are used to introduce potentially important diffusive pathways in a MMM. Pathway 2 is exactly the dual-mode mobility that Barrer describe with 4 diffusion coefficients as described in Section 2.2.3. Pathway 1 illustrates a diffusive pathway that takes a penetrant through interfacial polymer chains whose properties deviate from the bulk, glassy polymer—diffusion through interfacial polymer will be defined as D_{II}. Pathway 3 shows the bypass of a filler particle through an interfacial void. As Moore discusses in his thesis, diffusion through a void is dependent on the size of the void, but for simplicity a single diffusivity will be used to represent this possible path, D_V. The 4th path represents the different mobilities that may exist for a penetrant to get in and out of a filler particle through interfacial polymer (D_{IZ} and D_{ZI}) while the 5th pathway illustrates the possibility that diffusive jumps between zeolite particles, D_{ZZ}, may play an important role in overall diffusivity. Finally, pathway 6 represents transport through glassy polymer and a filler particle, D_Z.

Basically, the complexity of diffusion through a MMM is the result of introducing several new phases into the dual-mode mobility model for glassy polymers. Just as Barrer's model considers jumps within a phase and into and out of phases, accounting for diffusivities in a MMM of a glassy polymer and zeolite must do the same. The end result is no less than 12 potentially significant diffusion coefficients assuming that only one diffusivity is needed to describe transport through interfacial zones of influence and zeolite particles—an assumption that is not necessarily true since it is reasonable to model mobility in the interfacial polymer as multi-modal and since mobility in and out of a zeolite particle may be different from mobility through a zeolite particle [31]. Precisely

accounting for all the possible diffusivities in a MMM is a daunting task and of questionable value.

2.4.3 Gas Permeability in MMMs

Gas permeability in a MMM can be described as it is described for polymers and molecular sieving materials—with Equations 2.8 and 2.9. Just as solubility in a MMM is considered to be a volume fraction weighted combination of the individual phases' solubilities, permeation in a MMM can be described in a similar manner. In dense film MMM studies, the filler particles are typically small in relation to the film thickness and randomly dispersed throughout the polymer matrix. Many researchers [30, 32, 33] have shown that adapting Maxwell's model for electrical permittivity of dilute dispersions of metal spheres in a conducting fluid is a useful for understanding MMM permeation. Maxwell's model for gas permeability in a MMM is provided below [34].

$$P_{MMM} = P_p\left[\frac{P_d + 2P_p - 2\varphi_d\left(P_p - P_d\right)}{P_d + 2P_p + \varphi_d\left(P_p - P_d\right)}\right] \qquad \text{(Equation 2.14)}$$

As discussed in previous sections, the difficulties in accurately measuring diffusivity and permeability in microporous materials limits the predictive potential of Maxwell's model. However, it is still a useful gauge of MMM success and can be used quite effectively for comparing the properties of MMMs as a function of dispersed phase loading. Many other models may be considered for understanding MMM permeation properties, but only Maxwell's model will be considered in this work. Other MMM permeation models as well as Maxwell's are well discussed elsewhere [35, 36]. Some researchers have developed even more sophisticated models for understanding gas permeability in MMMs [30, 37]. The "3 phase Maxwell model" developed by Mahajan and Koros is noteworthy as it accounts for the contribution of interfacial zones of influence around particles.

2.4.4 Permeation Time Lag in MMMs

Permeation time lag is also observed in MMMs but has a more complex relationship with diffusivity than the case of a pure polymer film as described in Section 2.2. For example, a polymer dispersed with impermeable particles can increase the permeation time lag relative to the pure polymer due to tortuousity effects which can be greatly magnified by use of high aspect ratio particles aligned perpendicular to flow [38]. An increased time lag in such a sample does not mean that diffusivity in the polymer is inherently lower; it simply means that diffusional path lengths have increased due to tortuousity.

The case of permeable filler particles in MMMs is even more complex. Penetrants that permeate readily through the filler particles in a MMM can have longer time lags than impermeable penetrants due to the relatively high sorption capacities often seen in microporous filler particles relative to the polymer matrix. Higuchi *et al.* [39] and Paul *et al.* [40] were among the first to explore this time lag extension or immobilizing sorption phenomenon. Paul's work is especially useful as he shows that time lag extension (relative to pure polymer) for a microporous particle filled polymer matrix can be understood as a function of filler volume fraction, filler equilibrium sorption properties, and polymer matrix equilibrium sorption properties for the case of total penetrant immobilization (i.e. solubility is much higher and mobility is substantially lower in the dispersed particles than in the surrounding polymer matrix).

In general cases where penetrant mobility in the filler particles is comparable to or greater than the surrounding polymer, gas transport in porous filler-polymer systems is expected to show similar apparent increased sorption and corresponding extended time

lag effects. Many researchers studied partial penetrant immobilization in great depth [7, 8, 11, 41], resulting in permeation time lag expressions much more complex than equation 2.12. Regardless of the complexity of analysis, permeation time lag extension in glassy polymers or polymer-microporous filler systems are the results of the penetrant sorption in non-equilibrium microvoids or filler particles, respectively. In other words, non-equilibrium microvoids and filler particles act as mass sinks during the transient portion of a permeation experiment.

The MMMs studied in this work are unlikely to result in total immobilization due to the large windows of the zeolites and metal organic frameworks and low penetrant diffusivities in the polymer used, poly(vinyl acetate) (PVAc). However, the dispersed microporous particles will still act as mass sinks which must be filled by penetrant diffusion from the PVAc phase during the transient portion of permeation, thereby resulting in time lag extension and apparent diffusivity reductions for the MMMs compared to pure PVAc. While the likelihood of partial penetrant immobilization in these MMMs will make it difficult to understand whether transport enhancements are diffusivity based, solubility based, or combinations of both, use of Equation 2.12 as well as the relative gas solubilities in the microporous materials versus PVAc will assist in the characterization of the transport properties of the MMMs.

2.5 Dense Film Formation

Although this work focuses primarily on the gas transport properties of MMMs, creation of defect-free dense films is not trivial. Processing polymeric materials from polymer-solvent solutions may lead to defects in the final product. Pure polymer films can form pinholes, cracks, and curls that make transport measurements difficult. The

same defects along with interfacial adhesion problems, such as dilated or densified zones of influence and voids, can occur in low particle loading MMMs. High particle loading MMMs are subject to all of the same problems with the added complication of particle percolation—a phenomenon where the particle loading is so high that particles actually make direct contact. Particle percolation during MMM film formation may result in undesirable film morphology.

The relatively simple case of forming a dense film of a glassy polymer will be discussed first, followed by a discussion low loading MMM formation. Finally, some theoretical concepts of relevance to high loading MMM formation where particle percolation is likely will be presented.

2.5.1 Stress Accumulation in Glassy Polymer Films

Section 2.1 introduces the concept of the glass transition temperature, T_g, in polymers. Note that in the case of solvent evaporation, the glass transition is defined as the solvent volume fraction where the polymer vitrifies at the processing temperature, φ_s. Excess free volume leads to stress development in a polymer film formed on a rigid substrate. There is nothing inherently undesirable about stress development in a solution processed polymer so long as the stresses are accommodated in a non-destructive manner. The simplest way to accommodate the stress is for a polymer to relieve the stress as it continues to shrink in response to dropping temperature or loss of solvent. Given enough time, the excess free volume will diffuse out, and the polymer will be at its thermodynamic equilibrium—this is a non-destructive stress relief mechanism. [4, 42]

If the rate of thermal quenching or solvent evaporation is large enough, destructive stress relief mechanisms may occur. The stresses induced may exceed the

cohesive energy of the polymer resulting in fractures in a polymer film—typically polymers used in gas transport membranes have substantially high molecular weights that this is not a problem. A more common destructive relief mechanism (for coatings) is adhesive failure with the substrate [27]. Chapter 3 will describe the dense film formation procedure, but for now it is useful to note that the membranes used are initially applied as coatings on a rigid substrate and later removed. While it is ultimately necessary to remove the film from the substrate for gas transport testing, one wants to control when that happens. If the film delaminates from the substrate on its own, stresses not relieved by the delamination event may result in the film curling up. If the curled up film still contains enough solvent, the film may stick to itself resulting in a film with no suitable areas for testing.

Stress accumulation in polymer coatings has been studied extensively [4, 42, 43]. Figure 2.8 illustrates the difference between forming a free standing polymer sample versus a polymer adhered to a substrate as seen during dense film preparation.

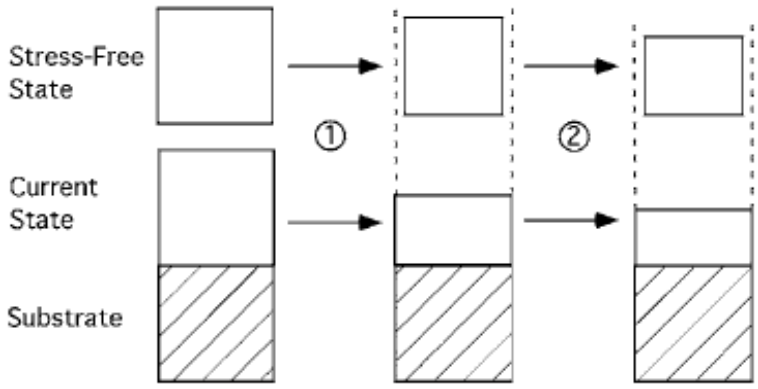

Figure 2.8: Residual Strain in solution processed polymers. [42]

The left most portion of Figure 2.8 represents a polymer sample processed from solution at zero time in film preparation. As solvent evaporates (depicted by arrows 1 and 2), the polymer sample shrinks to relax the excess volume left by the solvent molecules. The "stress-free" state shown on the top of Figure 2.8 shows the polymer sample shrinking in all directions whereas the lower portion shows that the sample adhered to a substrate can only shrink in the direction normal to the substrate. Compression towards the substrate results in tension in the plane of the film that can be described by Hooke's Law:

$$\sigma(t) = \frac{E_m}{1-\upsilon_m}\varepsilon(t) \qquad \text{(Equation 2.15)}$$

In Equation 2.15, σ(t) is the in plane stress at time, *t*, E_m is the elastic modulus of the membrane, υ_m is Poisson's ratio, and $\varepsilon(t)$ is the residual strain at *t*. The residual strain is defined as the difference between the strain of the stressed state (substrate-bound, solidified membrane) and the stress-free state that the membrane would adopt if removed from the substrate.

Note that the above case of a free standing sample versus a substrate bound sample only results in stress accumulation when the polymer solution sample reaches its T_g (or φ_s). Above T_g, stresses form but do not accumulate because of relaxations brought on by chain movement [42, 43]. At the glass transition, the sample gains enough elasticity to support a stress—in other words, the E_m term in Equation 2.15 only becomes significant as the sample passes through T_g. As solvent continues to evaporate, E_m becomes significant and stresses accumulate [4]. As discussed in Section 2.1, faster evaporation rates result in more excess free volume which results in more strain; thus, rapid evaporation accumulates greater stresses than slow evaporation in a solution processed polymer film.

2.5.2 Stress Accumulation in Low Particle Loading MMMs

Since MMMs are comprised of dispersed particles in a polymer matrix, it is important to understand the differences between stress accumulations in pure polymer films versus particle filled films. The concepts introduced in Section 2.5.1 still apply, and Equation 2.15 can be adapted to account for particle loading [4]. In his thesis, Moore provides an excellent snapshot of the implications of stress accumulation in MMMs [27]. Figure 2.9 considers a solution processed MMM at the moment enough solvent has evaporated to make the polymer matrix glassy.

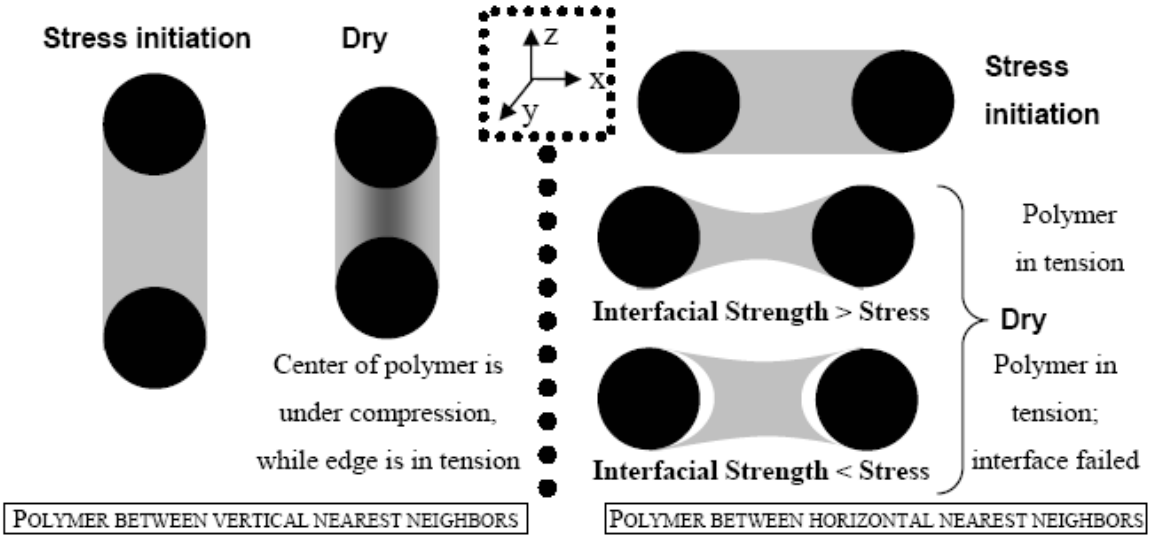

Figure 2.9: Stress accumulation behavior in a MMM. [27]

Since the MMM only shrinks towards the substrate, only vertically aligned particles move towards each other. Therefore, the horizontally aligned particles are subject to the in plane stresses that accumulate as solvent continues to evaporate. If the strength of the adsorbed polymer-particle adhesion is not strong enough, the adhesive bond can break in a stress relief mechanism.

The presence of particles also affects material properties in a way that magnifies stress accumulation. Many researchers have witnessed T_g and modulus increases proportional to filler concentration up to a plateau for cases of well adhered interfaces [4, 43-45]. Filler particles typically have a higher modulus than the polymer; therefore, particle filled polymeric composites have a higher modulus than the pure polymer for the case of good interfacial adhesion. Similarly, polymer-particle composites have a higher T_g than the pure polymer for the case of good interfacial adhesion. The modulus and T_g enhancements result in higher residual stresses for polymer-particle composites versus their corresponding pure polymers during processing. [43]

2.5.3 Stress Accumulation in High Particle Loading MMMs

The same concepts that apply to low particle loading polymer films applies to high loading films as well. There are 2 key differences: 1) higher loadings equate to more interfacial polymer which can increase the effective T_g and thus cause an earlier onset of stress accumulation; 2) particle percolation can disrupt the ability of a solution processed film to shrink even if the remaining solvent concentration leaves the polymer matrix above T_g.

Particle percolation occurs at specific particle loadings that are dictated by packing arguments. The boundaries for closest packing of monodisperse spheres are illustrated in Figure 2.10.

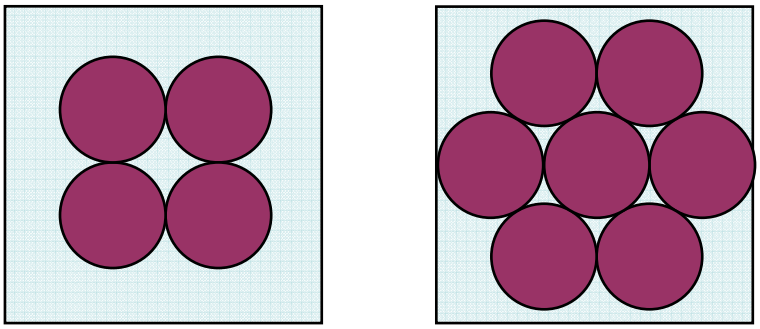

Figure 2.10: Closest packing of spheres. Left: simple cubic packing. Right : hexagonal closest packing.

The packing threshold for simple cubic arrangement of spheres is 52 vol.% (shown on left of Figure 2.10) whereas hexagonal closest packing is more efficient at 74 vol.% (shown on right of Figure 2.10). Random packing arrangements have been studied and fall between the boundaries of simple cubic and hexagonal closest packing [46].

Since some of the MMMs studied in this work are within or near the range of expected particle percolation, the effects of particle percolation on film formation are examined in Figure 2.11.

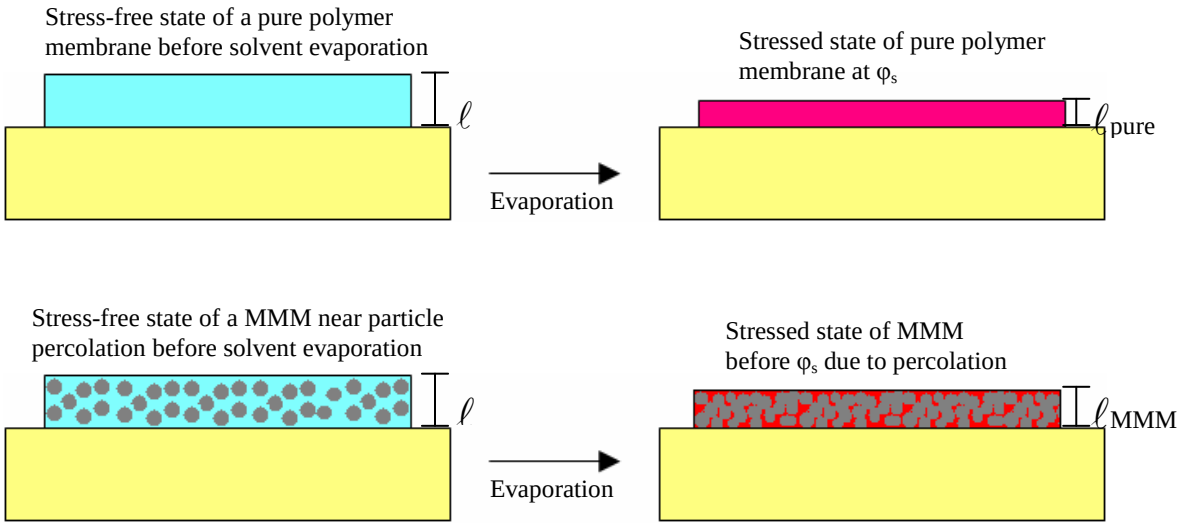

Figure 2.11: Pure polymer membrane vs. MMM. Initially both membranes are stress-free and have thickness = ℓ.

Figure 2.11 shows that homogenous shrinkage of the polymer towards the substrate can stop before φ_s in the event of particle percolation—this does not mean that polymer shrinkage stops. A MMM sample that reaches the percolation threshold effectively traps packets of polymer between particles. These packets will continue to undergo local polymer matrix contractions away from the immobile particles and will eventually reach φ_s and accumulate stress. Basically, percolation locks in an inflated film thickness which leads to even greater strain (and therefore stress) if the polymer matrix morphology is to remain homogenous throughout the volume of the film. This higher stress state is undesirable, and the sample has a tendency to form voids between percolated particle clusters and at particle-polymer interfaces. [47]

2.6 References

[1] Painter, P.C. and C. M.M., *Fundamentals of polymer science*. 2nd ed. 1997, Boca Raton, FL: CRC Press LLC.

[2] Rubinstein, M. and R.H. Colby, *Polymer physics*. 2003: Oxford University Press.

[3] Smith, J.M., H.C. Van Ness, and M.M. Abbott, *Chemical engineering thermodynamics*. 6th ed. 2001: McGraw-Hill.

[4] Croll, S.G., *Effect of titania pigment on the residual strain, glass-transition and mechanical-properties of a pmma coating.* Polymer, 1979. **20**(11): p. 1423-1430.

[5] Koros, W.J. and G.K. Fleming, *Membrane-based gas separation.* Journal of Membrane Science, 1993. **83**(1): p. 1-80.

[6] Kesting, R.E. and A.K. Fritzsche, *Polymeric gas separation membranes*. 1993: John Wiley & Sons, Inc.

[7] Vieth, W.R. and K.J. Sladek, *A model for diffusion in a glassy polymer*. Journal of Colloid Science, 1965. **20**(9): p. 1014-&.

[8] Paul, D.R. and W.J. Koros, *Effect of partially immobilizing sorption on permeability and diffusion time lag.* Journal of Polymer Science Part B-Polymer Physics, 1976. **14**(4): p. 675-685.

[9] Vieth, W.R., J.M. Howell, and J.H. Hsieh, *Dual sorption theory*. Journal of Membrane Science, 1976. **1**(2): p. 177-220.

[10] Koros, W.J., D.R. Paul, and A.A. Rocha, *Carbon-dioxide sorption and transport in polycarbonate.* Journal of Polymer Science Part B-Polymer Physics, 1976. **14**(4): p. 687-702.

[11] Tshudy, J.A. and Frankenb.Cv, *Model incorporating reversible immobilization for sorption and diffusion in glassy polymers.* Journal of Polymer Science Part B-Polymer Physics, 1973. **11**(10): p. 2027-2037.

[12] Neogi, P., ed. *Diffusion in polymers*. 1996, Marcel Dekker, Inc.

[13] Freeman, B.D., *Basis of permeability/selectivity tradeoff relations in polymeric gas separation membranes.* Macromolecules, 1999. **32**(2): p. 375-380.

[14] Barrer, R.M., *Diffusivities in glassy-polymers for the dual mode sorption model.* Journal of Membrane Science, 1984. **18**(MAR): p. 25-35.

[15] Graham, T., Philos. Mag., 1866. **32**.

[16] Wind, J.D., C. Staudt-Bickel, D.R. Paul, and W.J. Koros, *Solid-state covalent cross-linking of polyimide membranes for carbon dioxide plasticization reduction.* Macromolecules, 2003. **36**(6): p. 1882-1888.

[17] Breck, D.W., *Zeolite molecular sieves*. 1973, New York: Wiley.

[18] Karger, J., *Diffusion in zeolites and other microporous solids*. 2007, Wiley.

[19] Yang, R.T., *Gas separation by adsorption processes*. 1997: Imperial College Press.

[20] Shelekhin, A.B., A.G. Dixon, and Y.H. Ma, *Theory of gas-diffusion and permeation in inorganic molecular-sieve membranes.* Aiche Journal, 1995. **41**(1): p. 58-67.

[21] Karger, J. *Measurement of diffusion in zeolites - a never ending challenge?* 2003.

[22] Ruthven, D.M., *The window effect in zeolitic diffusion.* Microporous and Mesoporous Materials, 2006. **96**(1-3): p. 262-269.

[23] Yucel, H. and D.M. Ruthven, *Diffusion in 4a-zeolite - study of the effect of crystal size.* Journal of the Chemical Society-Faraday Transactions I, 1980. **76**: p. 60-70.

[24] Trzpit, M., M. Soulard, J. Patarin, N. Desbiens, F. Cailliez, A. Boutin, I. Demachy, and A.H. Fuchs, *The effect of local defects on water adsorption in silicalite-1 zeolite: A joint experimental and molecular simulation study.* Langmuir, 2007. **23**(20): p. 10131-10139.

[25] Caro, J. and M. Noack, *Zeolite membranes - recent developments and progress.* Microporous and Mesoporous Materials, 2008. **115**(3): p. 215-233.

[26] Caro, J., M. Noack, P. Kolsch, and R. Schafer, *Zeolite membranes - state of their development and perspective.* Microporous and Mesoporous Materials, 2000. **38**(1): p. 3-24.

[27] Moore, T.T., *Effects of materials, processing, and operating conditions on the morphology and gas transport properties of mixed matrix membranes*. 2004, The University of Texas at Austin, Ph.D. Thesis.

[28] Moore, T.T. and W.J. Koros, *Gas sorption in polymers, molecular sieves, and mixed matrix membranes.* Journal of Applied Polymer Science, 2007. **104**(6): p. 4053-4059.

[29] Moore, T.T. and W.J. Koros, *Non-ideal effects in organic-inorganic materials for gas separation membranes.* Journal of Molecular Structure, 2005. **739**(1-3): p. 87-98.

[30] Mahajan, R., *Formation, characterization, and modeling of mixed matrix membrane materials*. 2000, The University of Texas at Austin, Ph.D. Thesis.

[31] Walker, P.L., ed. *Chemistry and physics of carbon*. Vol. 2. 1966, Marcel Dekker.

[32] Shu, S., *Engineering the performance of mixed matrix membranes for gas separations*. 2007, Georgia Institute of Technology, Ph.D. Thesis.

[33] Das, M., *Membranes for olefin/paraffin separations*. 2009, Georgia Institute of Technology, Ph.D. Thesis.

[34] Maxwell, J.C., *A treatise on electricity and magnetism*. 1873: Oxford University Press.

[35] Petropoulos, J.H., *A comparative-study of approaches applied to the permeability of binary composite polymeric materials.* Journal of Polymer Science Part B-Polymer Physics, 1985. **23**(7): p. 1309-1324.

[36] Erdem-Senatalar, A., M. Tatlier, and S.B. Tantekin-Ersolmaz. *Questioning the validity of present models for estimating the performances of zeolite-polymer mixed matrix membranes*. 2003: Taylor & Francis Ltd.

[37] Pal, R., *Permeation models for mixed matrix membranes.* Journal of Colloid and Interface Science, 2008. **317**(1): p. 191-198.

[38] Liu, Q. and E.L. Cussler, *Barrier membranes made with lithographically printed fakes.* Journal of Membrane Science, 2006. **285**(1-2): p. 56-67.

[39] Higuchi, W.I. and T. Higuchi, *Theoretical analysis of diffusional movement through heterogeneous barriers.* Journal of the American Pharmaceutical Association, 1960. **49**(9): p. 598-606.

[40] Paul, D.R. and D.R. Kemp, *Diffusion time lag in polymer membranes containing adsorptive fillers.* Journal of Polymer Science Part C-Polymer Symposium, 1973(41): p. 79-93.

[41] Kasargod, S.S. and T.A. Barbari, *Permeation breakthrough models for associating and solvating penetrants in a membrane.* Industrial & Engineering Chemistry Research, 1997. **36**(2): p. 483-492.

[42] Francis, L.F., A.V. Mccormick, D.M. Vaessen, and J.A. Payne, *Development and measurement of stress in polymer coatings.* Journal of Materials Science, 2002. **37**(22): p. 4717-4731.

[43] Payne, J.A., *Stress evolution in solidifying coatings*. 1998, The University of Minnesota-Twin Cities, Ph.D. Thesis.

[44] Nielsen, L.E. and T.B. Lewis, *Temperature dependence of relative modulus in filled polymer systems.* Journal of Polymer Science Part a-2-Polymer Physics, 1969. **7**(10PA): p. 1705-&.

[45] Ruvo, A.D. and E. Alfthan, *Shifts in glass-transition temperatures of synthetic-polymers filled with microcrystalline cellulose.* Polymer, 1978. **19**(8): p. 872-874.

[46] Scott, G.D., *Packing of equal spheres.* Nature, 1960. **188**(4754): p. 908-909.

[47] Fishman, R.S., D.A. Kurtze, and G.P. Bierwagen, *Pigment inhomogeneity and void formation in organic coatings.* Progress in Organic Coatings, 1993. **21**(4): p. 387-403.

CHAPTER 3

MATERIALS AND METHODS

3.1 Introduction

The membranes studied in this work are comprised of polymers and molecular sieve filler particles. Creation of these membranes relied on the use of organic solvents, membrane casting substrates, laboratory equipment, and tailored experimental methods. Some of the raw materials as well as the membranes were characterized with a variety of gases and in-house built and commercially available equipment. In this chapter, the materials, equipment, and experimental methods used to create and test membranes are discussed.

3.2 Polymer

Poly(vinyl acetate) (PVAc) was the only polymer used for the membranes discussed in the forthcoming chapters. Most of these membranes used a single batch of PVAc from Aldrich (Milwaukee, WI): batch no. 08310AD, nominal molecular weight 500 kDa. Some PVAc from the same source with the same nominal molecular weight was also used: batch no. 1721220. A schematic of PVAc's structure is provided below.

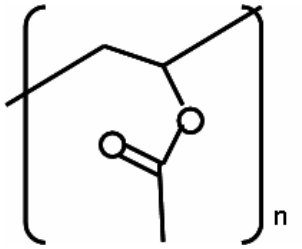

Figure 3.1: Repeat unit of poly(vinyl acetate).

One batch of PVAc was used (primarily) to establish a consistent baseline for comparison. Select gas transport properties of PVAc are provided in Table 3.1. These values are averaged over many samples tested in various permeation systems from pure gas permeation experiments performed in this work. All gases were tested at 35 °C with an upstream pressure of 65 psia (except carbon dioxide which was measured well below its plasticization pressure of 10 psia at 1.3 – 1.4 psia).

Table 3.1: Pure gas permeabilities and permselectivities of PVAc ± one standard deviation (all permeabilities in Barrers [=] 1 x 10^{-10} $cc_{STP} \cdot cm \cdot cm^{-2} \cdot s^{-1} \cdot cmHg^{-1}$).

P_{He}	P_{CO2}	P_{O2}	$\alpha_{He/CH4}$	$\alpha_{CO2/CH4}$	$\alpha_{CO2/N2}$	$\alpha_{O2/N2}$	$\alpha_{N2/CH4}$
14.8 ± 0.9	2.50 ± 0.25	0.501 ± 0.038	212 ± 2.0	34.9 ± 2.9	34.0 ± 3.4	6.58 ± 0.12	1.09 ± 0.043

Note that gas permeation measurements of low flux samples, such as those in this work, are quite lengthy (up to a month for 1 datum). Typically only 2 – 3 replicate measurements were made; thus, reported standard deviations are only rough estimates of errors. PVAc is an inexpensive, well-studied polymer that has been shown to adhere well to particles in MMMs [1-3]. Furthermore, PVAc has a low T_g (43.5 °C as measured in this work) which delays the onset of stress accumulation during solution processing until most of the solvent has evaporated. The strong adhesive properties and low T_g of PVAc make it an ideal polymer for basic MMM studies.

3.3 Molecular Sieves

Many molecular sieves were used in this work in order to probe the effects of molecular sieve pore size on the observed transport properties of MMMs. Zeolite 4A and a metal organic framework (MOF) of copper and terephthalic acid (CuTPA) were used in

the majority of the MMMs discussed in the forthcoming chapters, and their structures are provided in Figure 3.2.

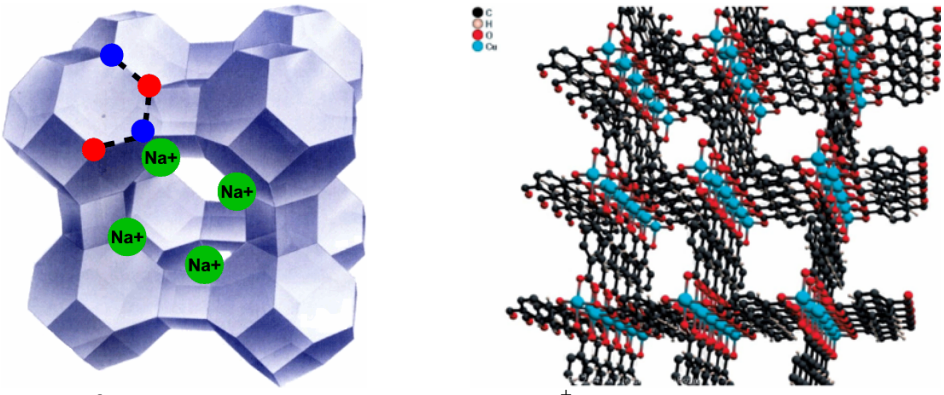

Figure 3.2: Left—zeolite 4A unit cell showing Na^+ ions in green at a pore window and silicon and aluminum atoms in red and blue [4]. Right—CuTPA repeat structure [5].

Figure 3.3 on the following page summarizes all molecular sieves used and provides their minimum and maximum pore access dimensions as well as providing some clarifying notes about their structures and sources.

Name	Min. Dim.	Max. Dim.	Notes and Source(s)
Zeolite 3A	3.3 Å	3.3 Å	Zeolite 3A is a synthetic zeolite with an LTA structure. It has the smallest pore opening of common type A zeolites due to the size and position of the K^+ ions that reside in the framework to maintain charge neutrality in the crystals. Zeolite 3A was acquired from ASGE (South Plainfield, NJ): lot # 947899110128, particle size ~ 1 – 5 µm. [6]
Zeolite 4A	3.9 Å	3.9 Å	Zeolite 4A is a synthetic zeolite with an LTA structure. Na^+ ions reside in the framework to maintain charge neutrality in the crystals. Type A zeolites are typically synthesized in the NaA form and later ion exchanged to the desired product. Zeolite 4A was acquired from ASGE (South Plainfield, NJ): lot # 942798110052, particles ~ 1 – 5 µm. In-house 4A synthesized by Tae-Hyun Bae were also used (particle sizes 0.1 – 2.0 µm). [6]
Zeolite 5A	4.2 Å	4.2 Å	Zeolite 5A is a synthetic zeolite with an LTA structure. Ca^{2+} ions reside in the framework to maintain charge neutrality in the crystals. Divalent Ca^{2+} ions maintain charge neutrality in the crystals with ½ as many ions compared to K^+ and Na^+; thus has a larger pore window. Zeolite 5A was acquired from ASGE (South Plainfield, NJ): lot # 943098110103, particles ~ 1 – 5 µm. [6]
CVX7	3.6 Å	5.1 Å	CVX7 is an alternative synthesis of the silica-alumina phosphate zeolite (SAPO17) by Chevron that results in unity aspect ratio particles rather than rod-shaped particles. It has an ERI-type structure. [7, 8]
CuTPA	5.2 Å	5.2 Å	CuTPA is a MOF of copper and terephthalic acid. The synthesis and properties of CuTPA will be discussed more in this chapter and others. Synthesis and material property details can be found elsewhere [5, 9, 10].
Zeolite NaY	7.4 Å	7.4 Å	Zeolite NaY is a synthetic zeolite with a faujasite structure. Na^+ ions maintain charge neutrality in the crystals. The faujasite structure has 12-membered ring pores that give NaY its large pore openings. Zeolite NaY was gifted by PQ Corp. (Valley Forge, PA): lot # 401F-003-04, particles < 1.0 µm. [6, 7, 11]

Figure 3.3: Summary of molecular sieves used in this work.

Two other molecular sieves were used that are not described in Figure 3.3. In efforts to improve the selectivities of zeolite 4A MMMs, 2 new tailored molecular sieves were created. Zeolite 4A synthesized by Tae-Hyun Bae was partially ion exchanged with

potassium ions to create batches of 6.76 % and 13.1 % K^+/Na^+ balance type A zeolites. The ion exchange procedure is described in Section 3.8. These materials and MMMs made with these materials will be discussed in more detail in Chapter 4.

3.4 Solvents and Gases

All solvents used were high purity, anhydrous solvents purchased from Sigma-Aldrich (Milwaukee, WI). Solvents were removed from bottles with a dry nitrogen purge through SureSeal® caps to maintain anhydrous conditions. Toluene was the most commonly used solvent as it was used for PVAc and PVAc MMM solution processing. N-N-dimethyl-formamide (DMF) was used in the synthesis of CuTPA. All gases used in permeation and sorption experiments (helium, carbon dioxide, oxygen, nitrogen, methane, and carbon dioxide-methane mixtures) were ultra-high purity grade from AirGas (Alpharetta, GA).

3.5 Dense Film Preparation

Many steps go into the preparation of dense polymeric and MMM films. These many steps can be best broken into 3 categories: 1) solution preparation, 2) dense film casting, and 3) dense film drying/annealing. Figure 3.4 summarizes the overall process.

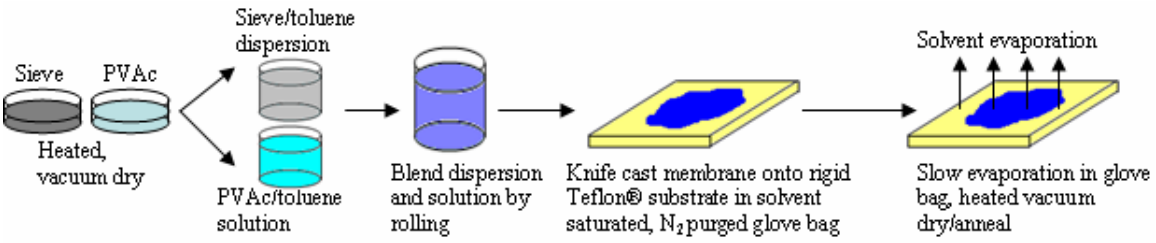

Figure 3.4: Summary of dense film preparation.

In the following subsections, individual parts of the overall procedure are described in greater detail.

3.5.1 Solution Preparation

Solutions for casting pure polymer membranes and MMMs follow the same general protocols used by previous researchers [3, 12]. Pure PVAc solutions were prepared:

1. PVAc beads were dried in clean glass vials at 100 °C under 29 in Hg vacuum in vacuum ovens for 18 – 24 hours and allowed to cool to room temperature under vacuum.
2. Toluene was added to the vials to create 25 wt.% PVAc-toluene mixtures. The vials were then placed on coaxial rollers to gently dissolve the PVAc beads without entraining excessive amounts of air for several days.

MMM solution preparation required many more steps. The PVAc-toluene solutions described above were used in the following procedure:

1. Molecular sieve particles were dried in clean glassware at 180 – 230 °C under 29 in Hg vacuum in vacuum ovens for 24 – 48 hours. Zeolites were only dried at 180 °C as they were already calcined prior to use and only atmospheric moisture had to be driven off. CuTPA particles were dried at 230 °C in order to drive off the large DMF molecules. Samples were allowed to cool to room temperature under vacuum.
2. After breaking the vacuum with a dry nitrogen purge to maintain dry conditions, toluene was added to the dry particles: 10 g toluene/g dry particles for 15 wt% MMMs and 20 g toluene/g dry particles for 50 vol.% MMMs. Excess solvent was

used for higher particle loading MMMs due to the use of a more intense dispersion protocol which adds more heat to the toluene-particle dispersion thus causes greater evaporative losses of toluene.

3. For 15 wt.% MMMs, a 130 W ultrasonic horn operating at 80% maximum amplitude was used to break up particle agglomerates and evenly disperse the particles in toluene. 3, 60 s ultrasonic cycles were used to disperse the particles—in some cases more than 3 cycles were used if agglomerates were visible on the vial walls. The 3 ultrasonic cycles were interrupted with ~ 30 s periods of shaking to allow for some cooling between cycles. 50 vol.% MMMs required a more intense ultrasonic dispersion protocol because much larger volumes of solvent were required to make a manageable amount of casting solution. A 1000 W ultrasonic horn operating at 66% maximum amplitude was used to disperse the particles. 5, 60 s ultrasonic cycles were performed with 30 s cool downs. Due to the large amounts of heat generated with the 1000 W horn, magnetic stirring (with a Teflon® coated stir bar) of the dispersion was used to help transfer heat away from the horn. The glass vessel that contained the dispersions was also surrounded by an ice bath to further facilitate heat transfer.
4. Immediately following the final ultrasonic burst, a small amount of PVAc-toluene solution was added to the dispersions. This technique, known as priming, has been shown to stabilize particle dispersions [2, 12, 13]. Due to the high viscosity of the 25 wt.% PVAc-toluene solutions, it was difficult to control the amount of solution added, but typically 5 – 10 % of the ultimate amount of polymer solution added was used. For the 15 wt.% MMM solutions, the vials were immediately

capped and shaken vigorously by hand to quickly homogenize the solution. Following shaking, primed 15 wt.% MMM solutions were allowed to tumble roll to maintain a homogenous dispersion in the low viscosity primed solution. For the 50 vol.% MMM solutions, the stirring speed was increased to maximum to homogenize the solution.

5. Primed, 15 wt.% MMM solutions were removed from tumble rolling after 12 – 24 hours and the remaining amount of polymer required was added from the same 25 wt.% PVAc solution used to prime. After vigorous shaking, the solution was allowed to coaxially roll to maintain a homogenous dispersion in the now viscous casting solution. Primed, 50 vol.% MMM solutions required much more care. After 4 – 6 hours of maximum mixing with the stir bar, the remaining amount of polymer required was added to the still mixing primed solution from the same PVAc solution used to prime. Since roughly the same ratio of solvent to dried particles was used to disperse particles for high loading dopes as was used for low loading dopes (and since high loading MMMs require much less polymer overall), high loading solutions had very low viscosity compared to low loading solutions at this stage. High loading solutions required substantial solvent evaporation before casting to increase the viscosity in order to achieve desired wetting on the casting substrate.
6. For 50 vol.% MMM solutions, the low viscosity solution (after bulk polymer addition) was transferred to a pre-weighed and zeroed clean glass one-neck flask. The mass of the solution was recorded (note that the stir bar within was pre-massed as well). The viscosity was then increased slowly (over 1 – 2 days) with a

slow dry N_2 purge through needles in the rubber plugged one-neck flask. Homogeneity was maintained with the stir bar during evaporation. When the desired viscosity was achieved (monitored indirectly by periodically checking the mass of the solution), the one-neck flask was allowed to coaxially roll at an angle to reincorporate any clumps on the walls of the flask for ~ 45 min. Finally, the solutions was poured into small, clean, glass vials and sealed. Note that this procedure is the result of a lengthy optimization study that will be described in greater quantitative detail in Chapter 6.

The samples were stored and mixed on a coaxial roller in order to prevent particle settling and the entrainment of air before film casting. Samples remained in storage for at least a few days before casting but often for weeks.

3.5.2 Dense Film Casting

Pure PVAc films were made directly from the 25 wt.% PVAc-toluene solutions described in Section 3.5.1. Films were made with casting knives by Paul N. Gardner & Co. (Pompano Beach, FL) with 8, 10, or 12 mil clearance (10 mil was used most):

1. The PVAc solution in a sealed glass vial, a low profile table with adjustable leg heights, a clean solid Teflon® plate, 2 Petri dishes, 20 – 30 mL toluene in a sealed glass vial, a flat bubble level, and the casting knife are put in a small AtmosBag (glove bag) from Aldrich (Milwaukee, WI).
2. The Teflon® plate is then centered on the table and the legs are adjusted until the bubble level indicates a balanced surface so that a uniform film can be made. The bag is then sealed with binder clips.

3. The bag is filled with dry N_2 through a small hole in the side of the glove bag and deflated by forcing the N_2 back out through the hole by hand 3 times. Following the 3rd deflation, the bag is partially refilled with dry N_2 such that one's hands can be easily inserted into the gloves while ensuring there is enough N_2 inside that the bag does not touch the Teflon® plate. The purpose is to maintain a dry, controlled atmosphere so that atmospheric water does not interfere with film formation.
4. 20 – 30 mL of toluene is poured into one of the Petri dishes positioned next to the table, and the bag is left to rest for 30 – 60 min so that toluene can evaporate into the dry N_2 atmosphere. This step is used to reduce the rate of solvent evaporation (and hence reduce stress accumulation) for the film to be cast. This is more of a concern for MMM casting but also done for pure PVAc.
5. The casting knife is positioned atop the Teflon® plate and a small amount of the viscous PVAc solution (5 – 15 mL) is poured before the knife. The knife is then slowly and steadily drawn over the solution to form a film.

MMM dense films were made an identical manner with the exception of solution degassing prior to step 1. Since the casting solutions were shaken vigorously and stored for long periods of time where the molecular sieve particles could sorb substantial amounts of gas, it was believed that a brief period of vacuum degassing prior to MMM casting would reduce the potential for bubble formation in the films. The MMM solutions were placed in vacuum ovens with the vial caps off. Partial vacuum (< 19 in Hg to prevent toluene from boiling) was applied for 10 – 20 min to liberate entrained gases. In some cases many bubbles appeared, surfaced, and popped.

3.5.3 Film Drying and Annealing

After films were cast, it was necessary to remove all toluene prior to characterization. Pure polymer films and low particle loading MMM films followed identical procedures:

1. The just-cast film is left in the glove bag for 12 – 18 hours to allow for some solvent evaporation so the film would be partially solidified.
2. After opening the glove bag, the plate is removed and quickly placed in a vacuum oven. The oven is closed, vacuum is applied (~ 29 in Hg vacuum), and the temperature is set to 130 °C. Solvent is allowed to evaporate under these conditions for at least 24 h but often as long as 48 h, after which the temperature is allowed to cool to room temperature under vacuum.
3. After closing the vacuum valve, vacuum is broken by allowing air in through the vent valve, and the plate (with the film still adhered) is removed.
4. A clean razor is used to gently delaminate the entire perimeter of the film from the plate. The solvent-free film is then gently peeled from the plate by hand and is ready for permeation testing.

High loading MMMs required a different procedure after casting. The reasons will be described in Chapter 6—for now, the procedure will simply be described:

1. The just-cast film is left in the glove bag for 36 – 48 hours to allow for substantial solvent evaporation so the film would be largely solidified.
2. After opening the glove bag, the plate is removed. A clean razor was used to gently delaminate the entire perimeter of the film from the plate. The film (which

still contains solvent) was extremely gently peeled from the plate by hand to prevent stretching and placed on (but not yet adhered to) a clean Teflon plate.

3. The plate and film were quickly placed in a vacuum oven and ~ 29 in Hg vacuum was applied for ~ 12 h.
4. The oven was then slowly and constantly ramped (over 24 h) from room temperature to 200 °C and kept at 200 °C for 24 – 48 hours. The oven was then slowly and constantly cooled (over 24 h) to room temperature under vacuum.
5. After closing the vacuum valve, vacuum is broken by allowing air in through the vent valve, and the plate (with the film now adhered) is removed.
6. A clean razor is used to gently delaminate the entire perimeter of the film from the plate. The solvent-free film is then gently peeled from the plate by hand and is ready for permeation testing.

3.6 Dense Film Permeation Testing

Nearly all data reported in this thesis comes from dense film permeation tests. The Koros Research Group has a long history of dense film permeation masking and testing. Permeation masking refers to the means by which a dense film sample is affixed to the permeation system—i.e. a circular sample of the dense film is "sandwiched" between 2 pieces aluminum-backed duct tape and stuck to the permeation cell with a 3rd piece of aluminum-backed duct tape. Excellent, detailed references describing the permeation systems and permeation masking procedures can be found elsewhere [2, 3, 12, 14-18]. For the sake of brevity, details of permeation masking and permeation systems that are common with previously described protocols will not be discussed here. Instead, this section will focus on some general aspects of the permeation system and

permeation testing as well as procedures that are substantially different from previously reported procedures.

3.6.1 Permeation System and Permeability Measurement Basics

Permeabilities reported in this work were measured in isothermal, isochoric permeation systems. Figure 3.5 illustrates the basics of the permeation system.

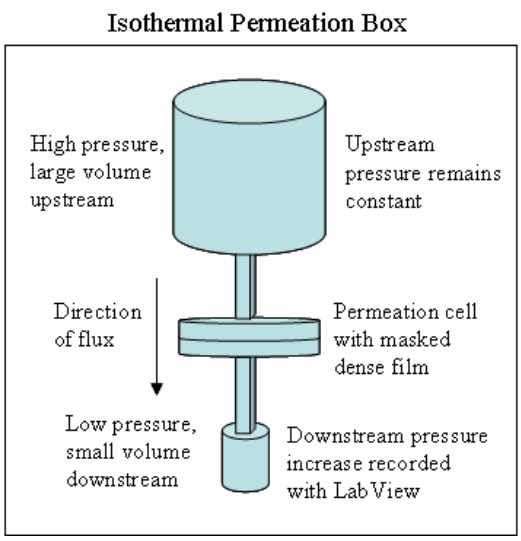

Figure 3.5: Basic cartoon of an isochoric, isothermal permeation system.

When a permeation cell is loaded into a permeation system, vacuum is applied to the entire system for some time to degas the dense film and the system itself. Then, through a series of valves, gases are introduced to the upstream and allowed to reach thermal equilibrium before exposure to the upstream surface of the masked membrane in the permeation cell. The rest of the system remains under vacuum during this time. Immediately before gas is exposed to the upstream face of the membrane, valves are turned in such a way that the upstream and downstream volumes are isolated from each other and from the vacuum source. The instant that gas is exposed to the membrane,

LabView® begins to record the downstream pressure as a function of time as illustrated in Figure 3.6.

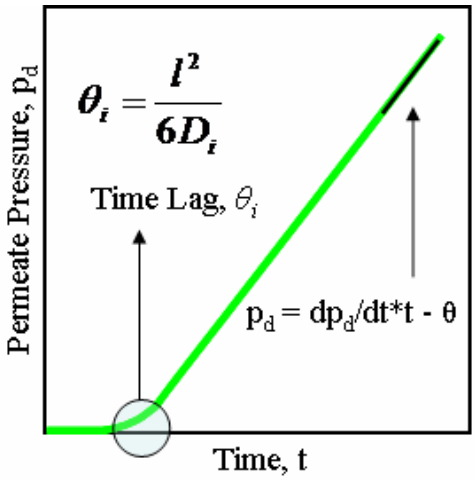

Figure 3.6: Cartoon of downstream pressure rise in a permeation experiment.

In Figure 3.6, the permeate pressure p_d initially remains constant while gas sorbs into the membrane and begins to transport across. This initial time lag period is followed by steady-state permeation. A linear fit of the steady-state pressure rise is made substantially far removed from the time lag portion of the permeation plot. The time lag, θ, was described in Chapter 2, can be related to apparent diffusivity by Equation 2.12, and is equal to the time intercept of the steady-state linear fit for zero initial permeate pressure. In this work, steady-state was assumed as 9 – 14 θ in order to be comfortably beyond the mathematically predicted steady-state of 2.5 θ [19].

Equation 3.1 describes how the steady-state pressure rise with respect to time was converted into permeability in Barrers.

$$Permeability(Barrer) = \left[\frac{dp}{dt}\left(\frac{torr}{s}\right)\right] \times \left[\frac{V_D(cc)}{62360\frac{torr \cdot cc}{mol \cdot K} \times T(K)}\right] \times \left\{\frac{22413 cc_{STP}}{mol}\right\} \times \left[\frac{l(cm) \times \left(\frac{14.696\, psia}{76 cmHg}\right)}{A(cm^2) \times p_F(psia)}\right] \times \frac{1 \times 10^{10}\, Barrer}{\frac{cc_{STP} \cdot cm}{cm^2 \cdot s \cdot cmHg}} \quad \text{(Equation 3.1)}$$

The term in curly brackets in Equation 3.1 converts to standard conditions. All other values in Equation 3.1 are known inputs or to convert to Barrer units. The experimenter must input the downstream pressure rise in *torr/s*, the downstream volume in *cc* (which is determined from calibration with a known volume attached to the downstream volume), the temperature in Kelvin (temperature is constant at 308.15 K for all permeation experiments in this work), the thickness of the dense film, *l*, in *cm* which is measured with high precision micrometers (in this work the average of 5 thickness measurements on the masked area was used—thicknesses varied from 25 to 90 μm), the area of the masked film (known due to the use of standard die cut circles with known areas to make the permeation masks—areas varied from 1 – 3 cm^2), and the feed pressure in *psia* which remains constant throughout the experiment due to the relatively large upstream volume and the relatively low flux through the dense film. In this work a feed pressure of 65 ± 0.3 psia was used for all gases except carbon dioxide where a feed pressure of 1.35 ± 0.5 psia was used to stay well below the plasticization pressure (unless otherwise noted).

Mixed gas permeation experiments are conducted in a similar manner. The main difference is the need for a retentate flow to keep the composition of the upstream constant. In a mixed gas permeation experiment, the valve configuration changes slightly

to allow the feed gas to flow through the upstream. This is done in such a way that the retentate flow is at least 100 X (but often much greater than 100 X) faster than the permeate flow rate so that the concentration of the feed does not change as the result of the enrichment of the slower gas due to the relatively high flux of the fast gas through the membrane. The retentate flow is checked periodically with a bubble flow meter. The need to analyze the composition of the permeate at steady-state is the other difference in mixed gas versus pure gas permeation tests. Once steady state flux is established, a portion of the permeate is fed to a calibrated gas chromatograph for compositional analysis. The permeability of an individual component can then be calculated by multiplying overall permeability (see Equation 3.1) by the ratio of permeate mole fraction to upstream mole fraction of said component. In this work, mixtures of 10 % carbon dioxide and 90% methane were used on some samples. Upstream pressures fluctuate a bit (± 2 psia) in mixed gas experiments since feed pressures are controlled by gas regulators.

3.6.2 Alteration of Established Permeation Testing Methods

Dense film permeation tests on the laboratory scale are typically performed with the downstream volume under vacuum as it simplifies analysis and is a suitable technique for low flux samples. As with any vacuum system, accounting for atmospheric leaks is an important step in data analysis. Section 3.6.1 mentions that vacuum must be applied to the entire permeation system for some time to degas the sample and the system itself. Other researchers report initial vacuum degassing times that range from a few hours to 24 hours [3, 12, 20]. Such short initial vacuum degassing times were found to be insufficient to attain the minimum leak rate of the permeation system in this work. In

order to make permeation testing and analysis as unambiguous as possible, it is critical to operate the system near its minimum leak rate. Figure 3.7 shows the leak trend of a 75 µm thick, 3 cm^2 area impermeable aluminum sheet that was prepared with the common aluminum-backed duct tape "sandwich" masking technique.

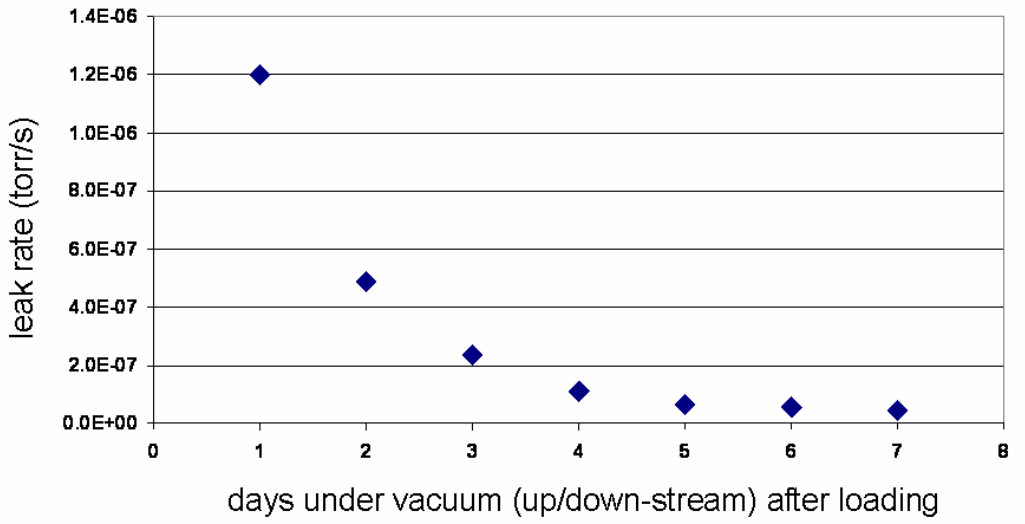

Figure 3.7: Leak trend of a freshly loaded aluminum-backed duct tape "sandwich"-style permeation mask.

Each of the points on Figure 3.7 represents leak rates that were measured for 1 – 2 hours. R^2 values of 0.99 or better were attained for each point. Clearly, 24 hours of high vacuum on the permeation system is insufficient to achieve a minimum leak rate. In fact, the leak rate measured after 5 days of vacuum was more than an order of magnitude lower than after 24 hours which is the longest initial vacuum exposure to permeation masks previously reported [3]. Note that the sample in this experiment was totally impermeable, i.e. the leak trend has nothing to do with sorbed gases in the sample. It is assumed that the adhesive polymer (probably a polyacrylate) that coats the aluminum-backed duct tape used for masking contains a substantial amount of sorbed gases—sorbed

gases that have long diffusive paths for desorption. The same leak trend experiment was done for almost every dense film sample reported in this thesis and comparable trends were observed.

There is nothing inherently wrong with initial vacuum exposure times that do not result in minimum leak rates although it is important to consider the potential leak rates with respect to the expected gas fluxes through a permeation sample. If the slowest gas to be tested gives a flux on the order of 1 x 10^{-3} torr/s (for example), there is little reason for concern if the leak trends are similar to Figure 3.7, and one may proceed with little regard for leak rates. However, if one expects the slowest gas flux to be on the order of 1 x 10^{-5} (as was common in this work and is not remarkably slow per se), then the consequences of improper leak accounting can be quite serious. Consider the data measured in this work for a 44 µm thick, 1.2 cm^2 area 15 wt.% ASGE 4A-PVAc MMM where leak rates were varied to illustrate their effect as shown in Figure 3.8.

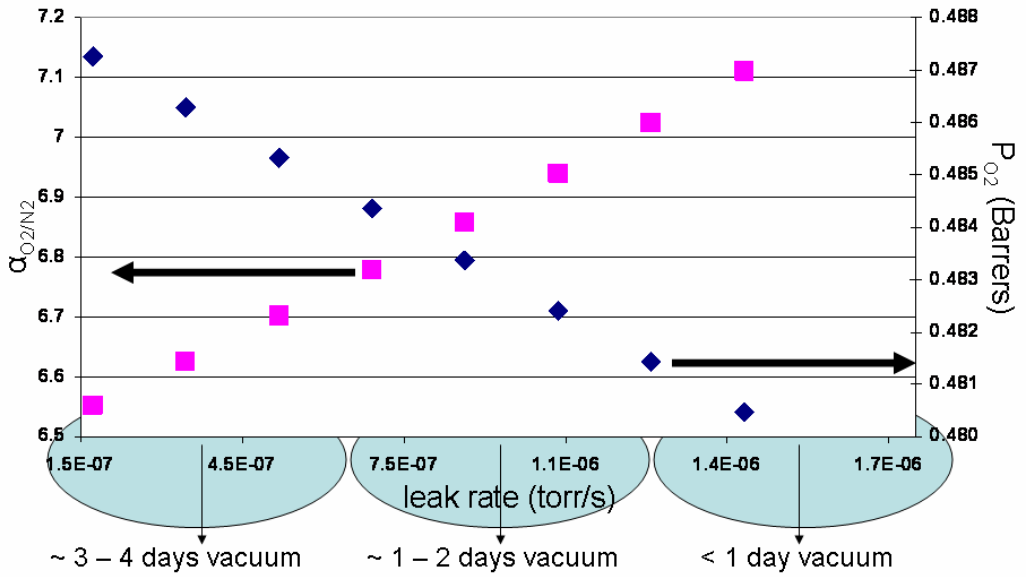

Figure 3.8: Impact of leak accounting on transport properties of a MMM.

Oxygen-nitrogen permselectivity appears on the left-hand y-axis while oxygen permeability appears on the right-hand y-axis. These values are plotted against the leak rate used to compute the values on the x-axis. It is clearly shown that using previously accepted experimental protocol can lead to inflated selectivity. Although oxygen permeability varies very little as a function of leak rate (all values within 2 % of each other), selectivity varies drastically (by ~ 10 %). Not only is this a substantial variation—it is the difference between concluding that the MMM has enhanced selectivity substantially or provides the same selectivity as pure PVAc. Data beyond 3 – 4 days of vacuum was deliberately excluded because the leak rate changes very little beyond 4 days of vacuum.

The order in which gases are tested as well as the vacuum exposure time between permeation tests must also be carefully considered. Consider the following example: a researcher loads a permeation cell, pulls vacuum overnight, performs a leak test, and immediately proceeds with an oxygen permeation test. The oxygen permeation test is completed within a few hours, and vacuum is applied to the entire system. If the researcher, for one reason or another, waits several days before the next permeation test (nitrogen for example) without conducting another leak test, the consequence would be an inflated oxygen-nitrogen permselectivity as illustrated in Figure 3.8. An analogous case would be a researcher who decides to avoid these issues by not even measuring leak rates. While it is true that such a method is really the most stringent since it would tend to under-report selectivities, it is only an acceptable method if one has ensured that the system is operating at minimum leak for all permeation tests—in other words, it is simply easier to be vigilant about accounting for leak rate. Out of consideration for such

possibilities, nearly every permeation test in this work was preceded by a leak test and the first gas tested was always preceded by at least 3 – 4 days of vacuum degassing. Furthermore, gases were always tested in this order, helium, oxygen, nitrogen, methane, and carbon dioxide which are fastest gas to slowest gas (except for carbon dioxide which was always measured last to avoid the possibility of sample conditioning by plasticization). Testing in this order ensured that the slower gases were always tested after longer vacuum exposures than the faster gases. The other benefit of testing in this order is illustrated in Figure 3.9.

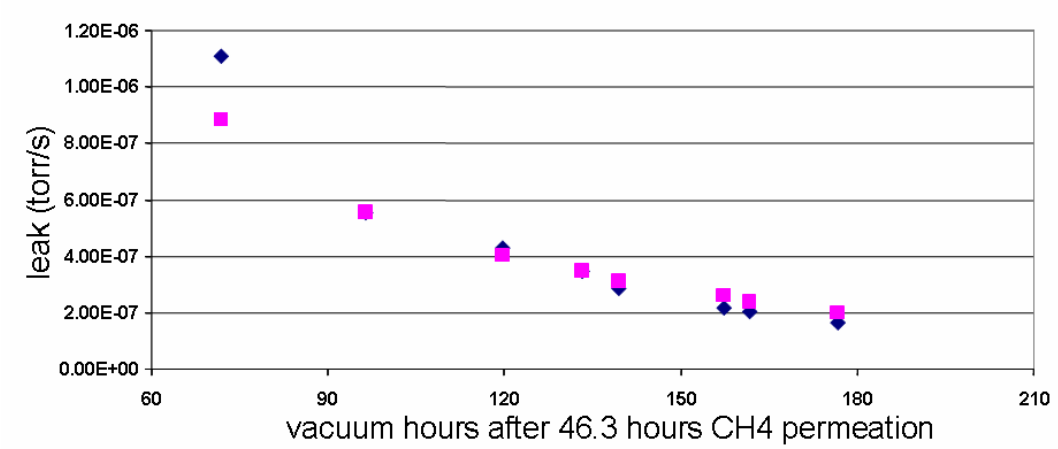

Figure 3.9: Leak trend of an aluminum-backed duct tape "sandwich" permeation mask after a long methane permeation experiment.

Due to time lags as long as 12 hours, some slow gases were exposed to membranes for long periods of time (up to a week or more) for a single permeation test. Figure 3.9 shows the leak trends of 2 different masks (blue and pink data markers) of the same membrane in 2 different permeation systems after long exposures to methane. Note that the first leak rates measured (after ~ 3 days of vacuum exposure) are on the order of the 24 hour vacuum exposure leak rate from Figure 3.7. This apparent inconsistency is

easily explained. The adhesive polymer in a fresh permeation mask is at absorption equilibrium with the atmosphere, i.e. mostly nitrogen and oxygen at low pressure. Gas absorption in polymers increases with pressure as shown in Chapter 2 and also tends to increase with the critical temperature of the sorbing gas [21, 22]. Since methane permeation tests were performed at 65 psia, it is no surprise that longer vacuum exposures are needed to reduce the leak rate to the minimum value.

The observations from Figure 3.9 added longer vacuum exposure times between gases on top of the longer initial vacuum exposures. These previously unreported findings on permeation testing procedures added substantial amounts of characterization time to each sample but also eliminate much uncertainty from the reported properties.

3.7 Pressure Decay Sorption

Pressure decay sorption was primarily used to determine the adsorption properties of molecular sieves but was also used on a few dense film samples. In this experiment, two volumes with pressure transducers are separated from each other by a valve. These two volumes are also separated from the feed line by a valve. Figure 3.10 illustrates the apparatus which is submerged in a water or oil bath with heated circulation up to the valve handles to maintain isothermal conditions (35 °C in this work).

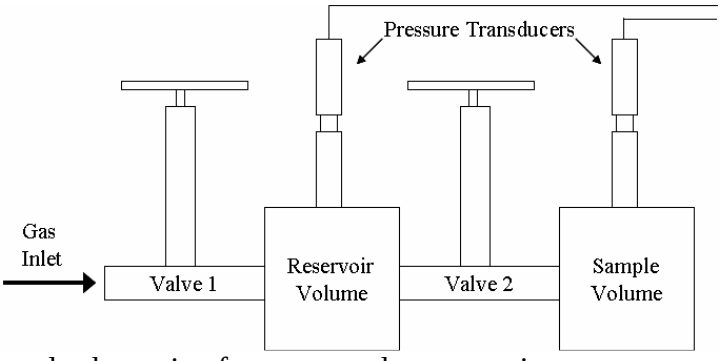

Figure 3.10: General schematic of a pressure decay sorption apparatus.

The pressure decay sorption experiment is quite simple. Samples are loaded into the sample volume and sealed with a nut (see Moore's dissertation for details regarding powder sample preparation [12]). The apparatus is then lowered into the liquid bath and vacuum is applied to the entire system (overnight vacuum is typically enough since the system only contains the sample and stainless steel parts). Following vacuum degassing, valve 2 is closed, gas is introduced to the reservoir volume, and valve 1 is closed. While data from the pressure transducers is collected via LabView®, the system is allowed to come to thermal equilibrium (in this work for at least 1 hour). Valve 2 is then quickly opened and closed to allow gas from the reservoir volume to expand into the sample volume, and data collection continues. After this expansion, a step change in reservoir pressure is seen due to the expansion. The sample pressure initially shows a step increase but is followed by a decay in pressure due to the sample absorbing gas (hence the term, "pressure decay sorption"). Data is monitored until the sample pressure signal decays to a constant value. Molecular sieve samples usually achieve equilibrium almost instantly, but data collection usually continues for at least an hour after expansion to ensure a thermally equilibrated post-expansion baseline pressure reading.

This concludes the acquisition of the 1st data point. If subsequent data points are desired in order to create a sorption isotherm (as described in Chapter 2), the same general procedure is used except vacuum is not necessarily required. As long as the reservoir pressure is higher than the sample pressure before an expansion, gas will go into the sample and be sorbed. Conversely, if pressure in the reservoir is lower than in the sample volume, a desorption experiment can be performed. Regardless of whether a sorption or desorption experiment has been done, the data are analyzed by manipulation

of the ideal gas law corrected for non-idealities with compressibility factors. Since the pressures and volumes of both the reservoir and sample are known, the discrepancy between the amount of gas lost from the reservoir and the amount gained by the sample volume (according to the pressure transducers) can be attributed to the sample sorbing or desorbing gas.

Since data are collected for the duration of the experiment, it is also possible to analyze the kinetics of gas absorption. Unfortunately, the molecular sieve particles used in this work are small and reach equilibrium within fractions of a second in most cases making kinetic analysis difficult. Furthermore, heat effects (the cooling of the gas upon expansion and the heating/cooling of the sample during sorption/desorption) obscure the nature of the kinetics. However, in cases where there is substantial transport resistance to sorb or desorb, kinetic analysis is used in a relative manner to compare different samples.

3.8 Potassium Ion Exchanging Zeolite 4A

Zeolite 4A that was synthesized in-house by Tae-Hyun Bae was used to make 2 batches of partially K^+ exchanged zeolite A. The batches were, nominally, 6.76 % K^+/balance Na^+ and 13.1 % K^+/balance Na^+ on a molar equivalent (A_z) basis described in Equation 3.2.

$$A_z \equiv \frac{\textit{no. equivalent exchange ions present}}{\textit{total equivalents present}} \qquad \text{(Equation 3.2)}$$

One molar equivalent of charge balancing ions is needed for type A zeolites with a Si:Al ratio of 1 [23, 24]. In other words, for a sample of perfect zeolite 4A (or NaA) with 0.1 mol of silicon and aluminum, there will be 0.1 mol of Na^+ in the framework balancing the charge (note that there is a 1+ valency discrepancy between Si^{2+} and Al^{3+} that gives rise to the charge imbalance in type A zeolites) [6]. Zeolite 4A is often synthesized with a

silicon to aluminum ratio slightly greater than 1 making it difficult to precisely ion exchange on an equivalent basis [6].

Roughly following the procedure of Yeh and Yang [25], the partially exchanged zeolites were made:

1. 0.42 – 0.44 g zeolite 4A were added to clean 250 mL Teflon® flasks with screw-on caps. This mass range of this batch of zeolite 4A contains approximately 0.0019 molar equivalents based on moles of sodium present. Sodium was used as the exchange basis because elemental analysis showed excess silicon in the framework which means less than 1 molar equivalent of ions is needed per mole of silicon or aluminum to balance the charge. The results of elemental analysis are provided in Chapter 4.
2. K^+ ions were then added to the flasks from a 0.6 mM KCl solution in deionized water. This resulted in approximately 70 mL of solution for the 6.76 % K^+/balance Na^+ and 98 mL for the 13.1 % K^+/balance Na^+.
3. The flasks were capped tightly and placed in a heated water shaker bath at 35 °C with a 150 rpm mixing speed for 4 days. According to the procedure of Yeh and Yang [23, 25] who used larger crystals, shorter exchange time, and lower temperature, this was ample time and conditions to complete the exchange.
4. Following the exchange, the zeolite was isolated by centrifugation and 120 mL deionized water was added to wash away any unincorporated ions. The zeolite-water mixtures were allowed to mix in a sonication bath overnight to complete the washing. This procedure of centrifugation and washing was repeated 5 times.

3.9 Other Experimental Techniques

A variety of complimentary experiments and techniques were used to characterize materials. Since the bulk of the data and analysis are based on gas permeation experiments, these other experiments and techniques (which were often kindly assisted by my colleagues) will only be discussed briefly.

Scanning electron microscopy (SEM) was used to image MMM cross-sections. Although most MMMs in this work were free of void defects, SEM is a great way of finding void defects and checking for particle dispersion homogeneity. X-ray diffraction (XRD) was used to confirm crystallinity of some molecular sieve samples. Differential scanning calorimetry (DSC) was used to determine the T_g of PVAc and some MMMs. Thermal gravimetric analysis (TGA) was used to investigate the desolvation of the CuTPA MOF and to confirm the particle loadings of some MMMs. Cryogenic nitrogen (or argon) physisorption was used to determine the sorption capacities and BET surface areas of some molecular sieve particles.

3.10 References

[1] Zimmerman, C.M., A. Singh, and W.J. Koros, *Tailoring mixed matrix composite membranes for gas separations.* Journal of Membrane Science, 1997. **137**(1-2): p. 145-154.

[2] Mahajan, R., *Formation, characterization, and modeling of mixed matrix membrane materials*. 2000, The University of Texas at Austin, Ph.D. Thesis.

[3] Shu, S., *Engineering the performance of mixed matrix membranes for gas separations*. 2007, Georgia Institute of Technology, Ph.D. Thesis.

[4] Xms. *Xinyuan molecular sieve*. 2009; Available from: http://www.molecularsieve.org/Zeolite_Molecular_Sieve.htm.

[5] Carson, C.G., K. Hardcastle, J. Schwartz, X.T. Liu, C. Hoffmann, R.A. Gerhardt, and R. Tannenbaum, *Synthesis and structure characterization of copper terephthalate metal-organic frameworks.* European Journal of Inorganic Chemistry, 2009(16): p. 2338-2343.

[6] Breck, D.W., *Zeolite molecular sieves*. 1973, New York: Wiley.

[7] Izasc. *Database of zeolite structures*. 2009 [cited 2009; Available from: http://www.iza-structure.org/databases/.

[8] Ward, J.K., *Personal communication*. 2009: Atlanta, GA.

[9] Seki, K., S. Takamizawa, and W. Mori, *Characterization of microporous copper(ii) dicarboxylates (fumarate, terephthalate, and trans-1,4-cyclohexanedicarboxylate) by gas adsorption.* Chemistry Letters, 2001(2): p. 122-123.

[10] Adams, R.T., C.G. Carson, J.K. Ward, R. Tannebaum, and W.J. Koros, *Metal organic framework mixed matrix membranes for gas separations.* Microporous and Mesoporous Materials, 2009. **in press**.

[11] Song, W.G., G.H. Li, V.H. Grassian, and S.C. Larsen, *Development of improved materials for environmental applications: Nanocrystalline nay zeolites.* Environmental Science & Technology, 2005. **39**(5): p. 1214-1220.

[12] Moore, T.T., *Effects of materials, processing, and operating conditions on the morphology and gas transport properties of mixed matrix membranes*. 2004, The University of Texas at Austin, Ph.D. Thesis.

[13] Husain, S., *Mixed matrix dual layer hollow fiber membranes for natural gas separation*. 2006, Georgia Institute of Technology, Ph.D. Thesis.

[14] Williams, P.J., *Analysis of factors influencing the performance of cms for gas separations*. 2006, Georgia Institute of Technology, Ph.D. Thesis.

[15] Perry, J.D., *Formation and characterization of hybrid membranes utilizing high-performance polyimides and carbon molecular sieves*. 2007, Georgia Institute of Technology, Ph.D. Thesis.

[16] Hillock-Mckittrick, A.M.W., *Crosslinkable polyimide mixed matrix membranes for natural gas purification*. 2005, Georgia Institute of Technology, Ph.D. Thesis.

[17] Das, M., *Membranes for olefin/paraffin separations*. 2009, Georgia Institute of Technology, Ph.D. Thesis.

[18] Moore, T.T., S. Damle, P.J. Williams, and W.J. Koros, *Characterization of low permeability gas separation membranes and barrier materials; design and operation considerations.* Journal of Membrane Science, 2004. **245**(1-2): p. 227-231.

[19] Paul, D.R. and Dibenede.At, *Diffusion in amorphous polymers.* Journal of Polymer Science Part C-Polymer Symposium, 1965(10PC): p. 17-&.

[20] Zhang, Y.F., I.H. Musseman, J.P. Ferraris, and K.J. Balkus, *Gas permeability properties of matrimid (r) membranes containing the metal-organic framework cu-bpy-hfs.* Journal of Membrane Science, 2008. **313**(1-2): p. 170-181.

[21] Koros, W.J. and G.K. Fleming, *Membrane-based gas separation.* Journal of Membrane Science, 1993. **83**(1): p. 1-80.

[22] Kesting, R.E. and A.K. Fritzsche, *Polymeric gas separation membranes*. 1993: John Wiley & Sons, Inc.

[23] Yeh, Y.T., *Diffusion and adsorption of gases in molecular sieves*. 1989, SUNY at Buffalo, Ph.D. Thesis.

[24] Yang, R.T., *Gas separation by adsorption processes*. 1997: Imperial College Press.

[25] Yeh, Y.T. and R.T. Yang, *Diffusion in zeolites containing mixed cations.* Aiche Journal, 1989. **35**(10): p. 1659-1666.

CHAPTER 4

EFFECTS OF PROCESSING CONDITIONS ON MMM MATERIALS AND MMM TRANSPORT PROPERTIES

4.1 Introduction

The processing conditions of complex materials such as polymers and molecular sieves can have significant effects on the observed gas transport properties. For polymeric membrane materials, synthesis atmosphere [1], physical aging [2], annealing temperatures [3], asymmetric hollow fiber membrane quenching conditions [4], and solvent removal procedures [4, 5] are just a few examples of how processing conditions can impact gas transport (and other) properties. Molecular sieving materials can exhibit drastically different material properties depending on post-synthetic washing procedures [6], conditions of solvent and structure directing agent removal by extractions [7], and milling conditions [8] for example.

Development of the MMMs discussed in the forthcoming chapters required careful attention to processing conditions. Major changes in conventional MMM solution preparation were needed to make void-free high loading MMMs. Also, it was found that the complex nature of gas transport in polymers, molecular sieves, and MMMs thereof can easily lead to erroneous hypotheses due to ignoring the effects of processing on material properties. This chapter will discuss cases where processing conditions had, or could have, large impacts on observed transport properties. Section 4.2 will focus on the role of processing conditions for creation of void-free high loading MMMs. Section 4.3 explores the impact of zeolite 4A source on observed transport properties. Section 4.4

discusses the impact of post-synthetic conditions on CuTPA properties. Conclusions are provided in Section 4.5.

4.2 Creation of Void-Free High Molecular Sieve Loading MMMs

A substantial amount of time was spent optimizing high loading MMM casting so that void-free MMM samples could be made for permeation testing. Samples with even a small amount of void and/or pinhole defects are known to have transport properties that are dominated by these low resistance diffusional pathways [9, 10]. Ultimately two critical processing parameters were identified for creation of void-free 50 vol.% zeolite 4A MMMs: 1) initial solvent concentration of the casting solution; 2) post-casting annealing temperature. Section 4.2.1 will discuss the impacts of initial solvent concentration on observed transport properties, and Section 4.2.2 will do the same for membrane annealing temperature.

4.2.1 Effect of Initial Solvent Concentration

Chapter 2 discusses the role of solvent evaporation rate on stress accumulation in solution processed polymers and polymer-filler composites. For MMM processing, it is also known that the three-way interactions between solvent, polymer, and filler play an important role in material morphology and properties [11, 12]. Furthermore, it has been hypothesized [13] (and investigated to some extent [14]), that stress accumulation in solution processed polymer-filler composites increases with increased filler loading. However, to our knowledge there have been no reports of a relationship between initial solvent concentration and subsequent material properties for filled polymer composites. In fact, Croll clearly states that the amount of solvent initially present in a coating solution of polymer with filler particles has no impact on coating properties since the

onset of stress accumulation is independent of the amount of solvent initially present [15].

In this work, it was found that the initial solvent concentration for high loading MMM casting solutions had an enormous impact on observed transport properties whereas low loading MMMs were not impacted by initial solvent concentration. Figure 4.1 shows three SEMs of 50 vol.% commercial zeolite 4A-PVAc MMMs cast from solutions with varying solvent (toluene) concentrations. While the SEMs in Figure 4.1 only represent 3 samples (one from each casting solution of varying initial solvent concentration), there were actually many samples prepared at all initial solvent concentrations that support the observations made for these samples.

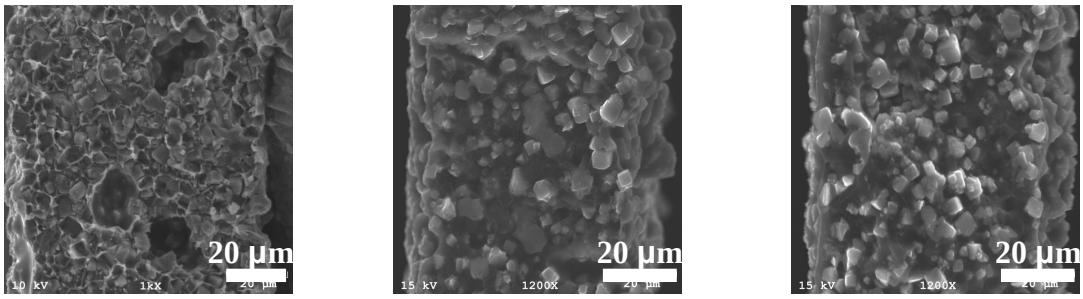

~ 75 wt.% toluene
P ~ 1000X; α < PVAc

~ 70 wt.% toluene
P ~ 100X; α < PVAc

~ 64 wt.% toluene
P ≤ PVAc; α ~ PVAc

Figure 4.1: High loading MMMs cast from solutions of varying solvent concentration.

Figure 4.1 shows the presence of large voids in the 50 vol.% 4A MMM cast from the solution with the highest initial solvent concentration. These voids easily explain the extremely high permeabilities measured. In fact, the transmembrane gas fluxes for samples processed from 75 wt.% toluene casting solutions were so high (approximately 1000 times that of pure PVAc) that it was difficult to accurately measure permeabilities

since the permeation systems were designed for much lower fluxes. This observation implies that the overall morphology of MMMs cast from this initial solvent concentration may be worse than the SEM suggests since such large increases in permeability are likely due to interconnected voids. These large voids can also lead to permselectivities substantially less than pure PVAc if the voids provide direct pathways through the membrane. A small decrease in casting solution toluene concentration (from 75 wt.% toluene to 70 wt.% toluene) yielded an SEM cross-section that appears to be free of voids; however, measured permeabilities were still ~ 100 times greater than and selectivities substantially less than pure PVAc suggesting that voids were still present. Reducing the initial solvent concentration just a bit more to ~ 64 wt.% not only produced cross-sectional images that were void-free, but also gave permeabilities that were approximately equal to pure PVAc. In fact, permeabilities of such samples were typically less than pure PVAc (as much as 60 % lower) with selectivities equivalent to pure PVAc. These undesirable transport properties in the void-free samples were the result of poor intrinsic transport properties of commercially available zeolite 4A as will be discussed shortly in Section 4.3.

The observations in this work are not totally without precedent. Chapter 2 cites the work of Fishman *et al* regarding void formation in filled polymer composites due to particle percolation [16]. The authors explain how local fluctuations in pigment (filler) density give rise to local percolation phenomena that can lead to void formation at filler loadings below the mathematical percolation threshold. In the case of 50 vol.% 4A MMMs studied in this work, it is reasonable to assume that “early” percolation could occur as described by Fishman *et al* due to the proximity to the mathematical percolation

threshold as described in Chapter 2. The MMMs in this work are prepared as coatings on a rigid substrate; thus, the film can only shrink towards the substrate and not in the plane of the film. This means that the starting in-plane particle spacing for solvent-rich casting solutions is greater than that of solvent-lean casting solutions of equivalent polymer to sieve loading. Since the final particle loadings on a polymer to sieve basis are equivalent regardless of initial solvent concentration, and the in-plane particle spacing cannot decrease once the film is applied to the rigid substrate unless pinhole defects develop in the just-cast film, final interparticle spacing between layers through the film is smaller for solvent-rich casting solutions. It is hypothesized that smaller interparticle spacing through the film increases the probability that percolation will occur; thus, voids are more likely to form in MMMs cast from solvent-rich casting solutions.

Chapter 2 also discusses how the rate of solvent evaporation can impact stress accumulation. While stress accumulation and solvent evaporation rate were not directly measured in this work, all MMMs were cast under roughly the same conditions with efforts to keep the solvent evaporation rate low as described in Chapter 3. Furthermore, PVAc has a low T_g (43.5 °C as measured by DSC) which should not accumulate stresses until nearly all solvent has been removed. While the initial solvent concentration effect can be greatly suppressed as the rate of solvent evaporation approaches zero, and if the films were not adhered to a rigid substrate where shrinkage is restricted in the plane of the cast films, these issues cannot be avoided in real situations so they must be "managed".

4.2.2 Effects of Annealing Temperature

Casting high loading MMMs from solutions of sufficiently low solvent concentration proved to be critical for formation of a void-free morphology, but the annealing conditions of these samples were also found to be important. Figure 4.2 shows SEMs of 2 different portions of a 50 vol.% zeolite 4A-PVAc MMM cast from a 64 wt.% toluene solution.

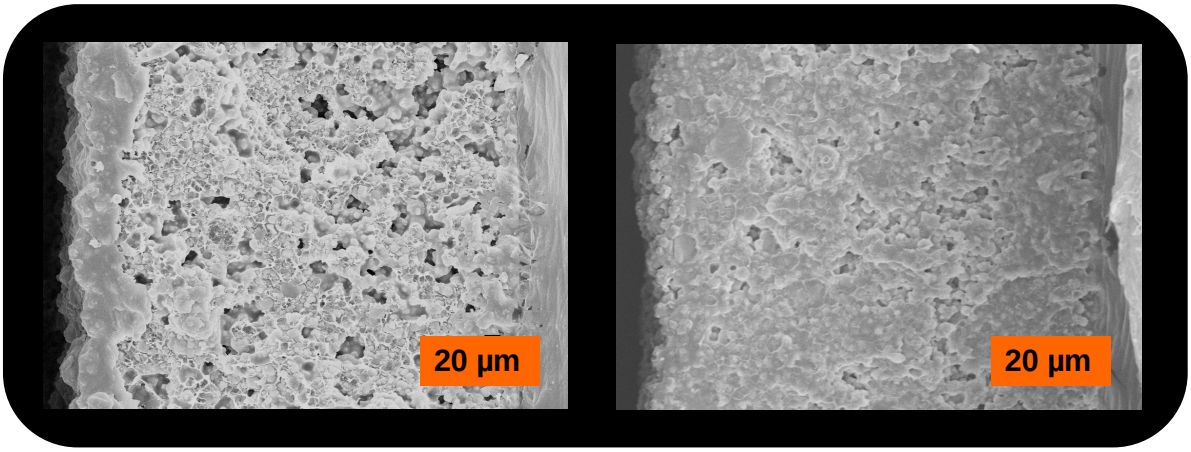

Figure 4.2: Effect of T_{anneal} on high loading 4A MMM morphology. Left: T_{anneal} = 130 °C; Right: T_{anneal} = 200 °C.

The left-hand image was from a portion of the MMM annealed at 130 °C whereas the right-hand image was from a portion of the same MMM annealed at 200 °C under vacuum. The low T_{anneal} sample has a heterogeneous morphology with a widespread presence of voids; thus, the measured permeabilities were orders of magnitude greater than pure PVAc with permselectivities less than pure PVAc. A homogenous, essentially void-free morphology is observed for the high T_{anneal} sample, and measured permeabilities were less than or equal to pure PVAc with permselectivities approximately

equal to pure PVAc (again, the poor transport properties in the void-free samples will be discussed in Section 4.3).

It is hypothesized that the high T_{anneal} case results in drastically increased PVAc chain mobility to a nearly liquid-like viscosity that allows the chains to readily flow, relieve stress, and fill in the voids. This is similar to observations of Shu regarding T_{anneal} for formation of void-free PVAc MMMs [17]. Photographs from her work are shown in Figure 4.3 (note that annealing time for each case was 30 min).

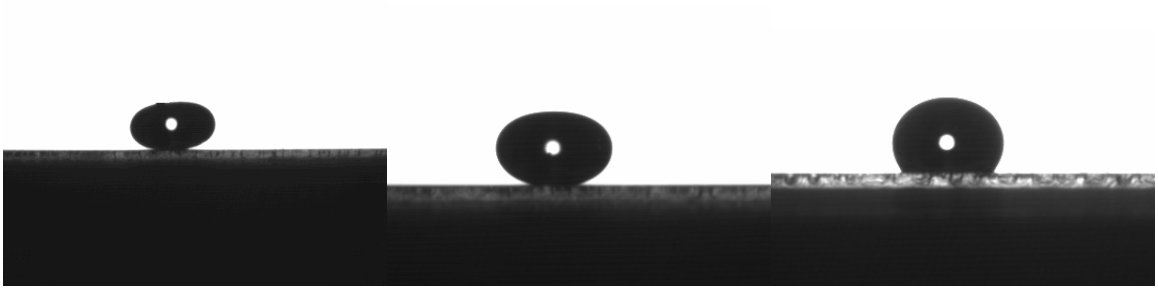

Figure 4.3: PVAc beads on glass plates under vacuum at different T_{anneal}. Left: No anneal. Center: T_{anneal} = 150 °C; Right: T_{anneal} = 200 °C. Images courtesy of Shu [17].

It is clear from Figure 4.3, that the high T_{anneal} condition resulted in deformation of the PVAc bead, reflecting a drastic reduction in the viscoelastic relaxation time constant. Shu's demonstration was reproduced on Teflon® substrates for T_{anneal} = 130 °C and 200 °C, and the same results were observed in the present work. Pure gas permeation experiments were also performed on PVAc dense films annealed at 200 °C to confirm the higher annealing temperature did not change the intrinsic transport properties. It should be noted that in some cases, void-free morphology was attained without a high temperature anneal, but in most cases, the high T_{anneal} improved morphology; thus, an

annealing temperature of 200 °C was adopted for all high loading MMMs discussed in Chapter 5.

4.3 Effects of Zeolite 4A Source on MMM Transport Properties

Zeolite 4A is a widely available molecular sieve that can be purchased from various companies. Due to this commercial accessibility, commercial zeolite 4A batches were initially used for MMMs in this work. Sections 4.2.1 and 4.2.2 briefly mention that the permeabilities of void-free 50 vol.% commercial zeolite 4A MMMs were up to 60 % lower than pure PVAc with permselectivities equivalent to pure PVAc. During the early stages of this work, it was unclear why the measured transport properties of high loading MMMs would be so poor, therefore the commercial zeolite 4A was used to make lower loading MMMs with which the MMM community is more familiar. Table 4.1 summarizes the pure gas permeabilities and permselectivities of 15 wt.% commercial zeolite 4A MMMs averaged over 7 samples. Pure PVAc data was averaged over 3 samples. All permeation tests used a 65 psia feed at 35 °C as described in Chapter 3. Note the last row are normalized values, i.e. MMM property divided by PVAc property.

Table 4.1: Permeabilities (Barrers) and selectivities of 15 wt.% commercial 4A MMMs.

	P_{He}	P_{O2}	P_{N2}	P_{CH4}	$\alpha_{He/CH4}$	$\alpha_{O2/N2}$	$\alpha_{N2/CH4}$
Pure PVAc	14.8 ± 0.9	0.501 ± 0.038	0.0762 ± 0.0067	0.0697 ± 0.0034	212 ± 1.8	6.58 ± 0.12	1.09 ± 0.04
15 wt.% com. 4A MMMs	12.9 ± 0.8	0.439 ± 0.022	0.0671 ± 0.0038	0.0604 ± 0.0034	214 ± 10.7	6.54 ± 0.13	1.11 ± 0.01
MMM/ PVAc	0.872	0.876	0.881	0.867	1.01	0.994	1.02

Table 4.1 clearly shows that all gas permeabilities were substantially decreased. In fact, the reductions of permeabilities relative to pure PVAc were nearly constant with an average reduction of 12.6 ± 0.6 %. Note that the standard deviations in Table 4.1 are only rough estimates of error since no more than 7 repeat measurements were made (see Section 3.2 for more details). Due to the differences in densities of PVAc and zeolite 4A (1.191 g/cc and 1.51 g/cc, respectively), 15 wt.% loading of zeolite 4A in PVAc equates to 12.2 vol.% loading. The 12.6 % average reduction in all gas permeabilities matches almost perfectly with predicted solubility reductions for the additive solubility model in MMMs (given as Equation 2.13 in Chapter 2) for impermeable fillers at 12.2 vol.%. The additive solubility model has been shown to be accurate [18], and the fact that the observed permeability reductions were slightly greater than the solubility reduction predictions is likely an indication that the seemingly impermeable commercial zeolite 4A particles created a more tortuous path for transport.

The permeation data in Table 4.1 can be used to compute gas diffusivities in PVAc and apparent diffusivities for the MMMs with the permeation time lag method (see Equation 2.12). Recall from Chapter 2, that use of Equation 2.12 for MMMs only gives apparent diffusivities due to a number of complicating factors that affect the transient approach to steady-state permeation. Table 4.2 on the next page summarizes these data (note that that the accuracy of the time lag method for helium is poor due to the high mobility of the helium molecule; thus, helium data are not included).

Table 4.2: Diffusivities and apparent diffusivities (cm^2/s) of PVAc and 15 wt.% commercial 4A MMMs, respectively.

	D_{O2}	D_{N2}	D_{CH4}
Pure PVAc	$4.5 \times 10^{-8} \pm 3.3 \times 10^{-9}$	$1.2 \times 10^{-8} \pm 5.1 \times 10^{-10}$	$2.9 \times 10^{-9} \pm 2.7 \times 10^{-10}$
15 wt.% com. 4A MMMs	$5.1 \times 10^{-8} \pm 6.0 \times 10^{-9}$	$1.3 \times 10^{-8} \pm 1.3 \times 10^{-9}$	$2.8 \times 10^{-9} \pm 3.8 \times 10^{-10}$

Table 4.2 shows that the apparent diffusivities in the commercial zeolite 4A MMMs match very closely to the actual diffusivities of pure PVAc. This directly conflicts with the concept of the filling of sorptive sinks as noted in Chapter 2 and implies that gases are bypassing, and not sorbing into, the commercial zeolite 4A particles in the MMMs. A variety of other experiments were performed to confirm that, over the timescale of the transient time lag, the commercial zeolite 4A particles were acting as impermeable fillers in the MMMs as discussed in the following subsections.

4.3.1 Gas Adsorption Properties of Zeolite 4A

Pure gas pressure decay adsorption experiments were done to confirm the commercial 4A from ASGE was effectively impermeable on the time scale needed to maintain local equilibrium with the surrounding polymer matrix as the MMM permeation properties suggested. The nitrogen adsorption isotherms (35 °C) for the ASGE zeolite 4A batch used in the MMMs from Sections 4.2 and 4.3, a previously reported but different batch of commercial zeolite 4A [12, 18], and an in-house synthesized batch of zeolite 4A are shown in Figure 4.4 on the next page.

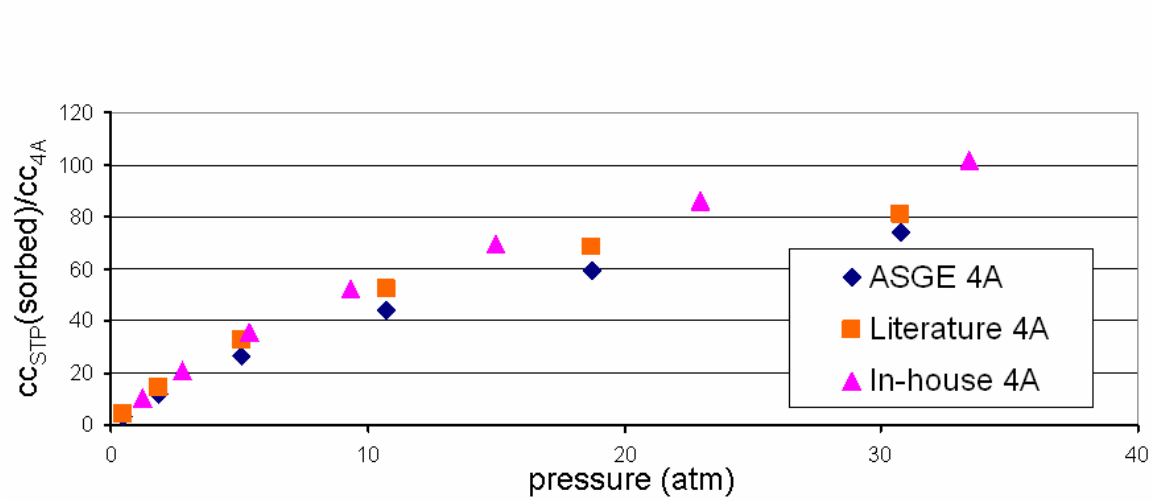

Figure 4.4: Nitrogen adsorption isotherms (35 °C) of commercial (ASGE) zeolite 4A, a literature reported zeolite 4A, and an in-house synthesized batch of zeolite 4A.

The seemingly contradictory factors noted with respect to the results in Table 4.2 and Figure 4.4 are important clues in explaining the surprising lack of enhancement in MMM performance in the high loading samples. The isotherm of the commercial 4A (from ASGE) used in this work compares well with previously reported isotherms for different commercially available zeolite 4A sources [12, 18]. Both of these isotherms fall short of the capacities measured for the in-house synthesized zeolite 4A; however, the discrepancy was not significant enough to explain the MMM data. Although determining gas diffusivities in zeolites is difficult (as described in Chapter 2), the nitrogen adsorption uptake kinetics of the commercial ASGE zeolite 4A were compared to those of the in-house synthesized zeolite 4A to probe the particle size normalized kinetic response. Find the uptake plots in Figure 4.5 on the following page.

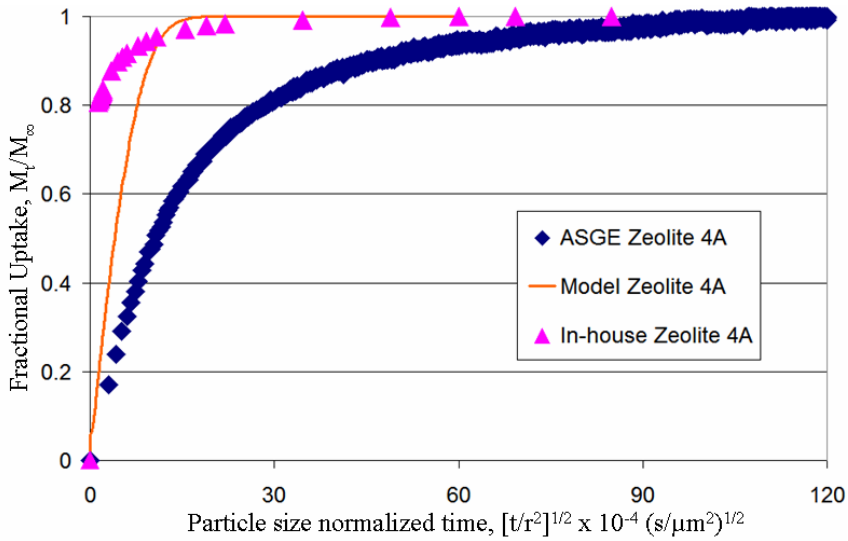

Figure 4.5: Nitrogen sorption kinetics (35°C) of zeolite 4A samples normalized by particle radius squared (r^2).

Note that the y-axis (M_t/M_∞) is the instantaneous fractional uptake of gas (i.e. the amount sorbed at a given time divided by the ultimate amount sorbed), and that the x-axis is plotted against the square-root of time (as is conventional) but normalized by particle radius squared to make a valid comparison of different size particles. It can be seen that the commercial zeolite 4A from ASGE has extraordinarily slow uptake kinetics compared to the in-house synthesized zeolite 4A and a model prediction of zeolite 4A nitrogen uptake based on Zimmerman's data [19].

It is hypothesized that the batch of zeolite 4A purchased from ASGE may have been improperly washed after synthesis and subsequently calcined by ASGE, thereby irreversibly fusing excess unreacted non-zeolitic aluminosilicate to the exterior of the zeolite 4A crystals. It has been reported that improper washing after zeolite synthesis can lead to such phenomena [20]; in fact, this type of observation lead to Chevron filing a patent on "super water washing" of zeolites to prevent this undesired excess on the external surfaces of crystals [6]. There are strong acid etching procedures for cleaning

such zeolite surfaces, but these techniques are too destructive for aluminum rich zeolites like zeolite 4A [20]. Note that a previous researcher confirmed this batch of zeolite 4A to have the correct crystal structure via XRD [17]. Elemental analyses of the ASGE and in-house synthesized zeolite 4A batches were made with the energy dispersive spectroscopic gun on the SEM as well as by ICP through Columbia Analytical Services. The results are provided in Table 4.3 below.

Table 4.3: Elemental analyses of commercial (ASGE) and in-house zeolite 4A.

Sample	wt.% oxygen EDS / ICP	wt.% sodium EDS / ICP	wt.% aluminum EDS / ICP	wt.% silicon EDS / ICP
In-house 4A	45.35 / na	13.23 / 11.93	18.41 / 17.50	23.01 / 27.64
Com. 4A	27.49 / na	15.82 / 14.69	26.29 / 17.14	30.40 / 23.74
Theoretical 4A	45.05	16.18	18.99	19.77

The in-house synthesized zeolite 4A has a chemical make-up that much more closely matches theory. It has a slightly higher Si:Al ratio than theory, but it is well documented that zeolite 4A can be synthesized with excess silicon [21]. Consequently fewer sodium ions needed to balance charge as the valency discrepancy between silicon and aluminum gives rise to charge imbalance in aluminum containing zeolites (as described in Chapter 2). The composition of the commercial zeolite 4A from ASGE was drastically different from theory according to EDS. There is a 49 % deficiency in oxygen, a 38 % excess of aluminum, and a 54 % excess of silicon. This compositional discrepancy from theory is consistent with the presence of non-zeolitic aluminosilicates such as alumina and silica as these materials have lower metal to oxygen ratios (3:2 and 2:1, respectively) compared to the 4:1 ratio for the silica and alumina tetrahedra that

make up the zeolite 4A framework. Since the commercial zeolite 4A from ASGE had the correct crystal structure and roughly correct adsorption capacities, it is assumed that there this excess alumina and silica resides on the surface of the crystals acting as a barrier for diffusion into the crystals. It is not clear why there is a large disagreement between the EDS and ICP results for the commercial zeolite 4A sample. Sample preparation for ICP involves digestion of the inorganic material with strong acids. Depending on the exact experimental protocol at Columbia Analytical Services, it is reasonable to assume that excess non-zeolitic aluminosilicate may have been washed away during sample preparation and not sent to the mass spectrometer.

4.3.2 Permeation in In-house Synthesized Zeolite 4A-PVAc MMMs

After confirming that the in-house synthesized zeolite 4A appeared to be "healthy", 15 wt.% in-house zeolite 4A-PVAc MMMs were made and subjected to the same permeation experiments done on the "bad" commercial 4A described in Section 4.3. Table 4.4 summarizes the permeabilities and permselectivities while Table 4.6 shows the apparent diffusivity data (Table 4.5 on next page).

Table 4.4: Permeabilities (Barrers) and selectivities of 15 wt.% in-house (IH) zeolite 4A MMMs.

	P_{He}	P_{O2}	P_{N2}	P_{CH4}	$\alpha_{He/CH4}$	$\alpha_{O2/N2}$	$\alpha_{N2/CH4}$
Pure PVAc	14.8 ± 0.9	0.501 ± 0.038	0.0762 ± 0.0067	0.0697 ± 0.0034	212 ± 1.8	6.58 ± 0.12	1.09 ± 0.04
15 wt.% IH 4A MMMs	14.2 ± 1.1	0.562 ± 0.103	0.0829 ± 0.0144	0.0697 ± 0.0097	206 ± 15.6	6.77 ± 0.08	1.19 ± 0.05
MMM/ PVAc	0.964	1.12	1.09	1.00	0.972	1.03	1.09

Table 4.5: Diffusivities and apparent diffusivities (cm^2/s) of PVAc and 15 wt.% in-house 4A MMMs, respectively.

	D_{O2}	D_{N2}	D_{CH4}
Pure PVAc	$4.5 \times 10^{-8} \pm 3.3 \times 10^{-9}$	$1.2 \times 10^{-8} \pm 5.1 \times 10^{-10}$	$2.9 \times 10^{-9} \pm 2.7 \times 10^{-10}$
15 wt.% com. 4A MMMs	$6.4 \times 10^{-9} \pm 1.1 \times 10^{-9}$	$7.6 \times 10^{-10} \pm 1.4 \times 10^{-10}$	$3.0 \times 10^{-10} \pm 7.6 \times 10^{-11}$

Unlike the commercial zeolite 4A MMMs, the in-house synthesized zeolite 4A MMMs provided both permeability and selectivity enhancements over pure PVAc (Table 4.4). Furthermore, the effects of transient filling of sorptive sinks that complicate the transient permeation in MMMs with fully accessible sieves are obvious from the reduced apparent diffusivities of the in-house zeolite 4A MMMs relative to pure PVAc (Table 4.5). Note that the standard deviations in Tables 4.4 and 4.5 are only rough estimates of error since no more than 3 repeat measurements were made (see Section 3.2 for more details).

This comparison of the commercial zeolite 4A batch and the in-house synthesized zeolite 4A batches suggests that much greater care must be taken when processing zeolites for MMM applications than for simple sorbent applications. It is not our intention to "bash" the commercially available source—ASGE provided a large, fairly monodisperse batch of small zeolite 4A crystals that have the proper crystal structure and adsorption capacities. This batch is simply not of the quality needed for use in MMM applications which require easy access to the internal micropores, or the gas molecules will tend to bypass the dispersed filler particles over the time scale needed for local equilibrium.

4.4 Effects of Desolvation on CuTPA·DMF Properties

The MOF, CuTPA, used to make MMMs in this work has not been well studied as a raw material or for use in MMMs. A detailed description of its synthesis and basic material properties can be found elsewhere [22], but some of this information is reproduced here to highlight the effects of processing on CuTPA properties. As mentioned in Chapter 3, CuTPA is synthesized as a CuTPA·DMF complex. The repeat unit of this complex is provided in Figure 4.6.

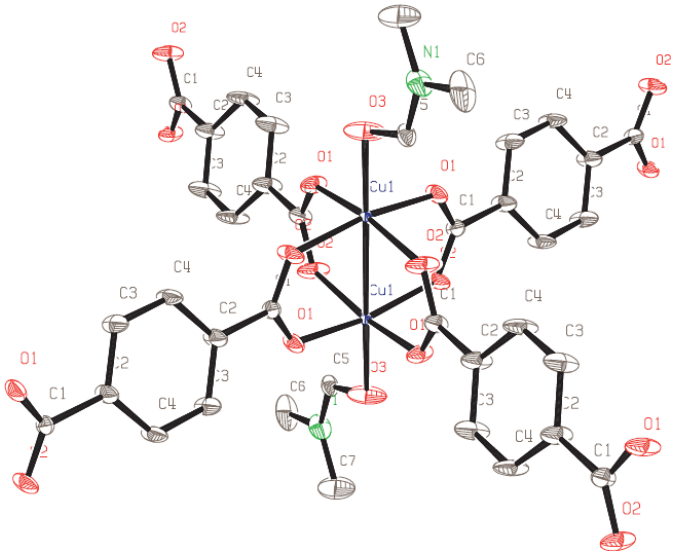

Figure 4.6: Repeat unit of CuTPA·DMF. The nitrogen of DMF appears in green.

XRD confirmed that the synthesized product shared the previously reported crystal structure [23]. The XRD of CuTPA·DMF is provided in Figure 4.7 on the next page.

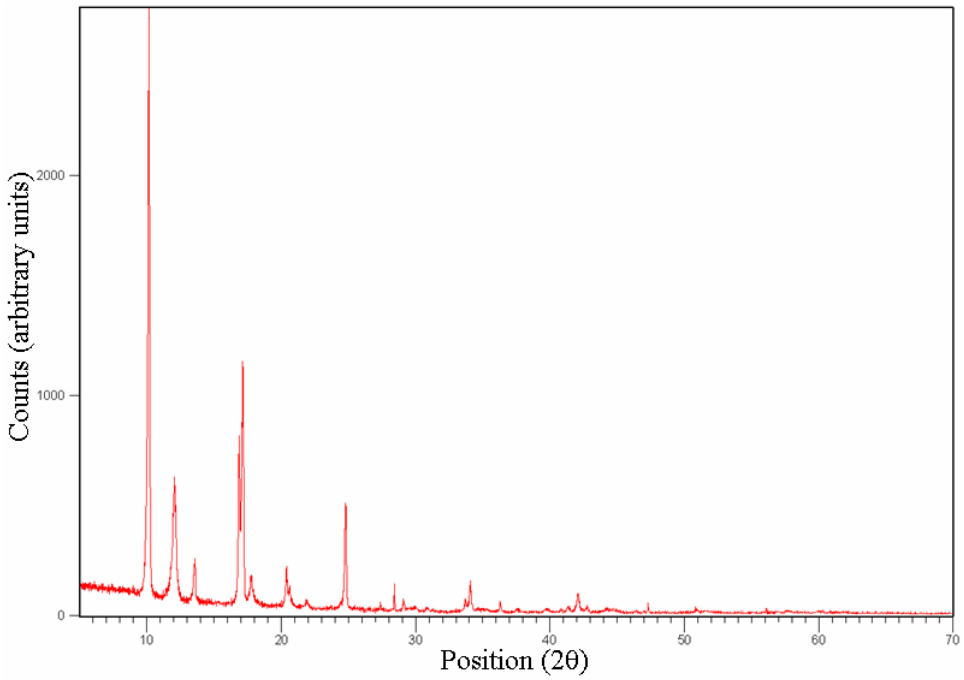

Figure 4.7: XRD of solvated CuTPA·DMF.

In order to determine the specific surface area and adsorption properties of this material, it was necessary to remove the DMF molecules coordinated with the copper atoms. TGA was performed to determine the desolvation temperature of CuTPA·DMF, and the results are given in Figure 4.8.

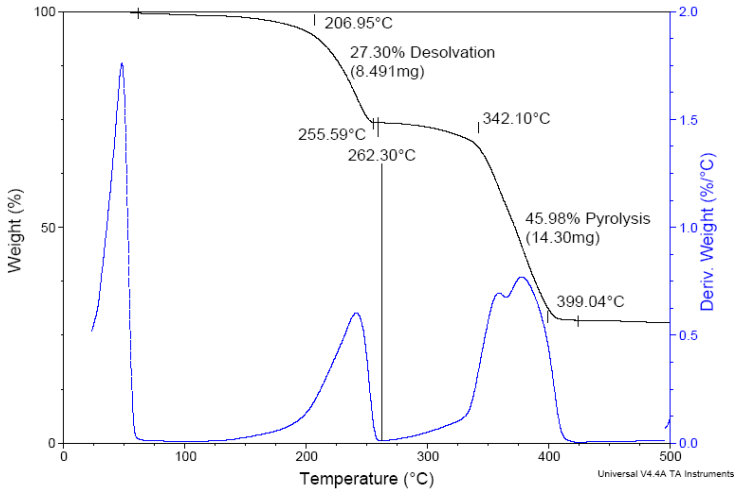

Figure 4.8: TGA of solvated CuTPA·DMF.

Figure 4.8 shows that desolvation begins around 200 °C and that degradation does not begin until over 300 °C. While this is a smaller window of thermal stability than for typical zeolitic materials, the thermal properties are good enough to use in the PVAc MMMs. When preparing CuTPA MMMs, the CuTPA·DMF was desolvated at 230 °C under vacuum for 24 – 36 hours, and it the mass loss was identical to the desolvation mass loss from the TGA experiment.

Although it was found that the CuTPA·DMF could be desolvated prior to degradation, there was a structural change upon desolvation as witnessed by the XRD of the desolvated CuTPA shown in Figure 4.9.

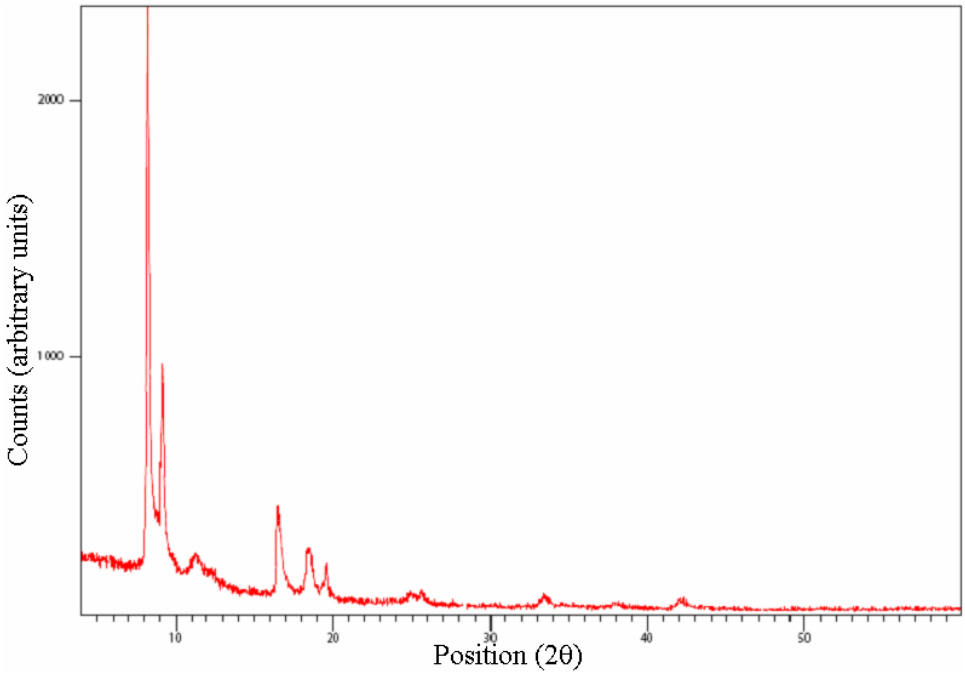

Figure 4.9: XRD of desolvated CuTPA.

The diffractogram in Figure 4.9 for the desolvated CuTPA is quite different from that of the solvated CuTPA·DMF. The peaks are less intense and broader, indicating that the

material underwent structural changes; however, the desolvated diffractogram still appears to that of a crystalline material.

To confirm that the desolvated CuTPA was indeed a microporous material with high surface area available for gas adsorption, cryogenic nitrogen physisorption measurements were made. Figure 4.10 shows these results.

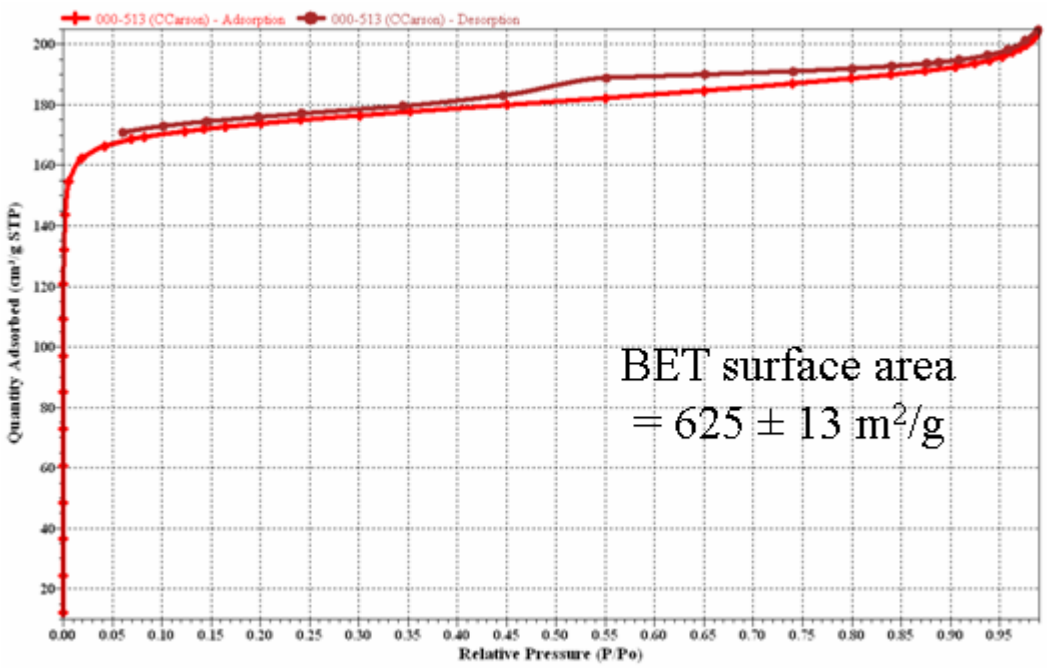

Figure 4.10: Cryogenic N_2 physisorption on CuTPA. Quantity adsorbed (cm^3/g STP) on y-axis; relative pressure (P/P_o) on x-axis. Red = sorption; Purple = desorption.

The shapes and magnitude of the cryogenic nitrogen adsorption/desorption isotherms confirm that the desolvated CuTPA is a microporous material despite the structural changes evident in the diffractogram in Figure 4.8. Chapters 5 and 6 discuss the transport properties of CuTPA MMMs, and Appendix A contains pure gas adsorption isotherms (35 °C) for desolvated CuTPA which further confirm the microporous nature of the material.

4.5 Conclusions

Formation of void-free high molecular sieve loading MMMs required significant alterations in MMM solution processing procedures. Two critical parameters were identified for successful formation of 50 vol.% zeolite 4A-PVAc MMMs: 1) sufficiently low initial solvent concentration; 2) sufficiently high annealing temperature. The effect of initial solvent concentration has not been previously reported and appears to be related to void formation caused by "early" particle percolation.

A variety of experiments confirmed that several commercial zeolite 4A sources may have been processed in a manner that restricts access to internal micropores. These apparent surface barriers effectively make the commercial zeolite 4A crystals impermeable in MMM applications despite showing the proper crystal structure and roughly correct adsorption capacities. It is hypothesized that improper washing and calcining by the supplier after synthesis left non-zeolitic aluminosilicate material on the external surfaces of the crystals that adds substantial diffusion resistance that undermine the sieves utility in MMMs. This is a significant finding as the reduced permeabilities in the commercial 4A MMMs could be easily misconstrued as the presence of rigidified polymer chains around the filler particles that provide extra transport resistance as observed in other MMMs [9, 13, 17, 24].

Processing the as-synthesized CuTPA·DMF for use in MMMs resulted in structural changes, but these changes did not destroy the material's microporous sieving properties. It later came to our attention that solvent extraction processes prior to thermal desolvation may have resulted in less structure alteration [7]. Future work should

investigate whether gentler processing would yield better pure CuTPA and CuTPA MMM properties.

4.6 References

[1] Das, M., *Membranes for olefin/paraffin separations*. 2009, Georgia Institute of Technology, Ph.D. Thesis.

[2] Rezac, M.E., P.H. Pfromm, L.M. Costello, and W.J. Koros, *Aging of thin polyimide ceramic and polycarbonate ceramic composite membranes.* Industrial & Engineering Chemistry Research, 1993. **32**(9): p. 1921-1926.

[3] Zhou, F.B. and W.J. Koros, *Study of thermal annealing on matrimid (r) fiber performance in pervaporation of acetic acid and water mixtures.* Polymer, 2006. **47**(1): p. 280-288.

[4] Kosuri, M.R. and W.J. Koros, *Defect-free asymmetric hollow fiber membranes from torlon (r), a polyamide-imide polymer, for high-pressure co2 separations.* Journal of Membrane Science, 2008. **320**(1-2): p. 65-72.

[5] Chafin, R.W., *Torlon(r) and silicalite mixed matrix membranes for xylene isomer purification*. 2007, Georgia Institute of Technology, Ph.D. Thesis.

[6] Miller, S.J., *Mixed matrix membrane with super water washed silica containing molecular sieves and methods for making and using the same*, U.S.P. Office, Editor. 2007.

[7] Liu, J.C., J.T. Culp, S. Natesakhawat, B.C. Bockrath, B. Zande, S.G. Sankar, G. Garberoglio, and J.K. Johnson, *Experimental and theoretical studies of gas adsorption in cu-3(btc)(2): An effective activation procedure.* Journal of Physical Chemistry C, 2007. **111**(26): p. 9305-9313.

[8] Perry, J.D., *Formation and characterization of hybrid membranes utilizing high-performance polyimides and carbon molecular sieves*. 2007, Georgia Institute of Technology, Ph.D. Thesis.

[9] Moore, T.T. and W.J. Koros, *Non-ideal effects in organic-inorganic materials for gas separation membranes.* Journal of Molecular Structure, 2005. **739**(1-3): p. 87-98.

[10] Husain, S., *Mixed matrix dual layer hollow fiber membranes for natural gas separation*. 2006, Georgia Institute of Technology, Ph.D. Thesis.

[11] Mahajan, R. and W.J. Koros, *Factors controlling successful formation of mixed-matrix gas separation materials.* Industrial & Engineering Chemistry Research, 2000. **39**(8): p. 2692-2696.

[12] Moore, T.T., *Effects of materials, processing, and operating conditions on the morphology and gas transport properties of mixed matrix membranes*. 2004, The University of Texas at Austin, Ph.D. Thesis.

[13] Mahajan, R., *Formation, characterization, and modeling of mixed matrix membrane materials*. 2000, The University of Texas at Austin, Ph.D. Thesis.

[14] Payne, J.A., *Stress evolution in solidifying coatings*. 1998, The University of Minnesota-Twin Cities, Ph.D. Thesis.

[15] Croll, S.G., *Effect of titania pigment on the residual strain, glass-transition and mechanical-properties of a pmma coating.* Polymer, 1979. **20**(11): p. 1423-1430.

[16] Fishman, R.S., D.A. Kurtze, and G.P. Bierwagen, *Pigment inhomogeneity and void formation in organic coatings.* Progress in Organic Coatings, 1993. **21**(4): p. 387-403.

[17] Shu, S., *Engineering the performance of mixed matrix membranes for gas separations*. 2007, Georgia Institute of Technology, Ph.D. Thesis.

[18] Moore, T.T. and W.J. Koros, *Gas sorption in polymers, molecular sieves, and mixed matrix membranes.* Journal of Applied Polymer Science, 2007. **104**(6): p. 4053-4059.

[19] Zimmerman, C.M., A. Singh, and W.J. Koros, *Tailoring mixed matrix composite membranes for gas separations.* Journal of Membrane Science, 1997. **137**(1-2): p. 145-154.

[20] Miller, S.J., *Discussion of impact of washing on zeolite properties.* 2007: Atlanta, GA.

[21] Breck, D.W., *Zeolite molecular sieves*. 1973, New York: Wiley.

[22] Carson, C.G., K. Hardcastle, J. Schwartz, X.T. Liu, C. Hoffmann, R.A. Gerhardt, and R. Tannenbaum, *Synthesis and structure characterization of copper terephthalate metal-organic frameworks.* European Journal of Inorganic Chemistry, 2009(16): p. 2338-2343.

[23] Seki, K., S. Takamizawa, and W. Mori, *Characterization of microporous copper(ii) dicarboxylates (fumarate, terephthalate, and trans-1,4-cyclohexanedicarboxylate) by gas adsorption.* Chemistry Letters, 2001(2): p. 122-123.

[24] Li, Y., H.M. Guan, T.S. Chung, and S. Kulprathipanja, *Effects of novel silane modification of zeolite surface on polymer chain rigidification and partial pore blockage in polyethersulfone (pes)-zeolite a mixed matrix membranes.* Journal of Membrane Science, 2006. **275**(1-2): p. 17-28.

CHAPTER 5

EFFECTS OF HIGH MOLECULAR SIEVE LOADING ON MMM PROPERTIES

5.1 Introduction

The ultimate goal of MMM design for improved gas separation performance is to maximize molecular sieve loading while retaining the ease of processing polymers from solution [1-3]. While there have been many reports of MMM gas transport properties for low to moderate molecular sieve loadings (10 – 40 vol.%) [3-21], there have been few studies of higher molecular sieve loading MMMs [5-7, 18, 19]. Understanding MMM transport properties at high molecular sieve loadings (> 40 vol.%) is critical to the future viability of MMMs as a gas separation technology.

Two molecular sieves (zeolite 4A and CuTPA) were used to make MMMs with loadings > 40 vol.% in PVAc. Successful formation of void-free MMMs at high molecular sieve loadings required changes to the processing procedures used for formation of low loading MMMs—these findings were discussed in Chapter 4. This Chapter focuses on the gas transport properties of void-free high loading MMMs. Section 5.2 will focus on the mixed gas transport properties of 50 vol.% zeolite 4A MMMs in PVAc while Section 5.3 does the same for 44 and 65 vol.% CuTPA-PVAc MMMs. Conclusions are drawn in Section 5.4.

5.2 High Loading Zeolite 4A-PVAc MMMs

Zeolite 4A is a well studied material (in fact it was the first reported synthetic zeolite [22]) and has been extensively used in MMMs [9-12, 17, 21, 23-26]. The long history of zeolite 4A as well as the promising results reported for low zeolite 4A loading

MMMs elsewhere [9, 23, 27] make zeolite 4A an ideal candidate for high loading MMM studies. Two 50 vol.% 4A MMMs were prepared from two different casting solutions which contained in-house zeolite 4A from 2 separate syntheses. Multiple samples were made and tested from each of these MMMs. SEM cross-sectional images of a 50 vol.% zeolite 4A MMM made in this work are provided in Figures 5.1 and 5.2.

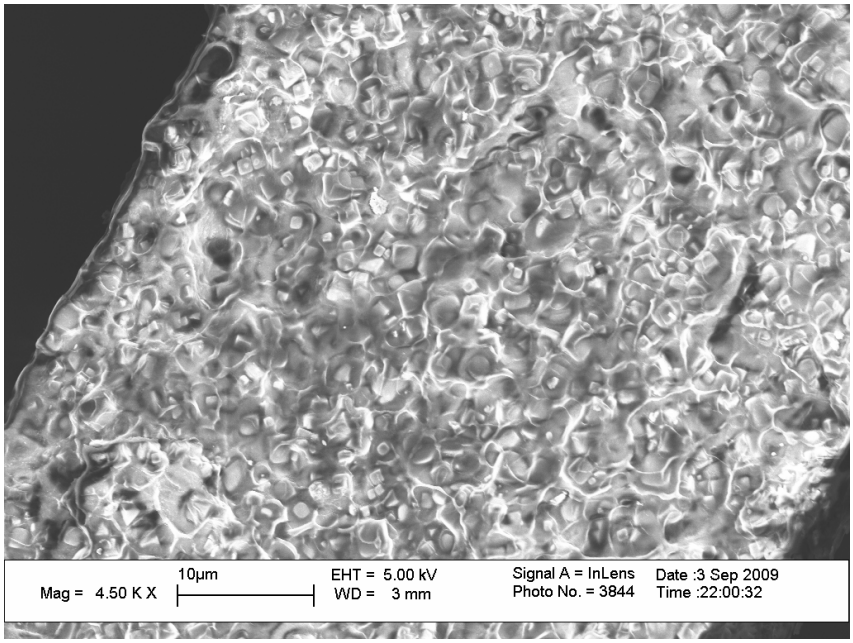

Figure 5.1: SEM of a 50 vol.% zeolite 4A-PVAc MMM overall cross-section.

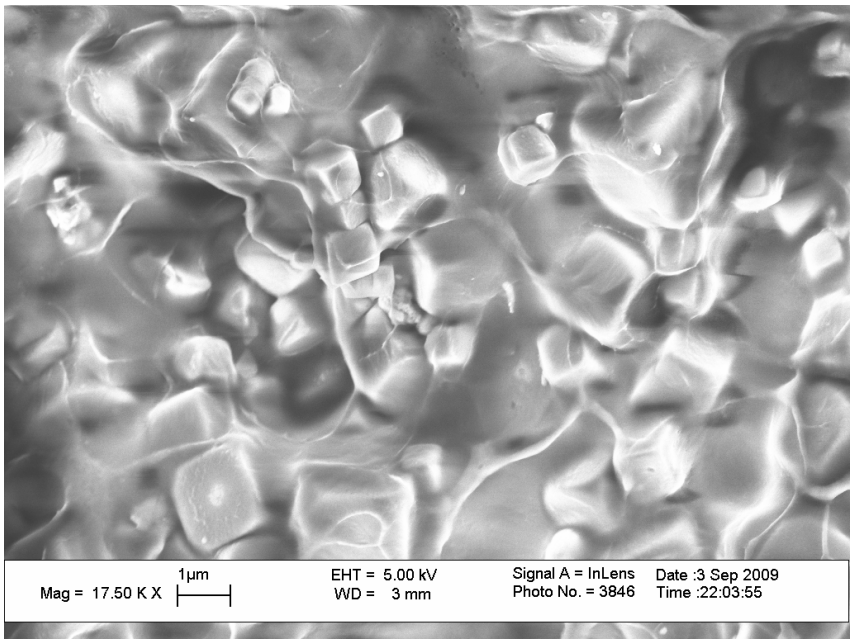

Figure 5.2: SEM of a 50 vol.% zeolite 4A-PVAc MMM zoomed in cross-section.

Figure 5.1 shows a homogenous dispersion of zeolite 4A particles and the absence of large voids. The zoomed in SEM in Figure 5.2 avoids the clutter in Figure 5.1 and confirms the absence of voids at the particle-polymer interfaces.

5.2.1 Low Pressure Mixture Permeation in 50 vol.% 4A MMMs

While pure gas permeation tests are a simple means to probe the quality of membrane materials and to gain a basic understanding of the transport properties and mechanisms, mixture permeation is the ultimate goal. Membrane materials are designed with the intention of separating mixtures of gases and have been found to provide the best tests of the MMMs studied here. Pure gas results are reported in Appendix B but provide less useful insights.

The transport properties of gas mixtures can deviate from pure gas transport properties [28, 29]. This is especially true for highly interacting gases such as carbon dioxide. Not only does carbon dioxide have strong interactions with itself (i.e. it is quite

compressible compared to other light gases) [30], it is also known to interact strongly with polymers and molecular sieves [31-37]. Furthermore, carbon dioxide is known to plasticize polymers further complicating analysis [31, 35, 37]. In order to investigate the mixed carbon dioxide-methane permeation properties of 50 vol.% zeolite 4A-PVAc MMMs without plasticizing the PVAc matrix, mixed gas permeation experiments were conducted with 10:90::CO_2:CH_4 mixtures at ~ 40 psia total pressure. Figure 5.3 shows the carbon dioxide permeability isotherm of pure PVAc to show that the p_{CO2} during mixed gas experiments was below the plasticization pressure.

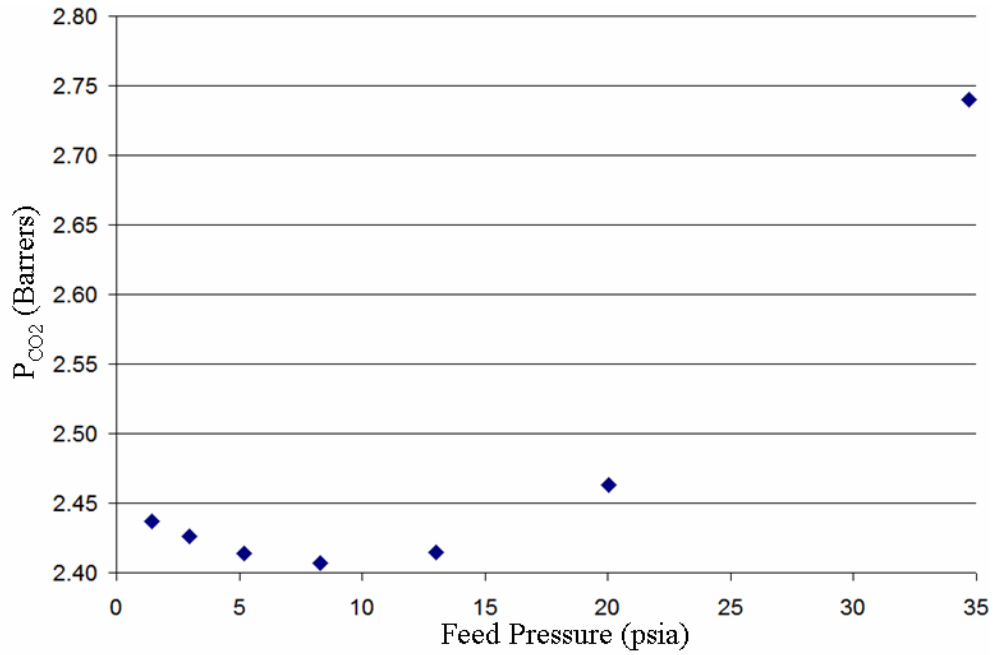

Figure 5.3: Carbon dioxide permeation isotherm of PVAc. Plasticization at ~ 10 psia (minimum of isotherm).

Two 50 vol.% 4A-PVAc samples were tested at the conditions described above. These samples were from separate casts and the 4A particles were from different batches.

A PVAc sample was also tested for comparison. The mixed gas permeation data of these MMMs and PVAc as well as the normalized MMM values are provided in Table 5.1.

Table 5.1: Low pressure mixed CO_2-CH_4 permeation data for 50 vol.% 4A MMMs.

	P_{CO2} (Barrers)	P_{CH4} (Barrers)	$\alpha_{CO2/CH4}$
Pure PVAc	2.15 ± 0.01	0.064 ± 0.001	33.5 ± 0.4
50 vol.% 4A MMM	4.33 ± 0.67	0.088 ± 0.013	49.4 ± 0.5
MMM/PVAc	2.01	1.36	1.47

Excellent transport enhancements are shown in Table 5.1. Note that standard deviations in Table 5.1 are only rough estimates of error since only 2 repeat measurements were made (see Section 3.2 for more details). Carbon dioxide permeability was doubled, and a 47 % increase in permselectivity was attained. Table 5.1 suggests that high loading MMMs in PVAc may be competitive with high performance polymer membranes; however, the conditions were mild, and many natural gas wells exist at much higher total pressures and partial pressures of carbon dioxide [38, 39]. While the low pressure mixed gas case for the high loading 4A MMMs in this work are similar to the conditions for carbon dioxide capture from the atmosphere or from coal-fired power plant flue gas [40], it was necessary to test these materials at conditions similar to natural gas feeds. Section 5.2.2 discusses the transport properties of 50 vol.% 4A-PVAc MMMs under aggressive (i.e. higher total and carbon dioxide partial pressures) mixed gas feeds.

5.2.2 High Pressure Mixture Permeation in 50 vol.% 4A MMMs

A 50:50 mixture of carbon dioxide and methane was used for 440 psia total pressure permeation experiments on 50 vol.% zeolite 4A-PVAc MMMs as well as a pure

PVAc sample. Results of these experiments are provided in Table 5.2 in the same manner results were presented in Table 5.1.

Table 5.2: Transport summary of high pressure mixed CO_2-CH_4 permeation.

	P_{CO2} (Barrers)	P_{CH4} (Barrers)	$\alpha_{CO2/CH4}$
Pure PVAc	11.4 ± 0.1	0.457 ± 0.008	25.0 ± 0.3
50 vol.% 4A MMM	12.7 ± 0.2	0.321 ± 0.014	39.8 ± 1.6
50 vol.% 4A/PVAc	1.12	0.702	1.59

The high pressure mixed carbon dioxide-methane transport properties of the 50 vol.% zeolite 4A MMM represent remarkable enhancements over the properties of pure PVAc under the same feed conditions. It is clear that plasticization has occurred in PVAc at these conditions as pure PVAc carbon dioxide permeability has increased by 429 %, methane permeability has increased by 611 %, and permselectivity has decreased by 26 %. Apparently the effects of plasticization on the PVAc matrix in the 50 vol.% zeolite 4A MMM did not outweigh the high permselectivity of zeolite 4A as the MMM gave a 59 % enhancement in permselectivity over pure PVAc. Note that this enhancement is actually much better than the permselectivity enhancement of 47 % for the low pressure mixed feed—this detail will be discussed more in Chapter 6. Carbon dioxide permeability enhancement in the high loading 4A MMM was not as high at these aggressive feed conditions as it was at the low pressure mixed feed conditions; however, a 12 % enhancement in desired permeant permeability was still observed. Furthermore, a 30 % reduction in undesired permeant (methane) permeability was observed. This difference in permeabilities for the two mixed feed conditions is likely the result of

higher penetrant permeabilities in the plasticized PVAc matrix (which dilutes the contribution from the filler particles) as well as Langmuir saturation in the zeolite 4A crystals (i.e. solubilities decrease with increasing pressure in materials that follow a Langmuir isotherm).

The excellent transport property enhancements of the high loading zeolite 4A MMMs over pure PVAc at both low and high pressure mixed gas conditions represent significant progress towards the properties of high-performance pure polymer membranes. The approach towards Robeson's upper-bound for the carbon dioxide-methane pair is shown in Figure 5.4.

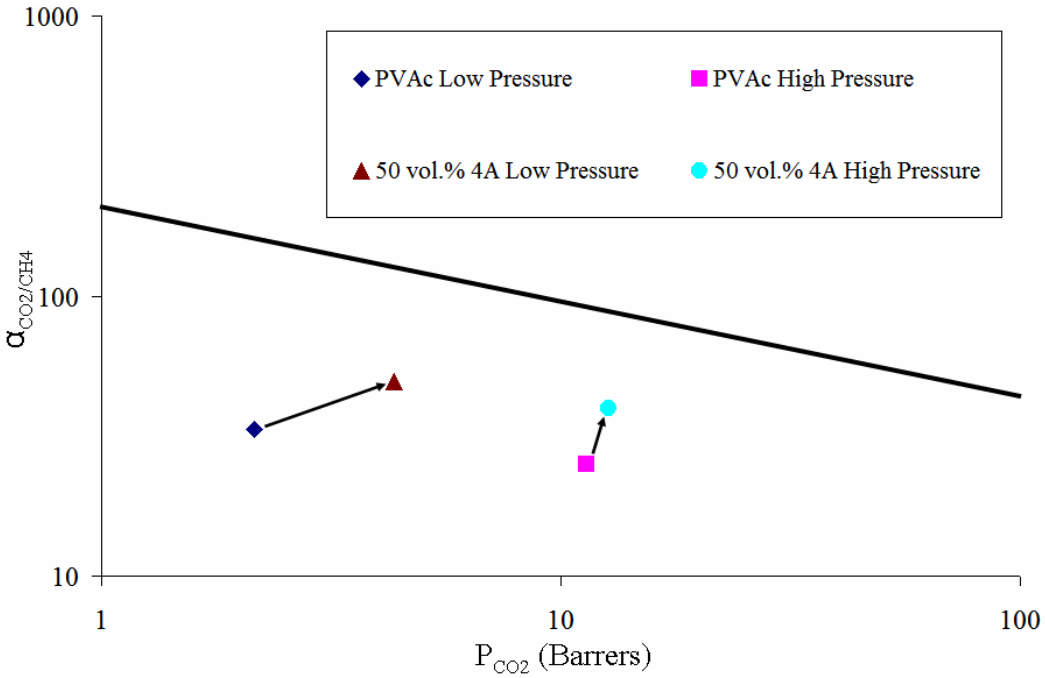

Figure 5.4: Pure PVAc and 50 vol.% zeolite 4A MMM performance vs. Robeson's 2008 upper-bound (shown as solid, black line) [41].

While the 50 vol.% zeolite 4A performance at each mixed gas condition fall well short of the upper-bound, it has been shown that the properties of a low cost, low performance

polymer can be drastically improved by inclusion of a low cost filler material. This ultimately was the goal of the present work.

Using a more rigid glass on the upper bound has been found, even at low sieve loading, to result in excessive stress accumulation during film formation which results in interfacial void defects unless complex "surface texturing" of the sieves is used [10, 11, 27, 42, 43]. In the present work, rather than combine the challenges of high sieve loadings and management of high stress accumulation due to the use of rigid matrices, the focus on PVAc was deemed wise. Also note that the performance of the high loading MMM for the high pressure mixed gas case was the closest to the so-called upper-bound despite plasticization in the polymer matrix. This fact is especially important since the Robeson upper-bound is merely a compilation of all reported data, most of which are not gathered under aggressive, mixed gas feeds so the high loading zeolite 4A-PVAc MMM performance under aggressive feeds reported here may, practically, be even more significant than they appear on Figure 5.4.

The successful formation of void-free 50 vol.% zeolite 4A-PVAc MMMs with substantially improved gas separation properties under industrially relevant, high partial pressure carbon dioxide conditions basically represents successful completion of the primary goal of this project. However, it was desired to investigate whether the lessons learned in Chapter 4 for creation of void-free high loading MMMs could be extended to other molecular sieves. Furthermore, the lack of a fundamental understanding of the nature of gas transport through MMMs (especially as a function of the pore sizes of molecular sieves) warranted an investigation of the performance of MMMs with varying pore window size.

5.3 High Loading CuTPA-PVAc MMMs

MOF MMMs have not been extensively studied outside of this work and a few others [44-47]. CuTPA is quite different from zeolite 4A in both composition and pore size. It was believed that formation of void-free, high loading CuTPA MMMs in PVAc using the same methods as for zeolite 4A would illustrate the generality of the techniques in Chapter 4 regarding formation of void-free high loading MMMs beyond conventional inorganic fillers. We expected in this case, however, that the reported large pore channel size of CuTPA (~ 5.2 Å [47]) should be too large to provide substantial improvements in diffusive selectivity of carbon dioxide over methane. This case would be very much the opposite of the case of effectively plugged commercial 4A MMMs discussed in Chapter 4 and should provide higher permeabilities with essentially the same selectivities as PVAc. However, CuTPA MMMs should show lower selectivities than the in-house synthesized 4A MMMs, thereby further illustrating the importance of pore size on MMM performance. Furthermore, this MOF material is easy to synthesize in large batches which facilitates high particle loading MMM preparation so it was easy to consider [47].

Two high loading CuTPA-PVAc MMMs were made and tested with pure and mixed gas permeation experiments. Due to the low density of CuTPA (0.63 g/cc [48]) relative to the density of PVAc (1.191 g/cc), small masses of CuTPA result in relatively large volume loadings in MMMs. 30 and 50 wt.% loading CuTPA MMMs equate to 44 vol.% and 65 vol.% MMMs, respectively. SEM cross-sectional images of the high loading MMMs are provided in Figures 5.5 – 5.8.

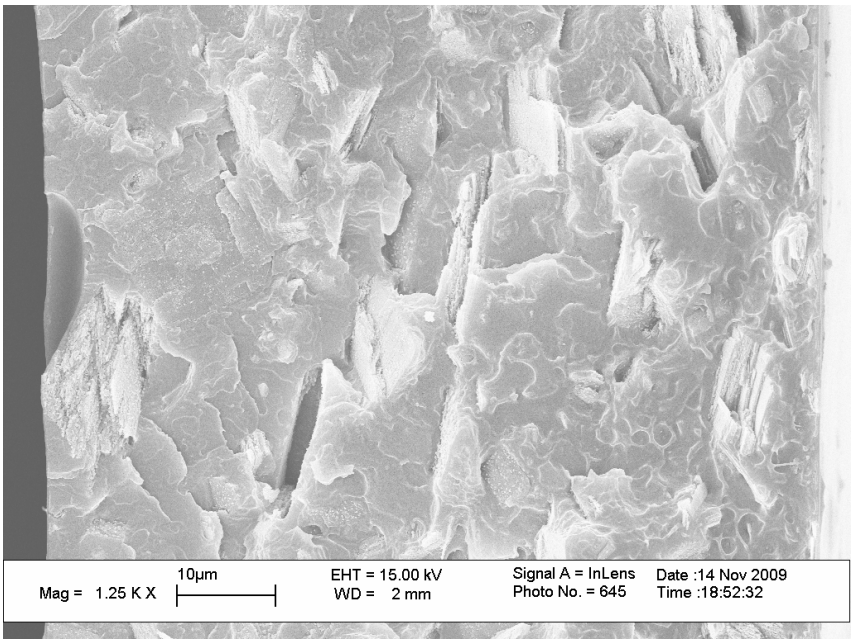

Figure 5.5: SEM of a 44 vol.% CuTPA-PVAc MMM overall cross-section.

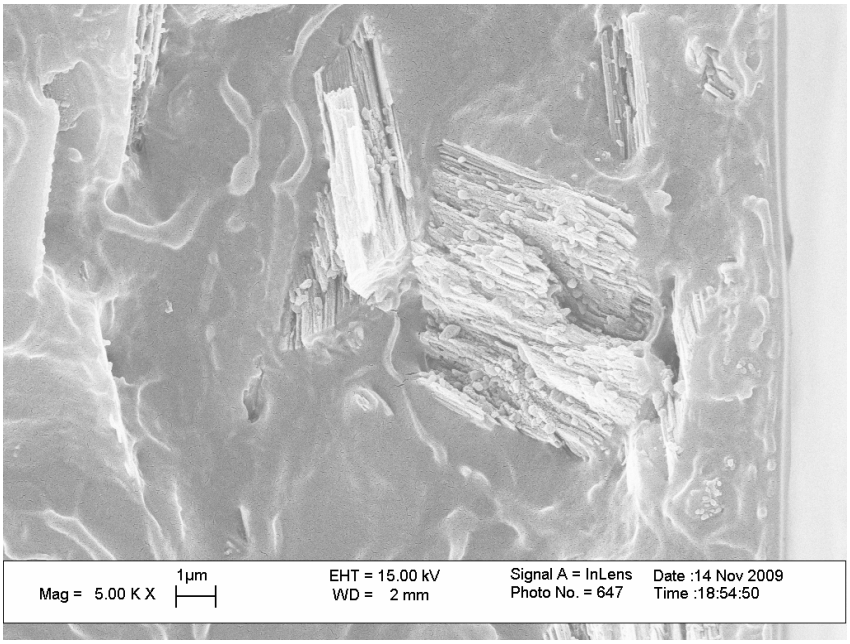

Figure 5.6: SEM of a 44 vol.% CuTPA-PVAc MMM zoomed in cross-section.

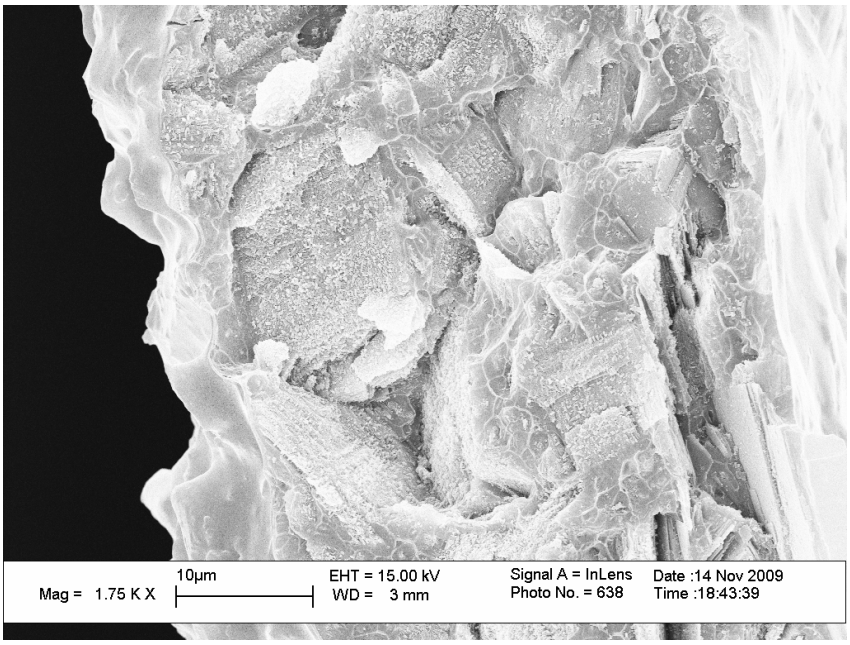

Figure 5.7: SEM of a 65 vol.% CuTPA-PVAc MMM overall cross-section.

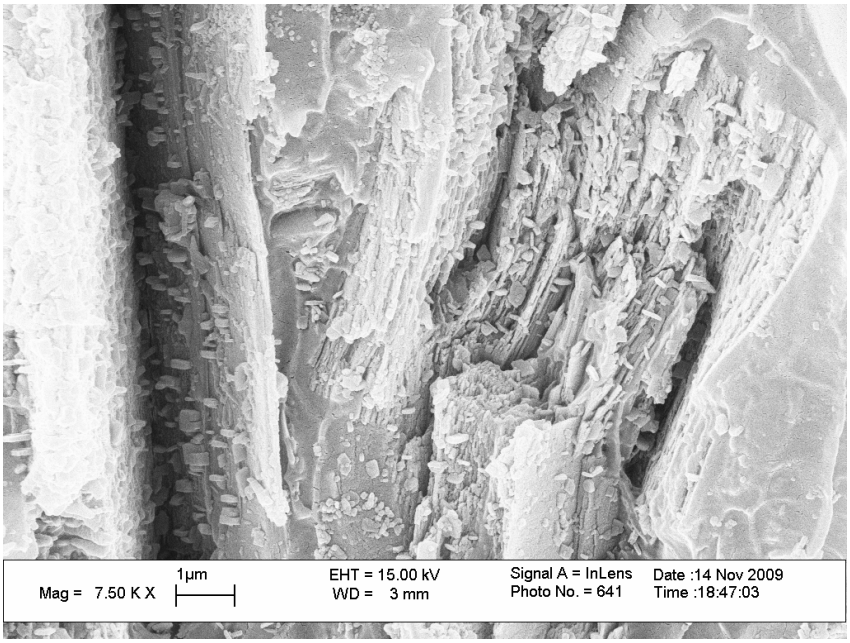

Figure 5.8: SEM of a 65 vol.% CuTPA-PVAc MMM zoomed in cross-section.

The cross-sectional images of the 44 vol.% CuTPA-PVAc MMM in Figures 5.5 and 5.6 show a high particle loading void-free MMM. These figures also display an

interesting property of the CuTPA particles and MMMs thereof, i.e. the particles appear to be stacks of platelets and many of these platelets are exfoliated and aligned perpendicular to the direction of flow. The solvated CuTPA crystals did not appear to be stacks of plates and certainly were not exfoliated platelets (see Figure 5.8).

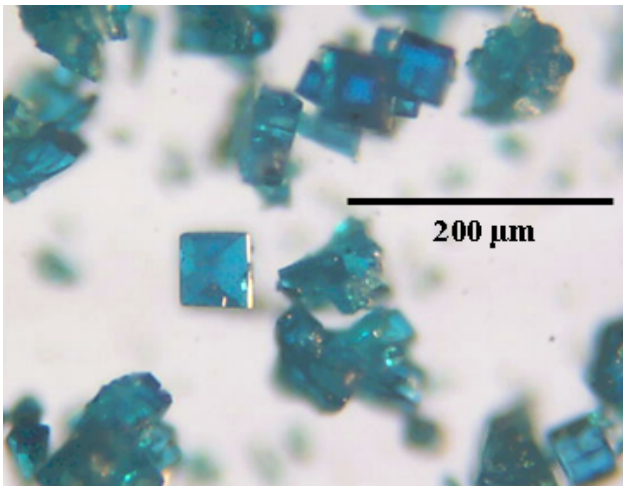

Figure 5.9: Optical micrograph of as synthesized CuTPA·DMF.

It is hypothesized that the desolvation and ultrasonic dispersion processes break the particles into platelets as suggested in Chapter 4. Platelets aligned perpendicular to the direction of gas transport in a MMM is a highly desired morphology [2, 49]. A MMM of aligned platelets has an effective volume fraction (which considers the alignment of and aspect ratio of particles) that can far exceed the actual volume fraction [49]. When the pore size of such platelets is large enough to permit the desired permeant and small enough to reject the undesired permeant, MMM transport enhancements far exceed that of unity aspect ratio particles in a MMM at the same actual volume fraction [49].

The cross-sectional images of the 65 vol.% CuTPA-PVAc MMM in Figures 5.7 and 5.8 suggest a complex picture for the morphology of the MMM. The extremely high

particle loading likely resulted in a highly irregular fractured surface. However, some useful information can be drawn from the figures. There does not appear to be any voids in the either SEM. Figure 5.8 also shows a lot small debris on the surface. Although the source and make-up of this debris is unclear, it is presumably smaller shards of CuTPA from the breaking up of the larger crystals during desolvation and ultrasonic dispersion as discussed in Chapter 4.

5.3.1 Pure Gas Permeability in CuTPA-PVAc MMMs

Unlike the high loading zeolite 4A MMMs, the pure gas data of the high loading CuTPA MMMs were logical extensions of the low loading pure gas data (see Appendix B). Select results will be discussed here, but all pure gas data are provided in Appendix C. Figure 5.10 shows the pure gas data for all CuTPA MMMs on Robeson's oxygen-nitrogen upper-bound [41].

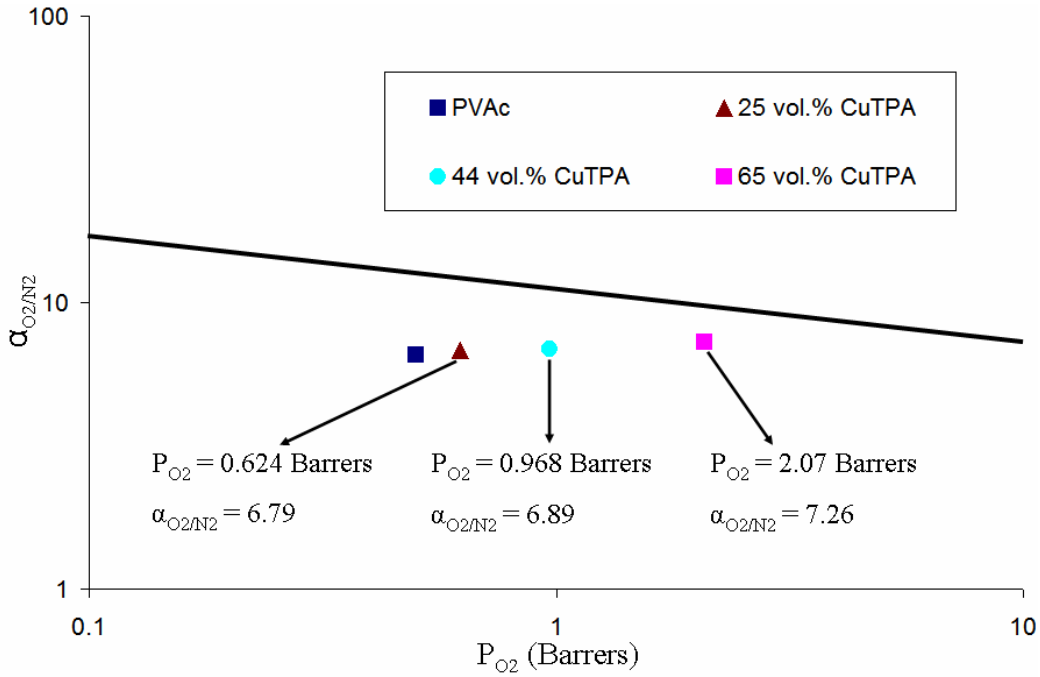

Figure 5.10: CuTPA MMM performance on O_2-N_2 upper-bound (shown as solid, black line) [41].

Figure 5.10 suggests that CuTPA-PVAc MMMs are approaching the performance of the state-of-the-art pure polymer membrane materials for selective removal of oxygen from nitrogen. Although the selectivity enhancements are modest (3.2 %, 4.9 %, and 10.5 % for 25 vol.%, 44 vol.%, and 65 vol.% MMMs, respectively), the permeation enhancements are quite large (28 %, 89 %, and 302 % for 25 vol.%, 44 vol.%, and 65 vol.% MMMs, respectively). As noted in Section 5.3, the large increases in permeability with small (relative to experimental uncertainty) changes in selectivity were exactly as anticipated.

The helium-methane gas pair transport properties are similarly impressive, and consistent with expectations, for high loading CuTPA MMMs. Figure 5.11 shows the CuTPA MMM performance on Robeson's helium-methane upper bound [41].

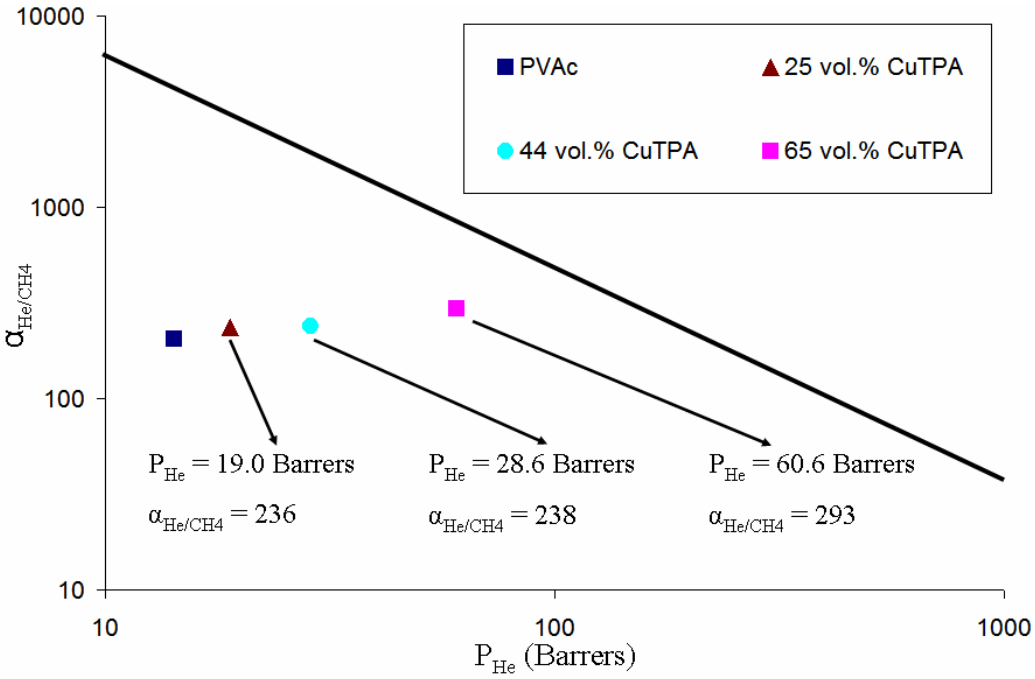

Figure 5.11: CuTPA MMM performance on He-CH_4 upper-bound (shown as solid black line) [41].

As in the oxygen-nitrogen case, the helium-methane performance of the high loading CuTPA MMMs is approaching the upper-bound. The nature of the enhancements echoes the oxygen-nitrogen case as well with modest selectivity enhancements (11 %, 12 %, and 38 % for 25 vol.%, 44 vol.%, and 65 vol.% MMMs, respectively) and substantial fast gas permeability enhancements (28 %, 94 %, and 311 % for 25 vol.%, 44 vol.%, and 65 vol.% MMMs, respectively).

Note that for each gas pair in Figures 5.9 and 5.10, there seems to be a disproportionate jump in permeability at the highest loading (65 vol.% CuTPA). Figure 5.12 shows the normalized apparent diffusivities (computed from the permeation time lags) of oxygen, nitrogen, and methane for MMMs at 25 vol.%, 44 vol.%, and 65 vol.% loadings.

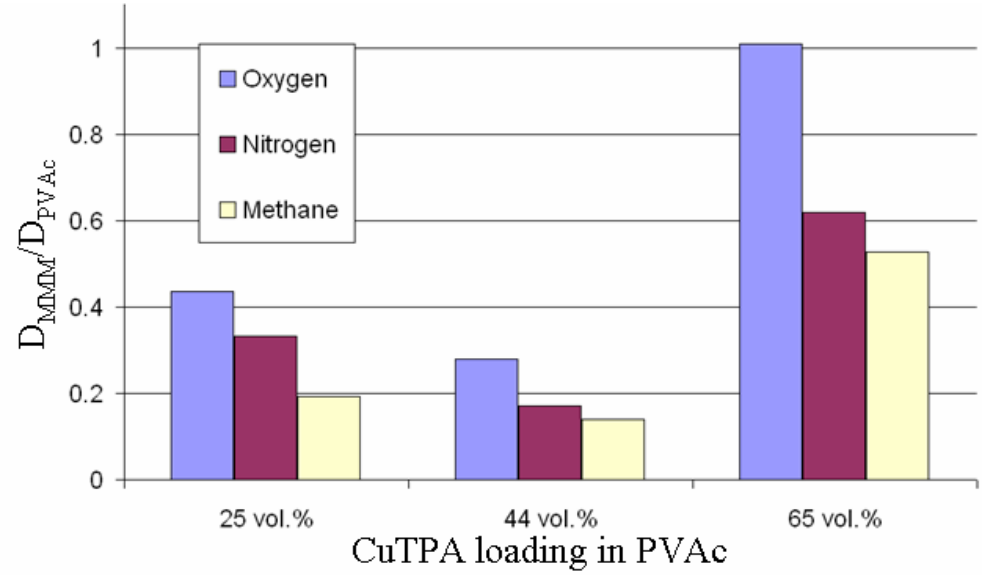

Figure 5.12: Normalized apparent diffusivities of CuTPA MMMs.

At 25 vol.% apparent diffusivity reductions are observed due to the effects of the transient filling of finite sorptive sinks in the CuTPA. These effects are magnified at 44

vol.%, i.e. higher particle loading equates to more sorptive sinks resulting in lower apparent diffusivities. This trend of lower apparent diffusivities appears to not hold at the highest CuTPA loading of 65 vol.%. This loading is well within the range of percolation (as discussed in Chapter 2 and elsewhere [50, 51]), and the SEMs in Figures 5.5 – 5.8 show large particles of stacked platelets (some approximately 10 µm and perhaps larger stacks exist elsewhere) that could act as nearly direct paths through large portions of the MMM thickness. These observations along with the disproportionate jump in permeabilities and the up-tick in apparent diffusivities at 65 vol.% suggest that CuTPA particles may begin playing a much larger role in overall transport via transport through percolated stacks of plates. Creation of a MMM where the dispersed phase dominates transport is a noteworthy achievement that has not been reported previously in the literature.

5.3.2 Low Pressure Mixture Permeation in 65 vol.% CuTPA MMMs

As described in Section 5.2.1, pure gas permeation experiments are important for basic membrane material characterization, but mixed gas experiments are a truer measure of the worth of gas separation membrane materials. To this end, low pressure mixed carbon dioxide-methane permeation experiments were carried out with the 65 vol.% CuTPA-PVAc MMM. The same conditions and mixed gas cylinder were used as in the mixed gas experiments on 50 vol.% 4A-PVAc MMMs. The results of mixed gas permeation on the high loading CuTPA MMM are organized in Table 5.3 on the next page (just as they were for the 4A MMMs in Tables 5.1 and 5.2).

Table 5.3: Low pressure mixed CO_2-CH_4 permeation data for 65 vol.% CuTPA MMM.

	P_{CO2} (Barrers)	P_{CH4} (Barrers)	$\alpha_{CO2/CH4}$
65 vol.% CuTPA MMM	9.30 ± 0.07	0.209 ± 0.007	44.5 ± 1.9
65 vol.% CuTPA/PVAc	4.32	3.25	1.33

For the low pressure mixed feed case, the carbon dioxide permeability enhancements for the 65 vol.% CuTPA MMM actually exceed those of the 50 vol.% 4A MMMs. Despite the unfavorable large pore size of the CuTPA, the 65 vol.% CuTPA MMM still offers a favorable increase in the permselectivity of carbon dioxide over methane relative to pure PVAc. However, it should be noted that the 65 vol.% CuTPA MMM provided less permselectivity enhancement than its high loading 4A counterpart (33 % versus 47 %) presumably since the zeolite 4A sieves offer both size discrimination and solubility selectivity advantages.

Although the performance of the high loading CuTPA MMM still falls short of high performance pure polymers (carbon dioxide permeabilities of high performance polymers are approximately 6 – 7 times higher for the same separation factor) [41], these results represent a drastic improvement over pure PVAc properties and show the basic principle pursued in this thesis. Moreover, the ability to enhance solubility selectivities of rigid chain, diffusion selective polymers on the upper-bound is an attractive avenue to pursue.

5.3.3 High Pressure Mixture Permeation in 65 vol.% CuTPA MMMs

The same cylinder of a 50:50 mixture of carbon dioxide and methane that was used for the materials in Section 5.2.2 was used for 440 psia total pressure mixed gas

permeation experiments on the 65 vol.% CuTPA-PVAc MMMs. Results of these experiments are provided in Table 5.4.

Table 5.4: Transport summary of high pressure mixed CO_2-CH_4 permeation.

	P_{CO2} (Barrers)	P_{CH4} (Barrers)	$\alpha_{CO2/CH4}$
65 vol.% CuTPA MMM	9.12 ± 0.02	0.292 ± 0.015	31.3 ± 1.7
65 vol.% CuTPA/PVAc	0.797	0.595	1.26

The 65 vol.% CuTPA-PVAc MMM did not fare as well as its high loading 4A counterpart under the high pressure mixed feed condition. Carbon dioxide and methane permeabilities were reduced by 20 % and 40 %, respectively, compared to pure PVAc at the same feed conditions. At the low pressure mixed feed condition, large permeability enhancements were observed for both penetrants. As with the high loading 4A MMM this discrepancy is due to both increased permeabilities in plasticized PVAc as well as Langmuir saturation in the molecular sieve crystals. Permselectivity of carbon dioxide over methane was improved 26 % over pure PVAc whereas a 33 % enhancement was observed in the low pressure mixed feed case. Note that the standard deviations in Table 5.3 and 5.4 are only rough estimates of error since no more than 7 repeat measurements were made (see Section 3.2 for more details). The low and high pressure mixed gas performance of the 65 vol.% CuTPA MMMs are compared to Robeson's upper-bound in Figure 5.13.

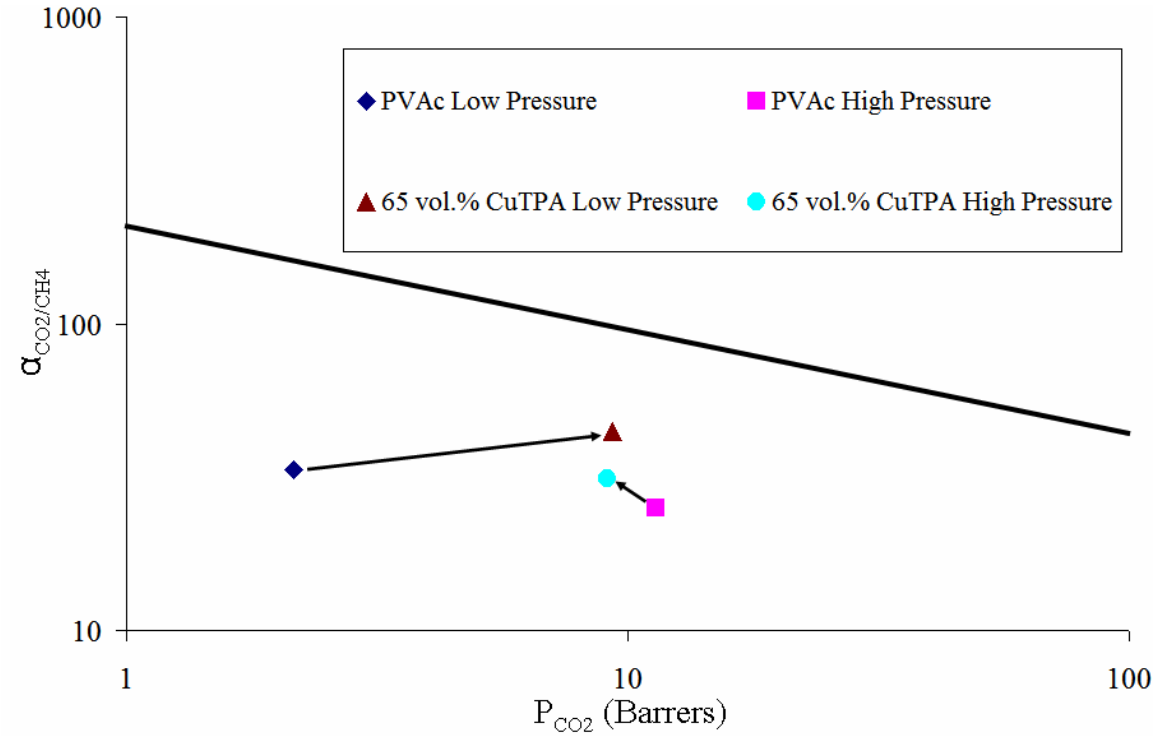

Figure 5.13: Pure PVAc and 65 vol.% CuTPA MMM performance vs. Robeson's 2008 upper-bound (shown as solid, black line) [41].

With regards to desired permeant permeability and separation factor, 65 vol.% CuTPA MMM performance under the aggressive, high pressure mixed feed was worse than at the low pressure mixed feed condition. This is contrary to the behavior of the 50 vol.% zeolite 4A-PVAc MMM; however, permselectivities were enhanced relative to pure PVAc for both the low pressure and high pressure mixed gas cases.

5.4 Conclusions

The investigation of high molecular sieve loading MMM transport properties produced extremely interesting and promising results. Section 5.2 showed that the parameters for void-free formation of high commercial zeolite 4A MMMs identified in Chapter 4 lead to impressive transport enhancements when a "healthy" batch of zeolite 4A is used. Impressive mixed carbon dioxide-methane separation properties were

attained for high loading zeolite 4A MMMs. Not only was the performance of 50 vol.% zeolite 4A-PVAc MMMs excellent at mild mixed gas conditions, the performance was even better for the more challenging high pressure mixed gas case. This was a surprising and pleasant discovery.

In Section 5.3, formation of void-free, high loading CuTPA-PVAc MMMs using the same principles for void-free formation of high loading zeolite 4A-PVAc MMMs suggests that the parameters and procedures identified in Chapter 4 (i.e. initial solvent concentration and annealing temperature) may have general applicability. Pure gas permeation of high loading CuTPA MMMs yielded expected results—with increased loading, increased permeabilities were measured for all gases. Furthermore, there was evidence of a shift towards CuTPA dominated transport at 65 vol.% CuTPA in PVAc as witnessed by the disproportionate jump in permeabilities and the apparent diffusivity trend. In fact, the oxygen-nitrogen and helium-methane performances of the 65 vol.% CuTPA-PVAc MMMs were competitive with upper-bound pure polymer membranes.

Although the excellent permeability and permselectivity enhancements observed for the high loading (and lower loading) CuTPA MMMs are very much desired properties, they raise important questions about the nature of gas transport in MMMs. As mentioned previously, the large pore channel size of CuTPA should not impart greatly improved diffusive selectivities on the PVAc matrix, yet impressive permselectivity enhancements were observed for CuTPA MMMs. It is not totally clear why the high loading CuTPA MMMs showed poorer performance for the high pressure mixed carbon dioxide-methane case than the low pressure mixed gas case (see Figure 5.13) while the high loading 4A MMMs displayed the opposite behavior (see Figure 5.4). One might

tentatively conclude that the sieve-polymer segment interactions were more favorable in the case of zeolite 4A versus CuTPA, and that this suppressed interfacial polymer chain plasticization for the zeolite 4A MMMs. However, this cannot be proven at this time. The large pore size of CuTPA would be expected to give larger permeability enhancements than the smaller pore size of zeolite 4A, and this is observed with the exception of high pressure mixed gas case. This exception suggests that gas solubility behavior may play a more significant role in overall transport behavior in MMMs than previously thought.

While the results of Chapter 5 were overwhelmingly positive, they raise many questions related to gas transport in MMMs as functions of molecular sieve pore size and the gas solubility properties of molecular sieves. These interesting results are explored in much greater depth in Chapter 6 where low molecular sieve loading MMMs are made with various pore size molecular sieves and investigated with pure gas permeation experiments.

5.5 References

[1] Zimmerman, C.M., R. Mahajan, and W.J. Koros, *Fundamental and practical aspects of mixed matrix gas separation membranes.* Abstracts of Papers of the American Chemical Society, 1997. **214**: p. 270-PMSE.

[2] Koros, W.J. and T.T. Moore. *Organic-inorganic hybrid membrane materials for gas separation*. 2003.

[3] Zimmerman, C.M., A. Singh, and W.J. Koros, *Tailoring mixed matrix composite membranes for gas separations.* Journal of Membrane Science, 1997. **137**(1-2): p. 145-154.

[4] Kulprathipanja, S., *Separation of fluids by means of mixed matrix membranes*, U.S.P. Office, Editor. 1988.

[5] Jia, M.D., K.V. Peinemann, and R.D. Behling, *Molecular-sieving effect of the zeolite-filled silicone-rubber membranes in gas permeation.* Journal of Membrane Science, 1991. **57**(2-3): p. 289-296.

[6] Tehennepe, H.J.C., D. Bargeman, M.H.V. Mulder, and C.A. Smolders, *Zeolite-filled silicone-rubber membranes .1. Membrane preparation and pervaporation results.* Journal of Membrane Science, 1987. **35**(1): p. 39-55.

[7] Clarizia, G., C. Algieria, and E. Drioli, *Filler-polymer combination: A route to modify gas transport properties of a polymeric membrane.* Polymer, 2004. **45**(16): p. 5671-5681.

[8] Chung, T.S., L.Y. Jiang, Y. Li, and S. Kulprathipanja, *Mixed matrix membranes (mmms) comprising organic polymers with dispersed inorganic fillers for gas separation.* Progress in Polymer Science, 2007. **32**(4): p. 483-507.

[9] Li, Y., T.S. Chung, C. Cao, and S. Kulprathipanja, *The effects of polymer chain rigidification, zeolite pore size and pore blockage on polyethersulfone (pes)-zeolite a mixed matrix membranes.* Journal of Membrane Science, 2005. **260**(1-2): p. 45-55.

[10] Mahajan, R. and W.J. Koros, *Mixed matrix membrane materials with glassy polymers. Part 1.* Polymer Engineering and Science, 2002. **42**(7): p. 1420-1431.

[11] Mahajan, R. and W.J. Koros, *Mixed matrix membrane materials with glassy polymers. Part 2.* Polymer Engineering and Science, 2002. **42**(7): p. 1432-1441.

[12] Moore, T.T. and W.J. Koros, *Gas sorption in polymers, molecular sieves, and mixed matrix membranes.* Journal of Applied Polymer Science, 2007. **104**(6): p. 4053-4059.

[13] Moore, T.T., R. Mahajan, D.Q. Vu, and W.J. Koros, *Hybrid membrane materials comprising organic polymers with rigid dispersed phases.* Aiche Journal, 2004. **50**(2): p. 311-321.

[14] Moore, T.T., T. Vo, R. Mahajan, S. Kulkarni, D. Hasse, and W.J. Koros, *Effect of humidified feeds on oxygen permeability of mixed matrix membranes.* Journal of Applied Polymer Science, 2003. **90**(6): p. 1574-1580.

[15] Hillock, A.M.W., S.J. Miller, and W.J. Koros, *Crosslinked mixed matrix membranes for the purification of natural gas: Effects of sieve surface modification.* Journal of Membrane Science, 2008. **314**(1-2): p. 193-199.

[16] Husain, S. and W.J. Koros, *Mixed matrix hollow fiber membranes made with modified hssz-13 zeolite in polyetherimide polymer matrix for gas separation.* Journal of Membrane Science, 2007. **288**(1-2): p. 195-207.

[17] Yong, H.H., N.C. Park, Y.S. Kang, J. Won, and W.N. Kim, *Zeolite-filled polyimide membrane containing 2,4,6-triaminopyrimidine.* Journal of Membrane Science, 2001. **188**(2): p. 151-163.

[18] Duval, J.M., B. Folkers, M.H.V. Mulder, G. Desgrandchamps, and C.A. Smolders, *Adsorbent filled membranes for gas separation .1. Improvement of the gas separation properties of polymeric membranes by incorporation of microporous adsorbents.* Journal of Membrane Science, 1993. **80**: p. 189-198.

[19] Tantekin-Ersolmaz, S.B., C. Atalay-Orala, M. Tather, A. Erdem-Senatalar, B. Schoeman, and J. Sterte, *Effect of zeolite particle size on the performance of polymer-zeolite mixed matrix membranes.* Journal of Membrane Science, 2000. **175**(2): p. 285-288.

[20] Wang, H.T., B.A. Holmberg, and Y.S. Yan, *Homogeneous polymer-zeolite nanocomposite membranes by incorporating dispersible template-removed zeolite nanocrystals.* Journal of Materials Chemistry, 2002. **12**(12): p. 3640-3643.

[21] Suer, M.G., N. Bac, and L. Yilmaz, *Gas permeation characteristics of polymer-zeolite mixed matrix membranes.* Journal of Membrane Science, 1994. **91**(1-2): p. 77-86.

[22] Breck, D.W., W.G. Eversole, and R.M. Milton, *New synthetic crystalline zeolites.* Journal of the American Chemical Society, 1956. **78**(10): p. 2338-2339.

[23] Mahajan, R., *Formation, characterization, and modeling of mixed matrix membrane materials*. 2000, The University of Texas at Austin, Ph.D. Thesis.

[24] Li, Y., H.M. Guan, T.S. Chung, and S. Kulprathipanja, *Effects of novel silane modification of zeolite surface on polymer chain rigidification and partial pore blockage in polyethersulfone (pes)-zeolite a mixed matrix membranes.* Journal of Membrane Science, 2006. **275**(1-2): p. 17-28.

[25] Huang, Z., Y. Li, R. Wen, M.M. Teoh, and S. Kulprathipanja, *Enhanced gas separation properties by using nanostructured pes-zeolite 4a mixed matrix membranes.* Journal of Applied Polymer Science, 2006. **101**(6): p. 3800-3805.

[26] Hu, C.C., T.C. Liu, K.R. Lee, R.C. Ruaan, and J.Y. Lai. *Zeolite-filled pmma composite membranes: Influence of coupling agent addition on gas separation properties*. 2006: Elsevier Science Bv.

[27] Shu, S., *Engineering the performance of mixed matrix membranes for gas separations*. 2007, Georgia Institute of Technology, Ph.D. Thesis.

[28] Kesting, R.E. and A.K. Fritzsche, *Polymeric gas separation membranes*. 1993: John Wiley & Sons, Inc.

[29] Koros, W.J. and G.K. Fleming, *Membrane-based gas separation.* Journal of Membrane Science, 1993. **83**(1): p. 1-80.

[30] Smith, J.M., H.C. Van Ness, and M.M. Abbott, *Chemical engineering thermodynamics*. 6th ed. 2001: McGraw-Hill.

[31] Koros, W.J., D.R. Paul, and A.A. Rocha, *Carbon-dioxide sorption and transport in polycarbonate.* Journal of Polymer Science Part B-Polymer Physics, 1976. **14**(4): p. 687-702.

[32] Koros, W.J. and D.R.B. Walker. *Gas separation membrane material selection criteria - weakly and strongly interacting feed component situations*. 1991.

[33] White, L.S., T.A. Blinka, H.A. Kloczewski, and I.F. Wang, *Properties of a polyimide gas separation membrane in natural-gas streams.* Journal of Membrane Science, 1995. **103**(1-2): p. 73-82.

[34] Bakker, W.J.W., F. Kapteijn, J. Poppe, and J.A. Moulijn, *Permeation characteristics of a metal-supported silicalite-1 zeolite membrane.* Journal of Membrane Science, 1996. **117**(1-2): p. 57-78.

[35] Bos, A., I.G.M. Punt, M. Wessling, and H. Strathmann, *Co2-induced plasticization phenomena in glassy polymers.* Journal of Membrane Science, 1999. **155**(1): p. 67-78.

[36] Baker, R.W., *Future directions of membrane gas separation technology*. Industrial & Engineering Chemistry Research, 2002. **41**(6): p. 1393-1411.

[37] Wind, J.D., S.M. Sirard, D.R. Paul, P.F. Green, K.P. Johnston, and W.J. Koros, *Carbon dioxide-induced plasticization of polyimide membranes: Pseudo-equilibrium relationships of diffusion, sorption, and swelling.* Macromolecules, 2003. **36**(17): p. 6433-6441.

[38] Bhide, B.D. and S.A. Stern, *Membrane processes for the removal of acid gases from natural-gas .2. Effects of operating-conditions, economic-parameters, and membrane-properties.* Journal of Membrane Science, 1993. **81**(3): p. 239-252.

[39] Baker, R.W. and K. Lokhandwala, *Natural gas processing with membranes: An overview*. Industrial & Engineering Chemistry Research, 2008. **47**(7): p. 2109-2121.

[40] Lively, R.P., R.R. Chance, B.T. Kelley, H.W. Deckman, J.H. Drese, C.W. Jones, and W.J. Koros, *Hollow fiber adsorbents for co2 removal from flue gas.* Industrial & Engineering Chemistry Research, 2009. **48**(15): p. 7314-7324.

[41] Robeson, L.M., *The upper bound revisited.* Journal of Membrane Science, 2008. **320**(1-2): p. 390-400.

[42] Mahajan, R., R. Burns, M. Schaeffer, and W.J. Koros, *Challenges in forming successful mixed matrix membranes with rigid polymeric materials.* Journal of Applied Polymer Science, 2002. **86**(4): p. 881-890.

[43] Shu, S., S. Husain, and W.J. Koros, *A general strategy for adhesion enhancement in polymeric composites by formation of nanostructured particle surfaces.* Journal of Physical Chemistry C, 2007. **111**(2): p. 652-657.

[44] Car, A., C. Stropnik, and K.V. Peinemann, *Hybrid membrane materials with different metal-organic frameworks (mofs) for gas separation.* Desalination, 2006: p. 424-426.

[45] Zhang, Y.F., I.H. Musseman, J.P. Ferraris, and K.J. Balkus, *Gas permeability properties of matrimid (r) membranes containing the metal-organic framework cu-bpy-hfs.* Journal of Membrane Science, 2008. **313**(1-2): p. 170-181.

[46] Perez, E.V., K.J. Balkus, J.P. Ferraris, and I.H. Musselman, *Mixed-matrix membranes containing mof-5 for gas separations.* Journal of Membrane Science, 2009. **328**(1-2): p. 165-173.

[47] Adams, R.T., C.G. Carson, J.K. Ward, R. Tannenbaum, and W.J. Koros, *Metal organic framework mixed matrix membranes for gas separations.* Microporous and Mesoporous Materials, 2009. **in press**.

[48] Carson, C.G., *Personal communication*. 2009.

[49] Johnson, J.R. and W.J. Koros, *Utilization of nanoplatelets in organic-inorganic hybrid separation materials: Separation advantages and formation challenges.* Journal of the Taiwan Institute of Chemical Engineers, 2009. **40**(3): p. 268-275.

[50] Scott, G.D., *Packing of equal spheres.* Nature, 1960. **188**(4754): p. 908-909.

[51] Fishman, R.S., D.A. Kurtze, and G.P. Bierwagen, *Pigment inhomogeneity and void formation in organic coatings.* Progress in Organic Coatings, 1993. **21**(4): p. 387-403.

CHAPTER 6

EFFECTS OF MOLECULAR SIEVE PORE SIZE ON MMM PERMEATION PROPERTIES

6.1 Introduction

Among the excellent properties observed and discussed in Chapter 5, there were some surprising results that suggest a better understanding of the effects of molecular sieve pore size on MMM gas transport properties is needed for designing ideal MMMs. In Chapter 2, Sections 2.3.2 and 2.3.3 discuss the difficulties of measuring gas diffusivities and permeabilities in molecular sieves. Section 2.4.2 illustrates the complexity of diffusivity in MMMs even if pure molecular sieve transport properties are known. The difficulties of measuring diffusivities in molecular sieves and MMM as well as the lack of an adequate framework for predicting MMM permeation properties necessitates an experimental screening of molecular sieve materials for use in MMMs that focuses on varying molecular sieve pore size.

In this Chapter, a series of low particle loading MMMs are made with molecular sieves of various pore dimensions. By using PVAc, which is known to adhere well to many fillers in MMMs [1-3] interfacial non-idealities are avoided. Firstly, attempts were made to engineer better MMMs by adjusting the pore size of zeolite 4A (a well studied molecular sieve in MMM applications)—Section 6.2 discusses these efforts. Section 6.3 is a survey of the overall transport properties of MMMs containing molecular sieves where pore sizes vary from 3.3 – 7.4 Å. Conclusions are drawn in Section 6.4.

6.2 Partial K^+ Exchanged Zeolite A MMMs

Chapter 5 showed that the pure gas permeability enhancements of CuTPA MMMs were quite high at all loadings and increased with increased loading. These observations are perfectly consistent with the conventional expectation that large pore size molecular sieves will give large enhancements in permeabilities [4-9]. However, the permselectivity enhancements for MMMs containing the large pore size CuTPA MOF are surprising, especially for the carbon dioxide-methane mixed feed cases, and are contrary to the conventional expectation that large pore accesses should not provide improved diffusive selectivities. In efforts to better understand how pore sizes affect the permselectivities of MMMs, 2 novel molecular sieves were made and studied in MMM permeation tests. Two different partially K^+ exchanged zeolite 4A batches were made, and their MMM transport properties are discussed below.

Yeh and Yang conducted an interesting study on the diffusion and adsorption properties of mixed Na^+/K^+ zeolite A [10, 11]. They were, in effect, creating zeolite A materials with pore sizes that fell between the pore sizes of zeolite 3A and zeolite 4A molecular sieves. A sample of their data is provided in Figure 6.1.

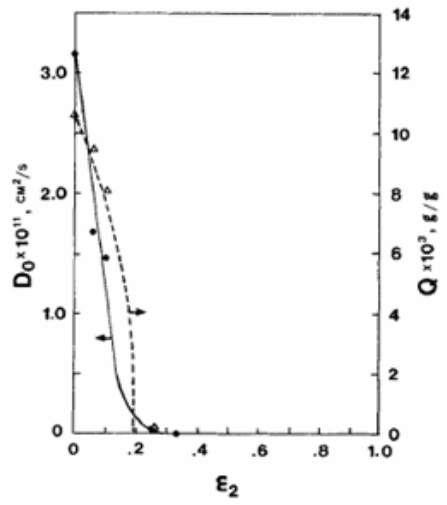

Figure 6.1: Methane diffusivity, D_o, and adsorption capacity, Q, plotted against fractional K^+ exchange, ε_2, (molar equivalent basis) of zeolite 4A. From Yeh & Yang [11].

The same data were generated for carbon dioxide, and it was shown that a properly tuned partial K^+ exchange of zeolite 4A could effectively block methane access while permitting CO_2 without taking zeolite A all the way to 3A where diffusion is undesirably low, with ultimate effective transport properties like the totally blocked ASGE zeolite 4A discussed in Chapter 4. Our goal was to do precisely the same "tuning" but for application in MMMs. By severely hindering access of methane while leaving carbon dioxide relatively unrestricted, the ability for molecular sieve particles to improve the diffusive selectivity of the host polymer matrix in a MMM will be put to the test.

One batch each of 13.1 % (#1) and 6.76 % (#2) K^+/Na^+ balance zeolite A molecular sieves were made as described in Chapter 3, and a 15 wt.% MMM in PVAc was made for each. Note that the percentages for samples #1 and #2 above are based on nominal molar equivalent loadings as described in Chapter 3. Actual extent of K^+ exchange was determined by elemental analysis from inductively coupled plasma (ICP)

mass spectrometry and the results for zeolite 4A and each partially K^+ exchanged batch are provided in Table 6.1.

Table 6.1: ICP elemental analysis of zeolite 4A and partially K^+ exchanged zeolite 4A.

	Silicon (wt. %)	Aluminum (wt. %)	Sodium (wt. %)	Potassium (wt. %)
Zeolite 4A	27.64	17.50	11.93	< 1.1
Partial K^+ # 1	27.08	17.39	8.98	2.87
Partial K^+ # 2	23.50	16.70	8.59	1.95

The results of elemental analysis confirm a good ion exchange procedure. The normalized transport data (i.e. MMM value divided by pure PVAc value) are presented in the following figures (raw data with errors are provided in Appendix D) and the zeolites are arranged in the order of increasing expected pore size, i.e. 13.1 % K^+/Na^+ balance zeolite A (smallest pore), 6.76 % K^+/Na^+ balance zeolite A (intermediate pore), and zeolite 4A (largest pore).

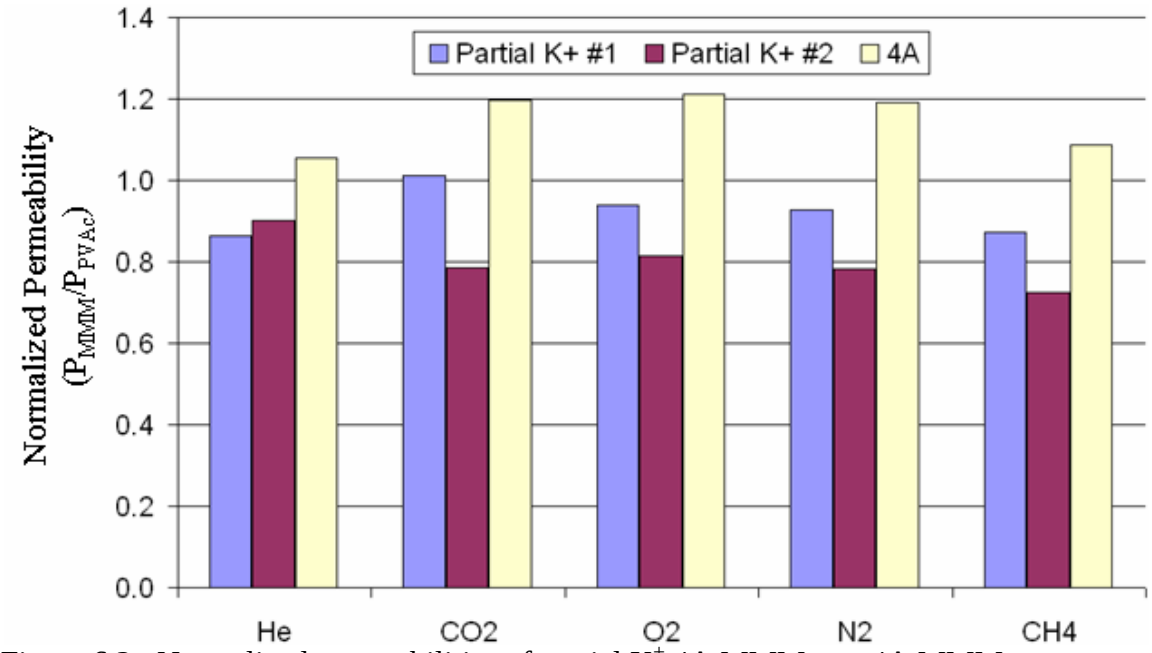

Figure 6.2: Normalized permeabilities of partial K^+ 4A MMMs vs. 4A MMMs.

Comparison of MMMs of any one batch of partially K^+ exchanged 4A versus zeolite 4A MMMs gives anticipated results; however, comparison of both batches simultaneously does not provide the expected results. Both batches of partially K^+ exchanged 4A MMMs give permeabilities that are lower than their 4A MMMs counterparts as expected since smaller pore type-A zeolites should have lower permeabilities. It is unclear why the partial K^+ #2 MMM had the lowest permeabilities for carbon dioxide, oxygen, nitrogen, and methane as its pore was expected to have an "intermediate" pore size; however, the "smallest" pore molecular sieve (partial K^+ #1) MMM did provide the lowest helium permeability. This inconsistency may be attributable to solubility effects; unfortunately time and material constraints did not allow for a sorption study on the partially ion exchanged 4A samples.

Normalized apparent diffusivities are summarized in Figure 6.3 on the following page.

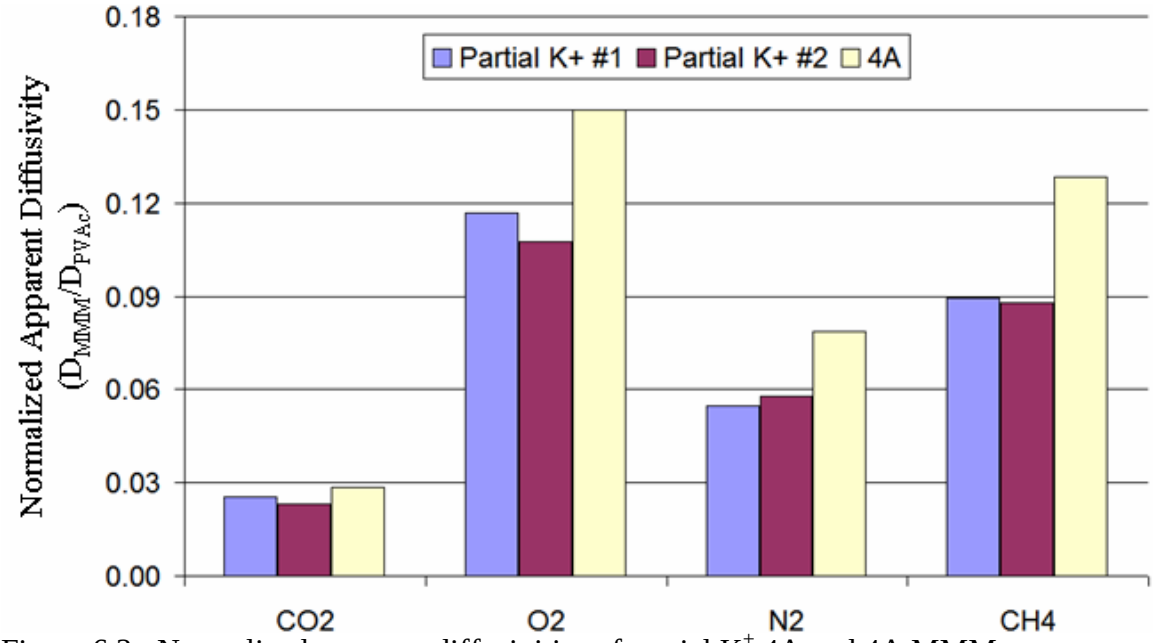

Figure 6.3: Normalized apparent diffusivities of partial K^+ 4A and 4A MMMs.

Figure 6.3 shows at least one noteworthy feature—the partially K^+ exchanged 4A MMMs show lower apparent diffusivities than the 4A MMMs. Based on the concept of site filling sorption during the permeation time lag for MMMs as discussed in Chapter 2, this suggests that the presence of K^+ ions in the zeolite A framework results in higher gas solubilities than Na^+ alone. As mentioned previously, gas solubilities were not measured for the partial K^+ exchanged zeolite samples, but this trend does match observations that increasing electronegativity of the cation in zeolite frameworks increases sorption affinities (the parameter, *b*, in Equation 2.4) [12]. However, the presence of K^+ ions, which are larger than Na^+ ions, actually reduces overall space available for sorption, i.e. lower Langmuir saturation constants ($C_H^{'}$ in Equation 2.4).

In other words, while the values in Figure 6.3 suggest that the partially ion exchanged zeolites have sorption properties that magnify the effects of site filling during the permeation time lag, gas solubilities were not directly measured and considering the

error associated with the time lag method, the small discrepancies in apparent diffusivities between the two partially K^+ exchanged zeolite A batches may not be significant. Furthermore, the phenomenon of site filling sorption during the permeation time lag does not necessarily outweigh the possibility that the low apparent diffusivities for the partially K^+ exchanged zeolite A MMMs are lower because actual diffusivities in these smaller pore zeolites are lower than those of zeolite 4A. There are multiple complex issues that can alter the apparent diffusivities of gases in MMMs. Molecular sieve pore sizes and gas solubilities are two such complex issues.

The permeability reductions for the partially K^+ exchanged zeolite A MMMs were expected. The main motivation for this study was to make zeolite A MMMs with enhanced permselectivities over zeolite 4A MMMs of the same particle loading by virtue of restricting methane diffusivity more than carbon dioxide diffusivity. Figure 6.4 summarizes the observed normalized selectivities. Note that Δd_k is the difference in kinetic diameters of a given gas pair (see Table 6.3)

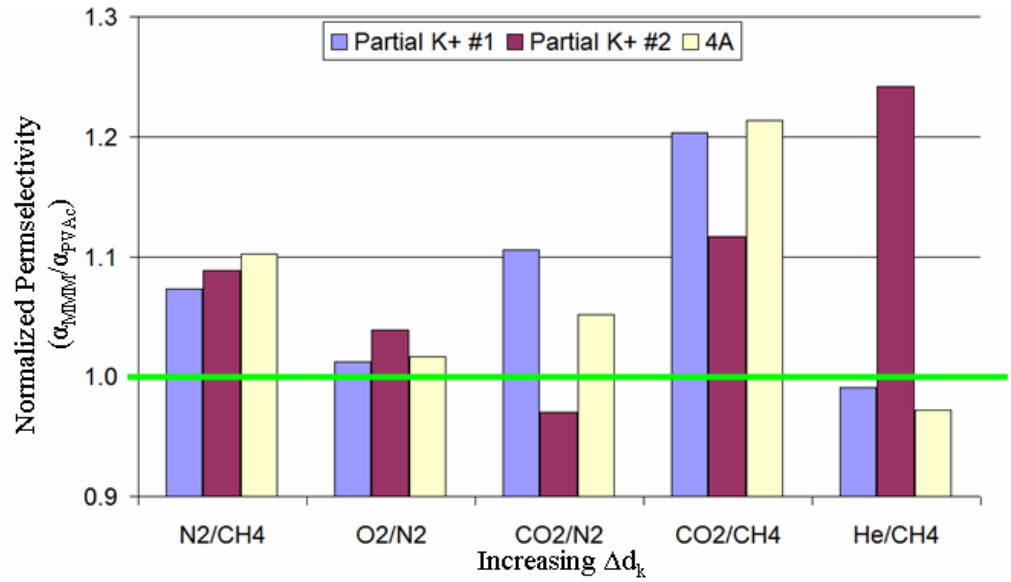

Figure 6.4: Normalized selectivities of partial K^+ 4A and 4A MMMs.

Unfortunately, the selectivity changes for the partially K^+ exchanged samples were not general improvements over 4A MMMs thereby suggesting that permselectivity enhancements in MMMs are, at the very least, not entirely due to improvements in diffusive selectivities as noted above. However, the partially K^+ exchanged zeolite A MMMs do provide the greatest selectivity enhancements over pure PVAc in 3 of the 6 gas pairs investigated suggesting that the desired result of improved selectivities was achieved. While the greatest permselectivity enhancements were observed for the gas pairs with the greatest Δd_k (i.e. the carbon dioxide-methane and helium-methane pairs), there was neither a general trend of improved permselectivities with increasing Δd_k nor a specific trend of improved permselectivities with increasing Δd_k for any given MMM. In both glassy polymers and molecular sieves, separation efficiency is shown to scale well with Δd_k [13-15].

While the results of the ion exchange study were ambiguous, many predictable results were attained. Partially K^+ exchanging undoubtedly reduces gas permeabilities compared to MMMs with the larger pore molecular sieve, zeolite 4A. This observation is completely consistent with traditional MMM wisdom. The partial K^+ exchanged samples had the best permselectivity enhancements in most cases, further supporting the conventional expectation that small pore molecular sieves are best for improving the permselectivities of small gas pairs. This "model" study of the effects of pore size on MMM permeation properties, perhaps, supports the complexity first seen in the CuTPA MMMs in Chapter 5. The facts that MMMs of the smaller pore window zeolites generally gave the lowest permeabilities, and that a MMM of a small pore molecular sieve gave the overall greatest permselectivity enhancement for the gas pair with largest

size discrepancy (i.e. the helium-methane pair), are not surprising. On the other hand the MMMs with the largest pore size molecular sieve, zeolite 4A, gave the best permselectivity enhancement for the gas pair with next largest size discrepancy (i.e. the carbon dioxide-methane pair), suggesting that gas solubilities in MMMs must be included in any complete analysis of MMM materials, as opposed to a strict, "size only" approach.

6.3 Overall Gas Transport Properties of 15 wt.% MMMs

The diverse array of molecular sieves described in Table 3.2 (see Chapter 3) were used to make 15 wt.% MMMs in PVAc. Table 3.2 organizes the sieves in order of increasing pore window size zeolite 3A is the smallest at 3.3 Å and zeolite NaY is the largest at 7.4 Å. Note that CVX7 has a slit-shaped pore that makes comparison to the aspect ratio 1 pores of the other molecular sieves investigated somewhat difficult so the various sieves are ranked based "pore area" (smallest pore dimension multiplied by largest pore dimension). Table 6.2 on the following page summarizes all of the transport data for the MMMs made from molecular sieves in Table 3.2 as well as pure PVAc. The following subsections discuss the observed trends in normalized MMM permeabilities, apparent diffusivities, and permselectivities of pure gases measured at 65 psia except carbon dioxide at 1.3 – 1.4 psia (as described in Chapter 3). Normalized MMM properties are simply MMM permeabilities, apparent diffusivities, and permselectivities divided through by their pure PVAc counterparts. Recall that apparent diffusivities reported in Table 6.2 are computed from permeation time lags with Equation 2.12. Note that standard deviations in Table 6.2 are only rough estimates of error since no more than 7 repeat measurements were made (see Section 3.2 for more details).

Table 6.2: PVAc and 15 wt.% MMM Transport Data Summary. P [=] Barrers, D [=] cm^2/s.
Values ± 1 standard deviation (except where only 1 sample tested).

	P_{He}	P_{CO2}	P_{O2}	P_{N2}	P_{CH4}	D_{CO2}	D_{O2}	D_{N2}	D_{CH4}	$\alpha_{CO2/N2}$	$\alpha_{O2/N2}$	$\alpha_{CO2/CH4}$	$\alpha_{N2/CH4}$	$\alpha_{He/CH4}$
PVAc	14.8 ± 0.9	2.50 ± 0.25	0.501 ± 0.038	0.0762 ± 0.0067	0.0697 ± 0.0034	$6.2 \times 10^{-9} \pm 4.8 \times 10^{-10}$	$4.5 \times 10^{-8} \pm 3.3 \times 10^{-9}$	$1.2 \times 10^{-8} \pm 5.1 \times 10^{-10}$	$2.9 \times 10^{-9} \pm 2.7 \times 10^{-10}$	34.0 ± 3.4	6.58 ± 0.12	34.9 ± 2.9	1.09 ± 0.04	212 ± 1.8
Zeolite 3A	12.7 ± 2.2	Not Tested	0.441 ± 0.051	0.0678 ± 0.0078	0.0599 ± 0.0067	n/a	$5.2 \times 10^{-8} \pm 7.7 \times 10^{-9}$	$1.5 \times 10^{-8} \pm 5.7 \times 10^{-10}$	$2.9 \times 10^{-9} \pm 1.3 \times 10^{-10}$	n/a	6.54 ± 0.10	n/a	1.13 ± 0.03	211 ± 16.4
Zeolite 4A	14.2 ± 1.1	2.71 ± 0.33	0.562 ± 0.103	0.0829 ± 0.0144	0.0697 ± 0.0097	$1.2 \times 10^{-10} \pm 1.1 \times 10^{-11}$	$6.4 \times 10^{-9} \pm 1.1 \times 10^{-9}$	$7.6 \times 10^{-10} \pm 1.4 \times 10^{-10}$	$3.0 \times 10^{-10} \pm 7.6 \times 10^{-11}$	34.9 ± 3.5	6.77 ± 0.08	40.8 ± 2.2	1.19 ± 0.05	206 ± 15.6
Zeolite 5A	20.1	3.00	0.630	0.0938	0.0799	3.8×10^{-10}	1.5×10^{-8}	1.6×10^{-9}	5.5×10^{-10}	32.0	6.72	37.6	1.17	252
CVX7	21.4 ± 1.0	3.07	0.657 ± 0.034	0.0950 ± 0.0044	0.0789 ± 0.0018	1.9×10^{-9}	$8.4 \times 10^{-9} \pm 2.9 \times 10^{-10}$	$1.3 \times 10^{-9} \pm 7.4 \times 10^{-11}$	$2.8 \times 10^{-10} \pm 3.3 \times 10^{-11}$	31.3	6.92 ± 0.037	38.2	1.20 ± 0.0278	271 ± 6.4
CuTPA	19.0 ± 0.5	3.26 ± 0.23	0.624 ± 0.026	0.0918 ± 0.0031	0.0806 ± 0.0035	$5.1 \times 10^{-9} \pm 1.5 \times 10^{-9}$	$2.0 \times 10^{-8} \pm 1.0 \times 10^{-8}$	$4.1 \times 10^{-9} \pm 2.9 \times 10^{-9}$	$5.7 \times 10^{-10} \pm 1.5 \times 10^{-10}$	35.4 ± 1.7	6.79 ± 0.14	40.4 ± 2.5	1.14 ± 0.02	236 ± 11.8
Zeolite NaY	27.3 ± 1.2	3.99 ± 0.09	0.918 ± 0.085	0.133 ± 0.007	0.107 ± 0.008	$5.5 \times 10^{-10} \pm 1.1 \times 10^{-11}$	$1.9 \times 10^{-8} \pm 4.1 \times 10^{-9}$	$2.2 \times 10^{-9} \pm 7.1 \times 10^{-10}$	$7.9 \times 10^{-10} \pm 1.6 \times 10^{-10}$	31.2 ± 0.1	6.84 ± 0.35	39.7 ± 1.0	1.25 ± 0.03	257 ± 14.7

6.3.1 Gas Permeabilities of 15 wt.% MMMs

Figure 6.5 shows normalized 15 wt.% MMM permeabilities with increasing molecular sieve pore window size on the x-axis.

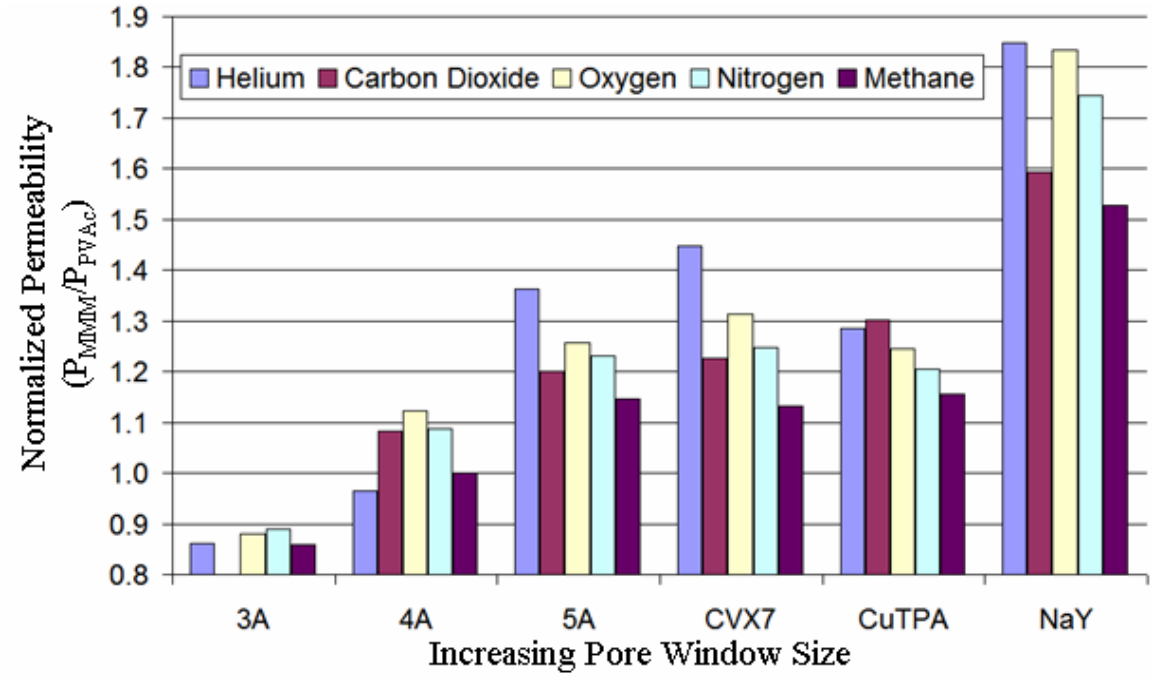

Figure 6.5: Normalized permeabilities of 15 wt.% PVAc MMMs.

A general trend of increasing permeabilities with increasing molecular sieve pore window size is observed. This trend confirms the expectation that larger pore molecular sieves give rise to greater permeability enhancements in MMMs. CuTPA MMMs are the one exception—this is likely attributable to the relatively low adsorption capacities of these gases in CuTPA (see Appendix A). Various other important observations can be made from this survey as well.

Zeolite 3A MMMs were the only MMMs to not enhance permeability. According to Breck, all gases except helium should be rejected from the small 3.3 Å pore window

[16]. The permeability decreases in the zeolite 3A MMMs are approximately equal for all gases tested. This trend is consistent with the additive sorption theory for MMMs discussed in Chapters 2 and 4 (see Equation 2.13)—since the gases are rejected from the sieve, permeability should decrease the same for all gases. In fact, the fractional permeability reductions in zeolite 3AMMMs are almost exactly equal (14 %, 12 %, 11 %, and 14 % for helium, oxygen, nitrogen, and methane, respectively) and nearly exactly match with the expected solubility reductions for an impermeable filler particle at this loading (13 % reduction expected based on Equation 2.13). Also recall that the "bad" commercial zeolite 4A used for MMMs in Chapter 4 showed a similar trend which emphasizes that impermeable fillers (or those with highly restricted access) reduce permeabilities by adding tortuousity and reducing solubility.

Permeability trends for zeolite 4A (in-house synthesized) MMMs are somewhat more confusing. Helium permeability is the least enhanced despite being the smallest gas permeated. This apparent discrepancy may be due to gas solubility effects. Aside from helium, permeability enhancements generally decrease with increasing kinetic diameters of the gases. Table 6.3 below summarizes the dimensions of the gases used.

Table 6.3: Kinetic diameters of gases used in permeation and sorption experiments.

	Helium	Carbon Dioxide	Oxygen	Nitrogen	Methane
Kinetic Diameter, d_k (Å)	2.6	3.3	3.46	3.64	3.8

Permeabilities for zeolite 5A, CVX7, CuTPA, and zeolite NaY MMMs seem to follow more logical trends. With the exception of carbon dioxide, MMMs containing all

of these molecular sieves show a trend of decreasing permeability enhancement with increasing gas kinetic diameter. This seems to indicate that the permeability enhancements are, at least in part, driven by a molecular sieving mechanism as is generally expected in MMMs [4, 6]. Zeolite NaY MMMs give substantially larger permeability enhancements than all other molecular sieves as its pore size is much greater than all the others and greater than the maximum dimensions of all gases. The carbon dioxide discrepancy is likely due to solubility effects.

6.3.2 Apparent Diffusivities of 15 wt.% MMMs

Chapter 2 introduces the concept of site filling sorption during the permeation time lag in MMMs. Consideration of this phenomenon through the use of Equation 2.12 to compute apparent diffusivities helps in the understanding of transport enhancements in MMMs. Figure 6.6 summarizes the normalized apparent diffusivity data (note that helium is excluded—the permeation time lag method is impractical with helium in these samples).

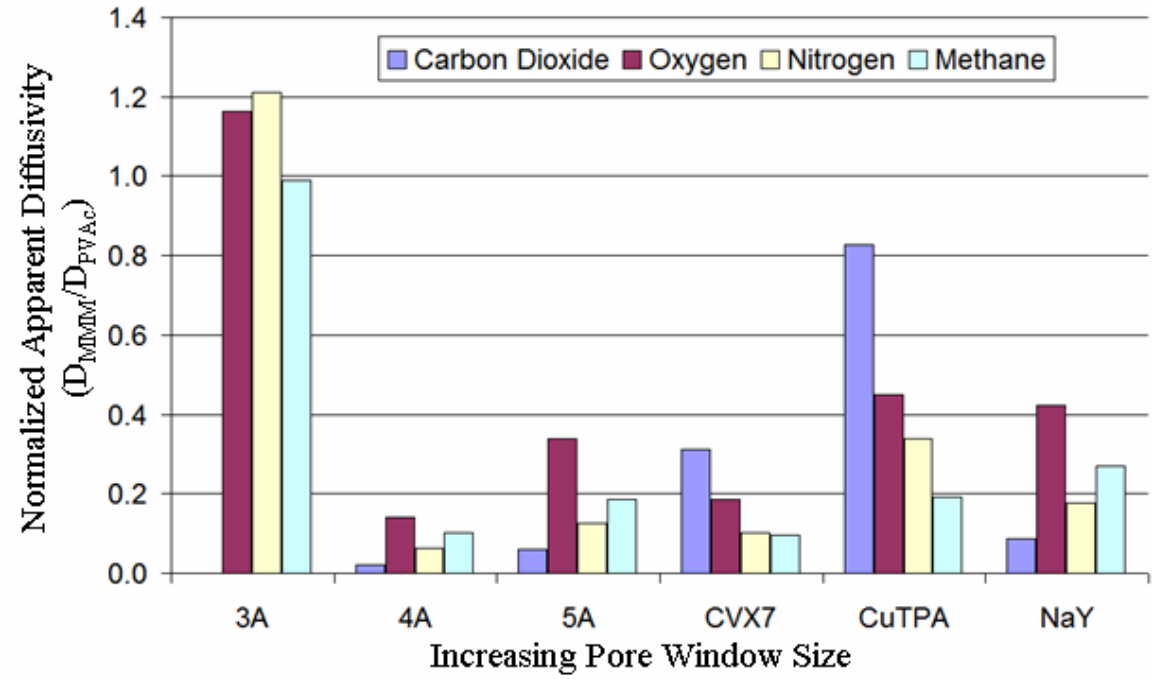

Figure 6.6: Normalized apparent diffusivities of 15 wt.% MMMs.

The most prominent feature in Figure 6.6 is the difference between apparent diffusivities in the 3A MMMs versus all other molecular sieve MMMs. Since access to the small 3.3 Å pore window of zeolite 3A is severely or completely restricted for all gases, no immobilizing sorption occurs, and apparent diffusivities for the MMMs are comparable to pure PVAc (similar to the behavior of the commercial zeolite 4A MMMs as discussed in Chapter 4). This simple observation is an excellent criterion for proving that penetrants in a MMM have easy access to the filler particles and are not bypassing the particles through voids or due to restricted access.

Drawing other conclusions from these data is somewhat questionable due to the multi-modal transport mechanisms that control transport in MMMs (as described Chapter 2, Section 2.4). However, there are some other noteworthy features to Figure 6.6. The aluminosilicate zeolites with charge balancing ions (zeolites 4A, 5A, and NaY) exhibit

nearly identical apparent diffusivity trends, i.e. normalized apparent diffusivities decrease in the same order for all 3 zeolites (oxygen, methane, nitrogen, and carbon dioxide in order of decreasing normalized apparent diffusivity). This trend suggests that these MMMs share the same solubility preferences relative to pure PVAc for these gases, i.e. sorption of carbon dioxide is most preferred and oxygen least preferred relative to PVAc.

The normalized apparent diffusivities of the CVX7 and CuTPA MMMs also stand out in Figure 6.6 as they show similar trends. Extending the argument used above for the aluminosilicate zeolites, it appears that CVX7 and CuTPA share a solubility preference for the gases tested: in order of increasing sorption preference relative to pure PVAc, carbon dioxide, oxygen, nitrogen, and methane.

6.3.3 Permselectivities of 15 wt.% MMMs

Section 6.3.1 shows that MMMs of all of the molecular sieves except zeolite 3A achieve one goal of the mixed matrix concept: permeabilities were enhanced. The other primary goal of a MMM is to improve permselectivities for important gas pairs; however, no significant improvements in permselectivity are expected from most of these molecular sieves due to their large pore windows unless gas solubility effects are considered. The 3.9 Å pore window of zeolite 4A and the minimum window dimension of 3.6 Å for CVX7 may be expected to improve the size based gas selectivities of PVAc. Figure 6.7 summarizes the normalized selectivity data for important gas pairs (note the exclusion of zeolite 3A MMMs due to 3A rejecting most gases—these data are provided in Table 6.2 however). The x-axis of Figure 6.7 groups the gas pairs in order of increasing differences in kinetic diameters, Δd_k. In both glassy polymers and molecular sieves, separation efficiency is shown to scale well with Δd_k [13-15].

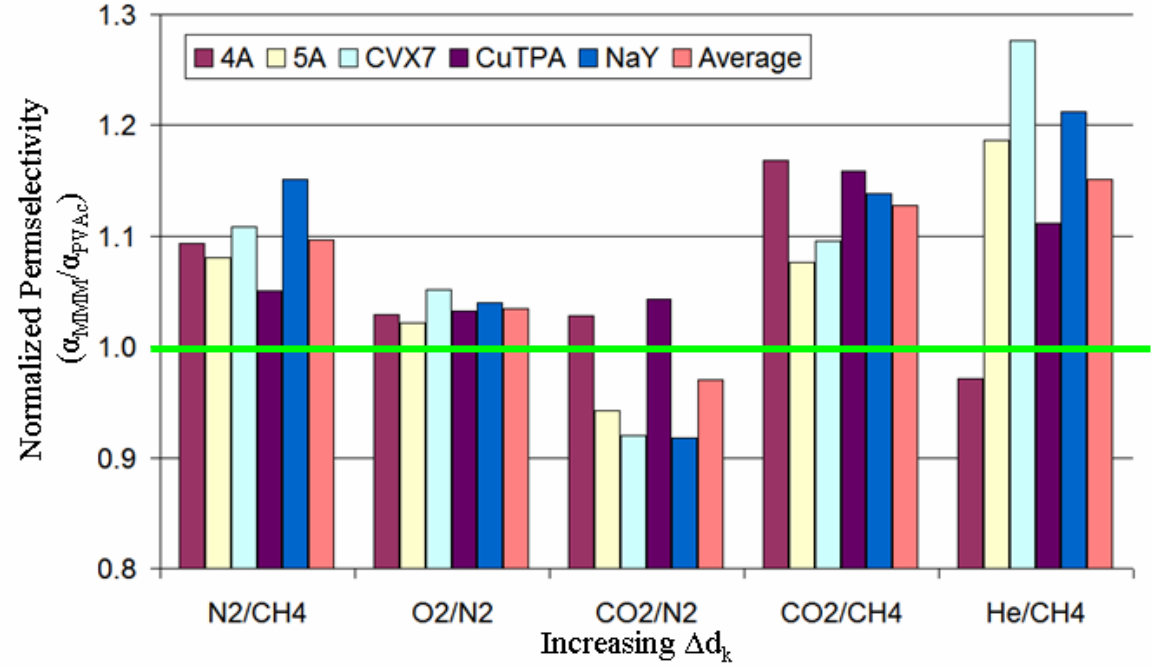

Figure 6.7: Normalized selectivities of 15 wt.% MMMs vs. increasing Δd_k.

The green line in Figure 6.7 corresponds to pure PVAc selectivities and shows that selectivity enhancements are observed for nearly every gas pair for all MMMs regardless of the molecular sieve used. To guide the eye, the normalized selectivities are averaged over all MMMs for each gas pair and appear in Figure 6.7 in pink. This was done to look for an overall trend of increasing selectivity enhancements with increasing Δd_k. While the largest Δd_k's give the best selectivity enhancements (i.e. the CO_2/CH_4 and He/CH_4 pairs show the best enhancements), the expected simplistic, "size only" basis for selectivity trend of increasing selectivity enhancements with increasing Δd_k is not seen in the average data. Furthermore, this expected trend is not seen for MMMs of any molecular sieve. The presence of selectivity enhancements for large pore molecular sieves (zeolite 5A, CuTPA, and zeolite NaY) as well as the lack of a trend relative to Δd_k

suggests that the nature of gas transport in MMMs is not strictly dominated by the size and shape-based selectivities of molecular sieves.

Perhaps the most interesting finding of this survey of MMMs with varying pore sizes was that large pore molecular sieves provided selectivity enhancements that were as good as or better than smaller pore molecular sieves—presumably a reflection of gas solubility effects in the sieves. Conventionally, material selection for MMM aims to match the transport properties of the sieve with the polymer [1, 2, 4]. The ideal matching is generally thought to occur where the fast penetrant permeability in the molecular is 3 times that of the polymer and where the slower penetrant is totally rejected [17].

Recently it was shown that MMMs comprised of MFI in a 6FDA-DAM polymer matrix illustrate and support the importance of these material selection criteria [9]. Although the permeabilities of gases in molecular sieves such as CuTPA and zeolite NaY are not exactly known, it is reasonable to assume that molecular sieves with pore sizes between $5 - 8$ Å (substantially larger than all gases tested) should have much higher permeabilities than a fairly good barrier polymer such as PVAc. Therefore, the observations of selectivity enhancements for these large pore sieves are contrary to previously reported theory and observations.

It may be possible that PVAc chains partially block access to the larger pore molecular sieves in these MMMs which would effectively reduce their pore sizes [8, 18]. In any event, the key finding is that large pore molecular sieves provide better than expected permselectivity enhancements which suggests that solubility effects require more attention than they have received to date in order to understand the full range of MMM performance.

6.4 Conclusions

It was demonstrated that desired changes in MMM transport properties can be achieved by engineering the pore size of zeolite A with mixed ion exchanges. However, the observed permselectivities for the ion exchanged zeolite A MMMs versus the zeolite 4A MMMs do not fully explain the effects of pore size on observed MMM properties, suggesting that other factors, like gas solubilities in MMMs, may play an important role in overall transport properties. The results do encourage further investigations as there are many cations of varying size and valency that can be exchanged in type A and other zeolites [10, 12, 16, 19-21].

Several logical, general trends were observed in Section 6.3. MMM permeabilities increased for all gases as a function of molecular sieve pore size. It was also shown that zeolite 3A MMMs give apparent diffusivities approximately equal to PVAc due to its small pore size (which largely rejects access of all gases) while all other molecular sieve MMMs result in apparently lower diffusivities due to the filing of sorptive sinks during the permeation time lag. Surprisingly, large pore molecular sieves (like zeolite NaY) showed permselectivity enhancements that were as good as or better than those of smaller pore molecular sieve MMMs. While improved permselectivities are a desired trait of MMMs, the survey of MMMs with varying molecular sieve pore sizes raises further questions about the nature of gas transport in MMMs.

Overall, the results presented in this Chapter suggest that the nature of gas transport in MMMs is not a “size only” affair, and that gas solubilities should be considered to fully understand MMM performance.

6.5 References

[1] Mahajan, R., *Formation, characterization, and modeling of mixed matrix membrane materials*. 2000, The University of Texas at Austin, Ph.D. Thesis.

[2] Mahajan, R. and W.J. Koros, *Factors controlling successful formation of mixed-matrix gas separation materials.* Industrial & Engineering Chemistry Research, 2000. **39**(8): p. 2692-2696.

[3] Shu, S., *Engineering the performance of mixed matrix membranes for gas separations*. 2007, Georgia Institute of Technology, Ph.D. Thesis.

[4] Zimmerman, C.M., A. Singh, and W.J. Koros, *Tailoring mixed matrix composite membranes for gas separations.* Journal of Membrane Science, 1997. **137**(1-2): p. 145-154.

[5] Zimmerman, C.M., R. Mahajan, and W.J. Koros, *Fundamental and practical aspects of mixed matrix gas separation membranes.* Abstracts of Papers of the American Chemical Society, 1997. **214**: p. 270-PMSE.

[6] Koros, W.J. and T.T. Moore. *Organic-inorganic hybrid membrane materials for gas separation*. 2003.

[7] Moore, T.T., R. Mahajan, D.Q. Vu, and W.J. Koros, *Hybrid membrane materials comprising organic polymers with rigid dispersed phases.* Aiche Journal, 2004. **50**(2): p. 311-321.

[8] Moore, T.T. and W.J. Koros, *Non-ideal effects in organic-inorganic materials for gas separation membranes.* Journal of Molecular Structure, 2005. **739**(1-3): p. 87-98.

[9] Liu, J.Q., T.H. Bae, W.L. Qiu, S. Husain, S. Nair, C.W. Jones, R.R. Chance, and W.J. Koros, *Butane isomer transport properties of 6fda-dam and mfi-6fda-dam mixed matrix membranes.* Journal of Membrane Science, 2009. **343**(1-2): p. 157-163.

[10] Yeh, Y.T., *Diffusion and adsorption of gases in molecular sieves*. 1989, SUNY at Buffalo, Ph.D. Thesis.

[11] Yeh, Y.T. and R.T. Yang, *Diffusion in zeolites containing mixed cations.* Aiche Journal, 1989. **35**(10): p. 1659-1666.

[12] Talu, O., S.Y. Zhang, and D.T. Hayhurst, *Effect of cations on methane adsorption by nay, mgy, cay, sry, and bay zeolites.* Journal of Physical Chemistry, 1993. **97**(49): p. 12894-12898.

[13] Freeman, B.D., *Basis of permeability/selectivity tradeoff relations in polymeric gas separation membranes.* Macromolecules, 1999. **32**(2): p. 375-380.

[14] Robeson, L.M., *Correlation of separation factor versus permeability for polymeric membranes.* Journal of Membrane Science, 1991. **62**(2): p. 165-185.

[15] Yang, R.T., *Gas separation by adsorption processes*. 1997: Imperial College Press.

[16] Breck, D.W., *Zeolite molecular sieves*. 1973, New York: Wiley.

[17] Perry, J.D., *Formation and characterization of hybrid membranes utilizing high-performance polyimides and carbon molecular sieves*. 2007, Georgia Institute of Technology, Ph.D. Thesis.

[18] Li, Y., T.S. Chung, C. Cao, and S. Kulprathipanja, *The effects of polymer chain rigidification, zeolite pore size and pore blockage on polyethersulfone (pes)-zeolite a mixed matrix membranes.* Journal of Membrane Science, 2005. **260**(1-2): p. 45-55.

[19] Karger, J., *Diffusion in zeolites and other microporous solids*. 2007, Wiley.

[20] Walton, K.S., M.B. Abney, and M.D. Levan, *Co2 adsorption in y and x zeolites modified by alkali metal cation exchange.* Microporous and Mesoporous Materials, 2006. **91**(1-3): p. 78-84.

[21] Bellat, J.P., M.H. Simonotgrange, and S. Jullian, *Adsorption of gaseous p-xylene and m-xylene on nay, ky, and bay zeolites .1. Adsorption equilibria of pure xylenes.* Zeolites, 1995. **15**(2): p. 124-130.

CHAPTER 7

CONCLUSIONS AND RECOMMENDATIONS

7.1 Summary and Conclusions

Mixed matrix materials have been shown to improve the gas separation performance of pure polymer membranes, which have potential as an efficient, non thermally-driven gas separation technology [1-7]. Ultimately, molecular sieve loadings must be maximized while maintaining the ease of processing polymer solutions for MMMs to reach their full potential [3, 6].

The primary goal of this work was to create high molecular sieve loading MMMs that improved the gas separation performance of poly(vinyl acetate). Chapters 4 and 5 demonstrate successful completion of this primary goal. Expectations for this project were achieved when excellent permselectivity enhancements for high loading MMMs were shown in aggressive feed conditions in Chapter 5.

There were many other noteworthy achievements and outcomes of this work as shown in the list below:

1. Investigations into experimental procedures for the permeation testing of low flux dense film samples in Chapter 3 illustrated the care which must be taken to avoid erroneous sample characterization. While the work of Moore *et al* introduced a useful and important new sample masking technique [8], it was found that extra sample degassing times were needed due to the sorptive nature of the masking tape adhesive.

2. Chapter 4 identified two critical parameters for the successful formation of void-free high particle loading MMMs. While one of the parameters, high annealing temperature, had been reported to be important by previous researchers for lower loading MMMs [9, 10], the initial solvent concentration effect had not been reported previously.
3. It was found that commercial zeolite 4A sources may contain excess non-zeolitic material on the external surface of particles, rendering these commercial sources ineffective in MMM applications. These findings were presented in Chapter 4.
4. High molecular sieve loading MMM transport properties presented in Chapter 5 show that the properties of a low cost, low performance polymer can be enhanced towards those of "upper-bound" polymers [11]. The large pure gas permeability enhancements and the permeation time lag behavior of 65 vol.% CuTPA MMM suggested that the filler particles are beginning to dominate overall gas transport—a first for MMMs. Under high pressure mixed carbon dioxide-methane feeds, the 50 vol.% zeolite 4A MMMs increased carbon dioxide permeability while reducing methane permeability resulting in a nearly 60 % enhancement in permselectivity.
5. Investigation into the effects of molecular sieve pore size on MMM transport properties in Chapter 6 suggested that the nature of gas transport enhancements in MMMs is not fully understood. Substantial permselectivity enhancements were attained for molecular sieves with pore window sizes previously considered too large to provide enhancements [3, 6, 9, 12, 13]. It was also shown that partial ion

exchanges of zeolites can be used to tailor the transport properties of MMMs as has been shown previously for sorbent applications [14].

7.2 Recommendations for Future Work

Overall, the outcomes of this project represent satisfactory completion of all goals and objectives described in Chapter 1. However, there were many aspects of this project that require further work as well as unexpected results that warrant further study. Specific recommendations for future work are provided in the following subsections.

7.2.1 Higher Molecular Sieve Loadings in PVAc MMMs

While this work achieved the primary goal of creating defect-free MMMs at particle loadings ≥ 50 vol.%, it is believed that loadings can be increased further. Due to time and material constraints, we were restricted to just a few 50 vol.% zeolite 4A MMMs. With the lessons learned in Chapter 4 regarding the quality variation in zeolite 4A sources, future researchers can continue with more confidence into higher zeolite 4A loadings in PVAc. The success with 65 vol.% CuTPA MMMs suggests that 50 vol.% loading is not an insurmountable limit. Moreover, working with molecular sieve batches with properly tuned particle size distributions could increase the particle percolation threshold to allow for creation of higher loading, defect-free MMMs [15, 16].

7.2.2 High Molecular Sieve Loading MMMs in Cellulose Acetate

Various industrial sponsors have expressed interest in cellulose acetate MMMs. Cellulose acetate is the industrial standard for polymeric gas separation membranes; thus, target users of MMM technology have a greater level of comfort with cellulose acetate based materials. Furthermore, cellulose acetate contains carbonyl groups which have been shown to play an important role in strong polymer-filler adhesion which is required

for MMMs. Cellulose acetate also has gas transport properties that are quite similar to PVAc thereby suggesting that transport enhancements similar to those shown in the PVAc MMMs in this work may be expected for cellulose acetate MMMs.

7.2.3 Metal Organic Framework Mixed Matrix Membranes

The CuTPA MOF MMMs studied in this work showed surprisingly good transport enhancements over pure PVAc performance despite having a large pore window that may not be ideal for maximum permselectivity enhancement. MOFs are a fairly new class of material that is in the early stages of research and development. As with traditional polymers, one can envision an effectively limitless set of potential MOF structures and compositions. This enormous reservoir of potential materials is perfectly suited for MMM applications as researchers can engineer the gas transport properties of the dispersed filler material around a particular polymer rather than searching for a polymer whose properties match well with a particular zeolite as is traditionally done in MMM design [3, 9, 10, 13, 17]. This is precisely the advantage pointed out by past researchers of carbon molecular sieve based MMMs [18]. Although there have been no reports of tuning MOF properties for MMM applications, there have been reports of the pure properties of MOFs containing halogenated organic linkages [19]. One can easily imagine using the large size of halogen atoms in halogenated organic linkages to decrease pore sizes of non-halogenated organic linkages in a similar way that fluorinated polyimides were shown to drastically improve the transport properties of their non-halogenated counterparts.

7.2.4 “Realistic” Mixed Matrix Membranes

Although there is still much to learn from pure gas transport studies on dense film MMMs, the fate of MMMs will ultimately depend on their performance in the asymmetric hollow fiber membrane morphology under realistic feed conditions [20, 21]. Since development of functional, high performance asymmetric hollow fiber membrane modules is difficult even for pure polymer membranes, MMM researcher cannot afford to delay development of asymmetric mixed matrix hollow fiber membrane modules. Such studies would be well served to investigate realistic feeds such as high pressure carbon dioxide mixtures as well as mixed gas feeds containing water, higher hydrocarbons, and other known natural gas contaminants as proof of good performance in such conditions would be extremely well received by potential users of MMMs in real applications. This recommendation ties in nicely with the recommendation studying cellulose acetate MMMs as cellulose acetate is a “comfortable” material for actual users of gas separation membranes. The Koros Research Group already has several such projects underway.

7.2.5 Investigate Anomalous Gas Transport in MMMs

Improvements in permselectivities with large pore molecular sieve MMMs shown in this work were unexpected and frankly confusing. Typically the pore size of the molecular sieve is used as the primary means for MMM design, i.e. a molecular sieve is chosen on the basis that the desired permeant is small enough to gain easy access to the sieve while the undesired permeant is large enough to be totally (or largely) rejected from accessing the sieve. While this certainly appears to be the logical approach to MMM design, many of the results in this work suggest a more complex set of rules apply. Fundamental gas transport studies on the precise nature of gas transport in MMMs as

related to molecular sieve pore sizes and gas solubilities are in great demand so that the full potential of MMM as an alternative gas separation technology can be known. Such studies should use a model polymer matrix, such as PVAc, and aim to break overall transport in MMMs down into the multi-modal diffusive and sorptive contributions in the same manner that is done for new polymeric materials via dual-mode transport considerations.

7.3 References

[1] Kulprathipanja, S., *Separation of fluids by means of mixed matrix membranes*, U.S.P. Office, Editor. 1988.

[2] Jia, M.D., K.V. Peinemann, and R.D. Behling, *Molecular-sieving effect of the zeolite-filled silicone-rubber membranes in gas permeation.* Journal of Membrane Science, 1991. **57**(2-3): p. 289-296.

[3] Zimmerman, C.M., A. Singh, and W.J. Koros, *Tailoring mixed matrix composite membranes for gas separations.* Journal of Membrane Science, 1997. **137**(1-2): p. 145-154.

[4] Mahajan, R. and W.J. Koros, *Mixed matrix membrane materials with glassy polymers. Part 1.* Polymer Engineering and Science, 2002. **42**(7): p. 1420-1431.

[5] Mahajan, R. and W.J. Koros, *Mixed matrix membrane materials with glassy polymers. Part 2.* Polymer Engineering and Science, 2002. **42**(7): p. 1432-1441.

[6] Koros, W.J. and T.T. Moore. *Organic-inorganic hybrid membrane materials for gas separation*. 2003.

[7] Li, Y., T.S. Chung, C. Cao, and S. Kulprathipanja, *The effects of polymer chain rigidification, zeolite pore size and pore blockage on polyethersulfone (pes)-zeolite a mixed matrix membranes.* Journal of Membrane Science, 2005. **260**(1-2): p. 45-55.

[8] Moore, T.T., S. Damle, P.J. Williams, and W.J. Koros, *Characterization of low permeability gas separation membranes and barrier materials; design and operation considerations.* Journal of Membrane Science, 2004. **245**(1-2): p. 227-231.

[9] Mahajan, R., *Formation, characterization, and modeling of mixed matrix membrane materials*. 2000, The University of Texas at Austin, Ph.D. Thesis.

[10] Shu, S., *Engineering the performance of mixed matrix membranes for gas separations*. 2007, Georgia Institute of Technology, Ph.D. Thesis.

[11] Robeson, L.M., *The upper bound revisited.* Journal of Membrane Science, 2008. **320**(1-2): p. 390-400.

[12] Moore, T.T. and W.J. Koros, *Non-ideal effects in organic-inorganic materials for gas separation membranes.* Journal of Molecular Structure, 2005. **739**(1-3): p. 87-98.

[13] Liu, J.Q., T.H. Bae, W.L. Qiu, S. Husain, S. Nair, C.W. Jones, R.R. Chance, and W.J. Koros, *Butane isomer transport properties of 6fda-dam and mfi-6fda-dam mixed matrix membranes*. Journal of Membrane Science, 2009. **343**(1-2): p. 157-163.

[14] Yeh, Y.T. and R.T. Yang, *Diffusion in zeolites containing mixed cations.* Aiche Journal, 1989. **35**(10): p. 1659-1666.

[15] Scott, G.D., *Packing of equal spheres.* Nature, 1960. **188**(4754): p. 908-909.

[16] Fishman, R.S., D.A. Kurtze, and G.P. Bierwagen, *Pigment inhomogeneity and void formation in organic coatings.* Progress in Organic Coatings, 1993. **21**(4): p. 387-403.

[17] Moore, T.T., *Effects of materials, processing, and operating conditions on the morphology and gas transport properties of mixed matrix membranes*. 2004, The University of Texas at Austin, Ph.D. Thesis.

[18] Perry, J.D., *Formation and characterization of hybrid membranes utilizing high-performance polyimides and carbon molecular sieves*. 2007, Georgia Institute of Technology, Ph.D. Thesis.

[19] Yang, C., X.P. Wang, and M.A. Omary, *Fluorous metal-organic frameworks for high-density gas adsorption.* Journal of the American Chemical Society, 2007. **129**(50): p. 15454-+.

[20] Moore, T.T., T. Vo, R. Mahajan, S. Kulkarni, D. Hasse, and W.J. Koros, *Effect of humidified feeds on oxygen permeability of mixed matrix membranes.* Journal of Applied Polymer Science, 2003. **90**(6): p. 1574-1580.

[21] Husain, S. and W.J. Koros, *Mixed matrix hollow fiber membranes made with modified hssz-13 zeolite in polyetherimide polymer matrix for gas separation.* Journal of Membrane Science, 2007. **288**(1-2): p. 195-207.

APPENDIX A

GAS ADSORPTION ISOTHERMS OF MOLECULAR SIEVES

A.1 Introduction

Throughout this thesis, there are references to the pure gas adsorption properties of some of the molecular sieves used in this work. Pure gas adsorption isotherms (measured by the author at 35 °C) for ASGE zeolite 4A, in-house synthesized zeolite 4A, CuTPA MOF, and zeolite NaY with fitted Langmuir parameters (see Equation 2.4) are provided in sections A.2, A.3, A.4, and A.5, respectively. Note that the Langmuir saturation constant, $C_H^{'}$ (or $C^{'}$), has units of cc_{STP} sorbed/cc sample and the Langmuir affinity constant, *b*, has units of atm^{-1} for all isotherms shown in Appendix A.

A.2 Pure Gas Adsorption Isotherms of ASGE Zeolite 4A

For this molecular sieve, helium, oxygen, and nitrogen isotherms were completed. See Figures A.1, A.2, and A.3.

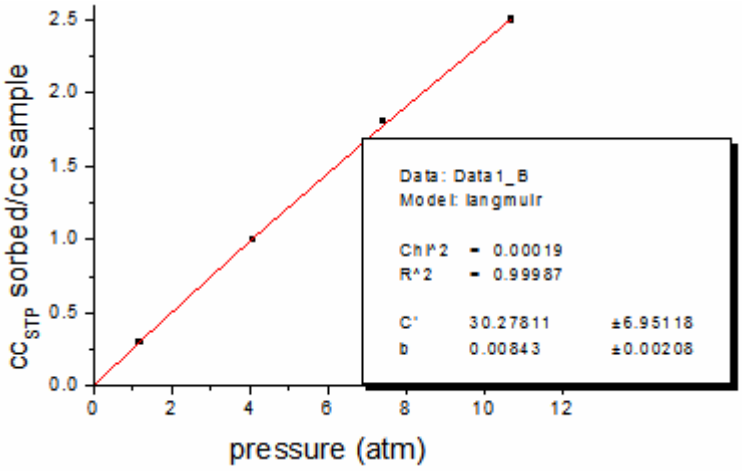

Figure A.1: Helium isotherm (35 °C) of ASGE zeolite 4A.

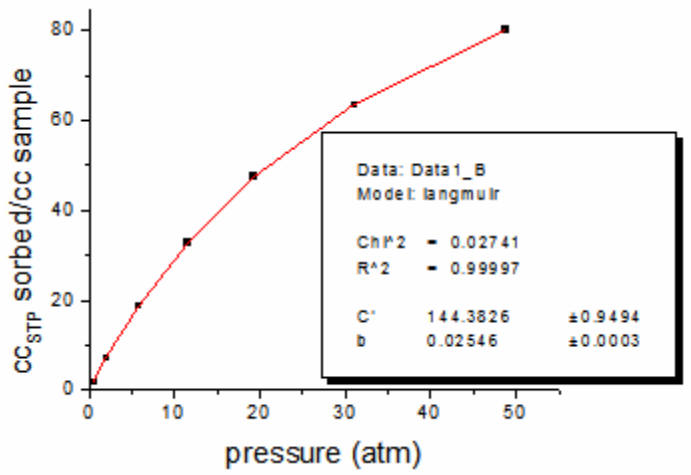

Figure A.2: Oxygen isotherm (35 °C) of ASGE zeolite 4A.

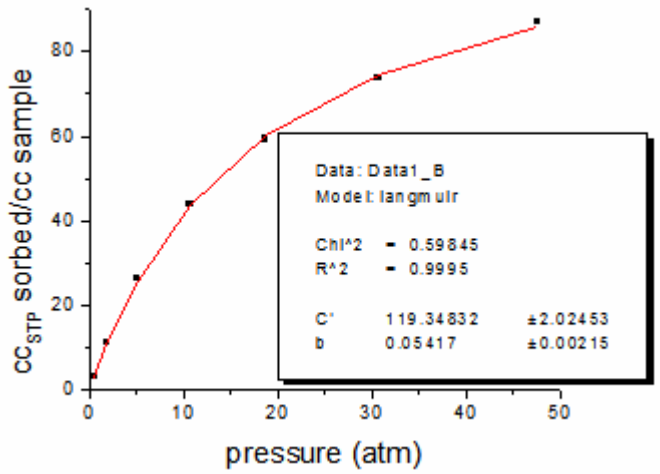

Figure A.3: Nitrogen isotherm (35 °C) of ASGE zeolite 4A.

A.3 Pure Gas Adsorption Isotherms of In-house Zeolite 4A

For this molecular sieve, oxygen, nitrogen, methane and carbon dioxide isotherms were completed. See Figures A.4, A.5, A.6 and A.7.

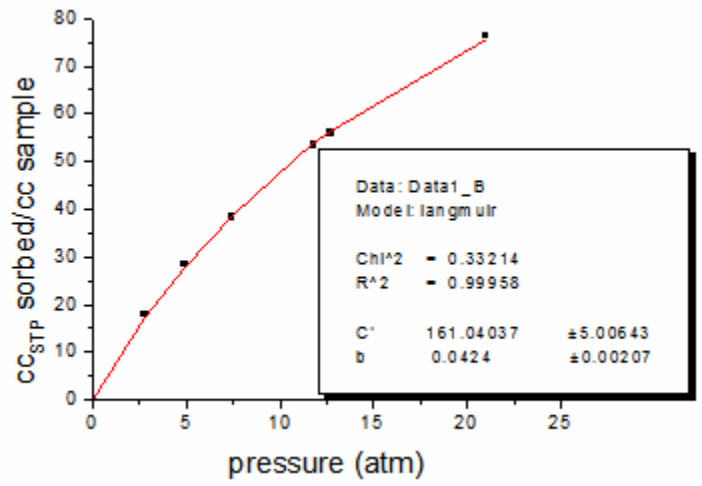

Figure A.4: Oxygen isotherm (35 °C) of in-house zeolite 4A.

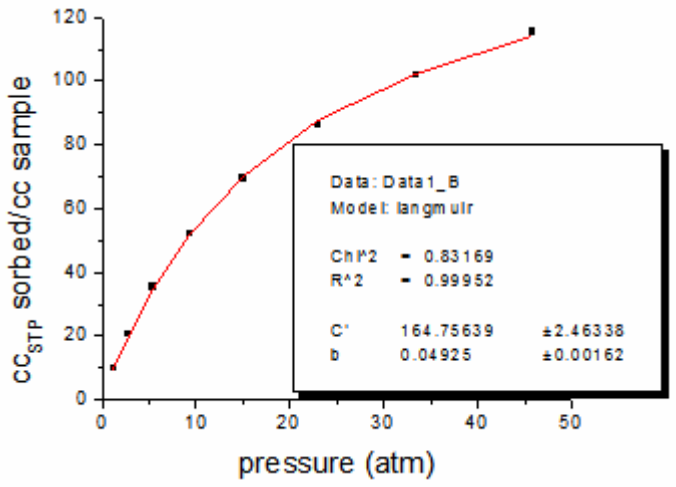

Figure A.5: Nitrogen isotherm (35 °C) of in-house zeolite 4A.

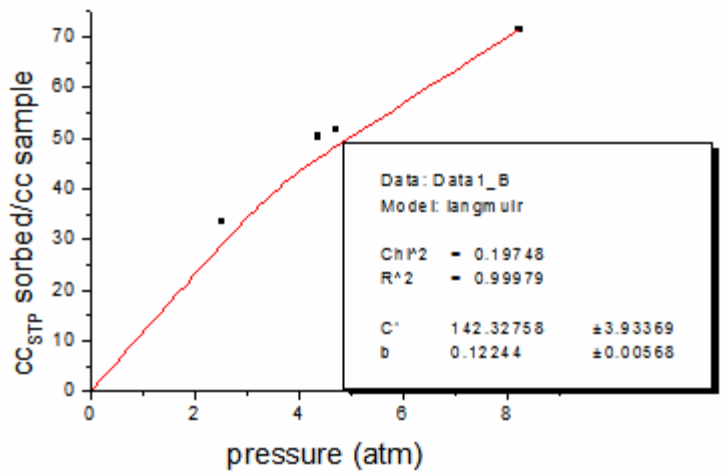

Figure A.6: Methane isotherm (35 °C) of in-house zeolite 4A.

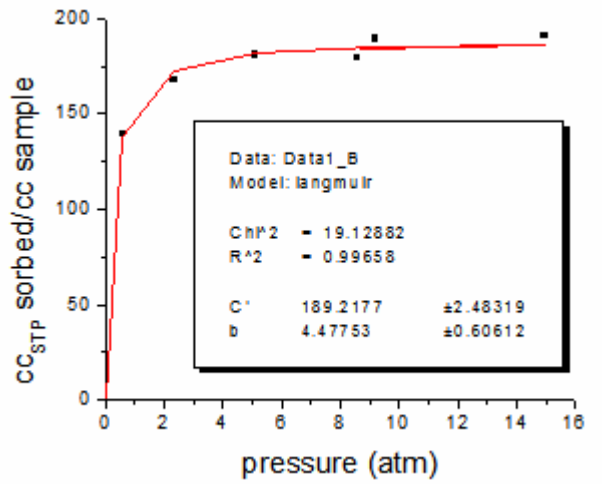

Figure A.7: Carbon dioxide isotherm (35 °C) of in-house zeolite 4A.

A.4 Pure Gas Adsorption Isotherms of CuTPA

For this molecular sieve, oxygen, nitrogen, methane and carbon dioxide isotherms were completed. See Figures A.8, A.9, A.10 and A.11.

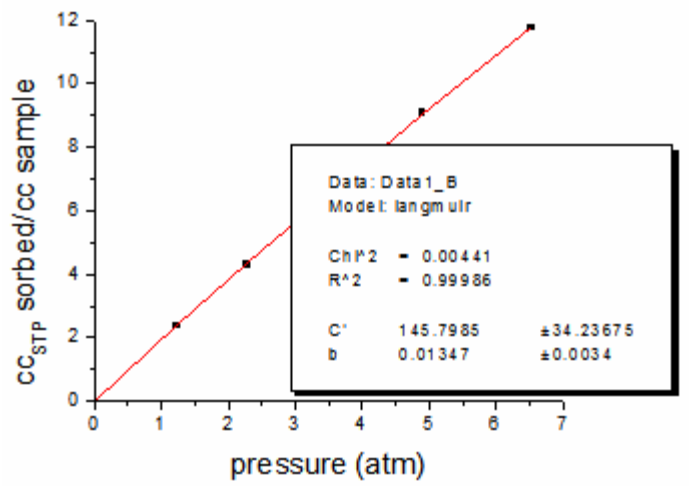

Figure A.8: Oxygen isotherm (35 °C) of CuTPA. Note the Langmuir fit is bad.

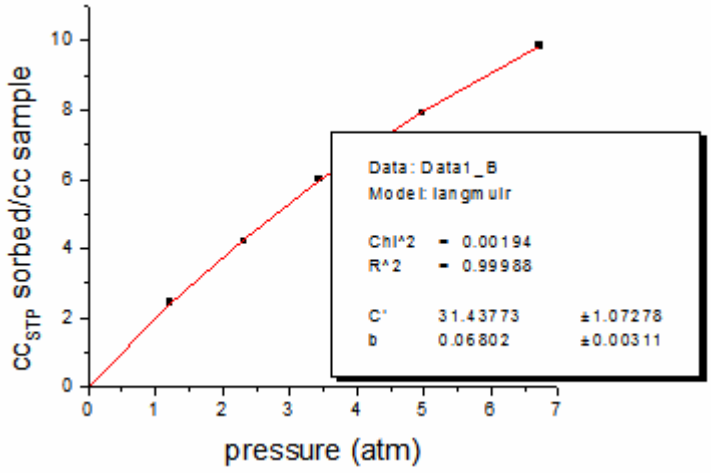

Figure A.9: Nitrogen isotherm (35 °C) of CuTPA.

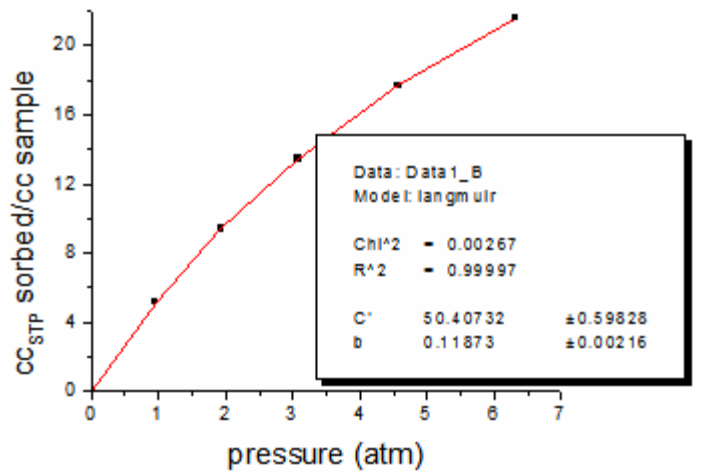

Figure A.10: Methane isotherm (35 °C) of CuTPA.

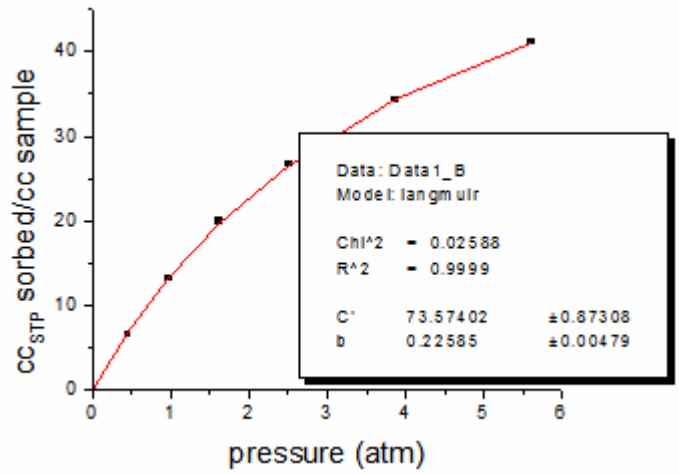

Figure A.11: Carbon dioxide isotherm (35 °C) of CuTPA.

A.5 Pure Gas Adsorption Isotherms of Zeolite NaY

For this molecular sieve, helium, oxygen, nitrogen, and methane isotherms were completed. See Figures A.12, A.13, A.14 and A.15.

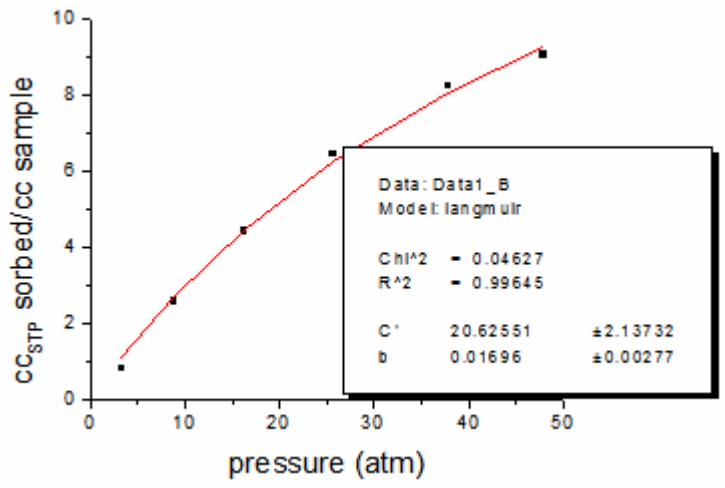

Figure A.12: Helium isotherm (35 °C) of zeolite NaY.

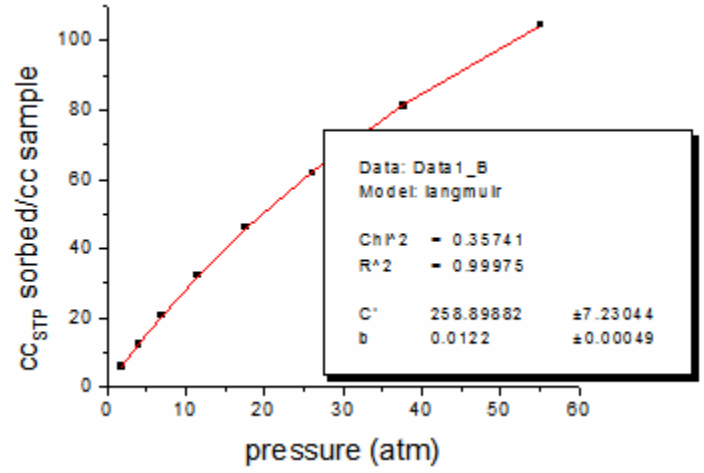

Figure A.13: Oxygen isotherm (35 °C) of zeolite NaY.

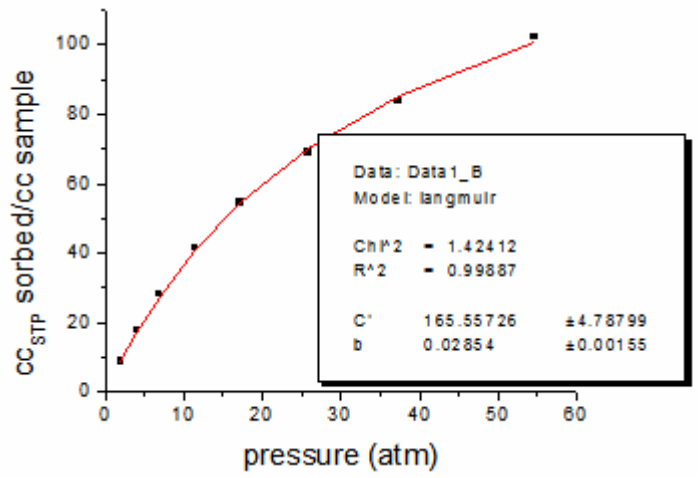

Figure A.14: Nitrogen isotherm (35 °C) of zeolite NaY.

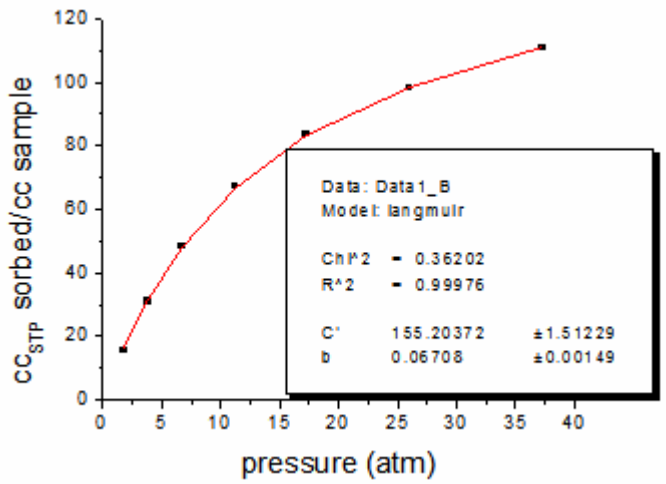

Figure A.15: Methane isotherm (35 °C) of zeolite NaY.

APPENDIX B

PURE GAS PERMEATION IN HIGH LOADING ZEOLITE 4A MMMS

B.1 Introduction

The first experiments performed on 50 vol.% zeolite 4A MMMs were pure gas permeation tests. Much to our surprise, these pure gas permeation tests yielded results that cannot be fully explained despite great experimental and theoretical efforts. The following subsections discuss the pure gas permeation results in detail. Pure helium permeation data are provided in Section B.2. These data appear to be logical extensions of pure helium permeation data on lower loading zeolite 4A MMMs. Section B.3 discusses the results of pure oxygen and nitrogen permeation experiments. These data showed unusual behavior that is not fully understood; however, a tentative hypothesis and recommendations to test the hypothesis are provided.

B.2 Pure Helium Permeability in High Loading Zeolite 4A-PVAc MMMs

Table B.1 compares pure helium permeabilities of pure PVAc, 15 wt.% (or 12.2 vol.%) 4A MMMs, 30 wt.% (or 25.3 vol.%) 4A MMMs, and 56 wt.% (or 50.0 vol.%) 4A MMMs.

Table B.1: Pure helium permeabilities (at 65 psia) of PVAc and 4A MMMs.

	Pure PVAc	12.2 vol.% 4A	25.3 vol.% 4A	50.0 vol.% 4A
P_{He} (Barrers)	14.8 ± 0.9	14.2 ± 1.1	12.5 ± 0.7	7.77 ± 0.36

Table B.1 shows that helium permeabilities decrease with increased zeolite 4A loading. The values (± one standard deviation) of MMM helium permeability in Table B.1 were

used to make low and high (i.e. low predictions from minus one standard deviation and high predictions from plus one standard deviation) helium permeability predictions for zeolite 4A using Maxwell's model (see Equation 2.14). These values are provided in Table B.2.

Table B.2: Low and high Maxwell model predictions of P_{He} in zeolite 4A.

	From 12.2 vol.% MMM	From 25.3 vol.% MMM	From 50.0 vol.% MMM
$P_{He,4A}$ (Barrers)	3.99 to 20.2	4.97 to 9.26	2.15 to 3.23

In general, the predicted helium permeabilities in zeolite 4A are quite low. When the low and high predicted values at each loading are averaged, $P_{He,4A} = 7.30 \pm 6.78$ Barrers. Although the predictions at each loading do not match exactly, the close proximity of the predictions at each loading suggest that all of these MMMs are largely free of the complications of non-idealities and that Maxwell's model is a useful tool for validation MMM transport properties as a function of loading. The relatively low predicted $P_{He,4A}$ values for the 50.0 vol.% MMMs may be attributable to reduced mobility in the PVAc matrix as a greater percentage of chains will be adsorbed to surfaces; hence, overall chain mobility is reduced [1, 2]. TGA showed a marginal increase in T_g as function of particle loading: T_g's of 43.49 °C, 43.53 °C, 43.88 °C, and 44.24 °C were measured for pure PVAc, 12.2 vol.% 4A, 25.3 vol.% 4A, and 50.0 vol.% 4A MMMs, respectively.

B.3 Pure Oxygen and Nitrogen Permeation in 50 vol.% Zeolite 4A MMMs

As described in Chapter 3, pure gases were typically tested in the following order: helium, oxygen, nitrogen, methane, and carbon dioxide. Helium permeation experiments provided results that agreed reasonably well with lower loading zeolite 4A MMM data as shown in Section B.2. Pure oxygen and nitrogen permeation experiments provided highly unusual results. Figure B.1 is a plot of the derivative of permeate pressure as a function of time during a permeation experiment.

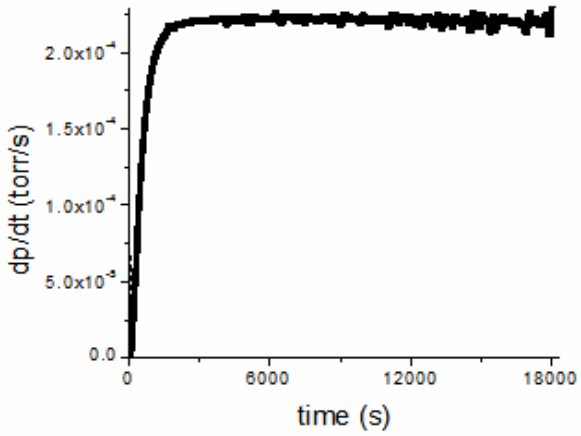

Figure B.1: Derivative of permeate pressure versus time for a 65 psia oxygen permeation in a 12.2 vol.% zeolite 4A-PVAc MMM.

The approach to steady-state permeation can be clearly seen in Figure B.1. Initially, the derivative equals zero because little or no gas breaks through the sample immediately after gas is exposed to the upstream face of the sample. This is followed by a steady increase in the derivative as the gas breaks through the sample thickness and begins to approach a steady-state flux. Steady-state flux is evidenced by the plateauing of the derivative of permeate pressure with respect to time. Since the upstream pressure is

much greater than the permeate pressure, the driving force for flux remains constant, and flux remains constant for the duration of the experiment.

Markedly different behavior was observed for 50 vol.% zeolite 4A MMMs. Figure B.2 shows the derivative response for a 65 psia oxygen permeation experiment on a 50 vol.% zeolite 4A MMM.

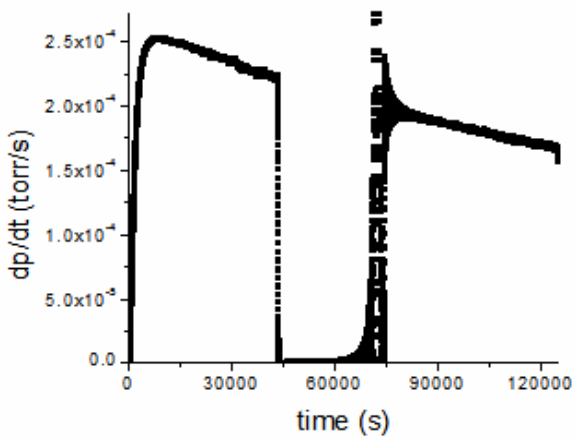

Figure B.2: Derivative of permeate pressure versus time for a 65 psia oxygen permeation in a 50.0 vol.% zeolite 4A-PVAc MMM.

The response in Figure B.2 is strikingly different from the response in Figure B.1. Initially, the response is "normal", i.e. the derivative is zero before break through and begins to increase rapidly as time progresses beyond the time lag portion of the experiment. However, there is no plateau at a global maximum as shown in Figure B.1. The derivative reaches a maximum value and then begins a slow, and seemingly never ending, descent. Eventually, the experiment was stopped because there appeared to be no end in sight. Note that the "maximum" flux results in a reasonable value for oxygen permeability based on low loading zeolite 4A MMM data. P_{O2} ~ 0.8 Barrers at "maximum" flux which is roughly expected based on the lower loading zeolite 4A MMM

oxygen permeability increases. Note that the sudden step decrease to zero flux in the middle of Figure B.2 was the result of pulling active vacuum on the permeate.

The 65 psia oxygen experiment was followed by a 65 psia nitrogen experiment after several days of vacuum degassing. Unfortunately, the same behavior was observed for nitrogen, and the experiment was stopped before steady-state flux could be established. Note that the "maximum" flux results in a reasonable value for nitrogen permeability based on low loading zeolite 4A MMM data. P_{N2} ~ 0.1 Barrers at "maximum" flux which is roughly expected based on the lower loading zeolite 4A MMM nitrogen permeability increases. This left us quite confused—properly designed and controlled permeation experiments should not behave this way, and we had no reason to believe there was anything wrong with the system, the feed gas, or the experimental methods as countless "normal" experiments had been conducted by the author for several years including the weeks leading up to these confounding experiments.

There was one obvious difference with this sample—this was the first high loading "good" zeolite 4A-PVAc MMM to be tested in this work. Membranes with gas permeabilities that decrease with time are actually well known although had not been witnessed in this work until now. Physical aging of glass polymers is a phenomenon where excess free volume slowly diffuses out of the sample [3-5]. This process is directly related to the concepts introduced in the beginning of Chapter 2. When glassy polymers are processed in such a way that excess free volume is trapped between dilated chain segments, there is a thermodynamic driving force to move the system to its denser, lowest free energy chain conformation.

While aging effects are typically not observed during a permeation experiment, nor with materials being tested so near their glass transition, a combined "heat of sorption-aging" hypothesis was formulated and tested for the 50 vol.% zeolite 4A MMMs. A conventional aging response would not "reset" itself between permeation experiments. In other words, a conventional aging response does not agree with the fact that the two consecutive 65 psia oxygen and nitrogen permeation experiments showed basically identical responses of no flux before breakthrough, followed by an increase up to an apparent maximum that agrees with expectations from low loading MMM data, and finally followed by an never ending decrease in flux.

Zeolites, especially aluminum rich zeolites with charge balancing ions, can have fairly high heats of sorption. These high heats of sorption can result in substantial releases of thermal energy when penetrants sorb. Equation B.1 describes this phenomenon.

$$n \cdot \Delta H_{ads} = m \cdot C_p \cdot \Delta T \qquad \text{(Equation B.1)}$$

In Equation B.1, n is the number of moles sorbed, H_{ads} is the exothermic heat of sorption in J/(g·K), m is the mass of sample in grams, C_p is the isobaric heat capacity in J/g·K, and ΔT is the temperature change in Kelvin. Equation B.1 was used to estimate the potential temperature change, ΔT, of zeolite particles upon adsorption of 65 psia nitrogen. Breck provides a $-\Delta H_{ads}$ for zeolite 4A of 27196 J/mol [6], Qiu *et al* give a C_p of 0.94 J/mol·K at permeation experiment temperature of 35 °C [7], and n/m can be directly computed from the nitrogen adsorption isotherm of zeolite 4A provided in Appendix A (n/m = 0.000865 mol/g). The resulting ΔT = 25 °C. Considering the T_g of PVAc is only 43.49 °C (as measured in this work) and that the permeation test temperature is 35 °C, PVAc

chains could feel temperature spikes that are as high as 16.5 °C above T_g. Since the adsorbed chains are in direct contact with the zeolite particles, this ΔT could be reasonably expected to dilate interfacial polymer. If the heat generated dissipates much faster than the PVAc chain segments can relax such a dilation (which is quite likely), than it is possible to envision a heat of sorption induced aging event where fluxes start high due to interfacial polymer dilation from the heat of sorption followed by a slow decrease as the dilated polymer relaxes.

This hypothesis was put to the test by starting with a fresh sample of 50 vol.% zeolite 4A-PVAc that had never been exposed to elevate pressures. Low pressure (~ 5 psia) oxygen and nitrogen permeation experiments were done. Since such low pressures should only give a maximum ΔT of 2.3 °C, no appreciable dilation should occur as all chains would still be below T_g. If no dilation occurs, there should be no evidence of aging in the derivative of the permeate pressure with respect to time as was shown for the higher pressure case in Figure B.2. Figure B.3 shows the permeate pressure derivative for 5 psia nitrogen permeation on the fresh 50 vol.% zeolite 4A-PVAc MMM sample.

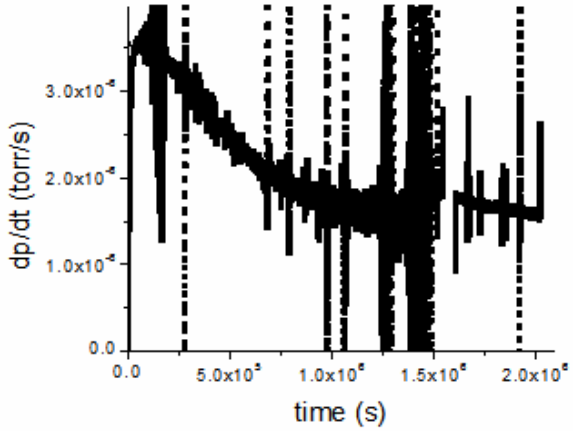

Figure B.3: Derivative of permeate pressure versus time for a 5 psia nitrogen permeation in a 50.0 vol.% zeolite 4A-PVAc MMM.

One can clearly see that low pressure experiment has the same "derivative signature" (note that the noise is due to the intrinsically low flux of low pressure nitrogen through PVAc MMMs). In this case, the permeation was allowed to proceed for a very long time (over 23 days!), and flux never reached steady-state although it did finally appear to approaching a steady state value. Roughly identical "derivative signatures" for the low and high pressure pure gas cases basically proves that there is no heat of sorption induced, reversible aging phenomenon at play, but it does not explain what is actually causing the unusual behavior.

Mixed carbon dioxide-methane permeation was also done on high loading zeolite 4A MMMs (as discussed in Chapter 5). Figure B.4 shows the permeate pressure derivative with respect to time for the low pressure mixed feed case. While it has already been argued that heats of sorption did not induce an aging event, this experiment would, if anything, show a much greater effect as the heat of methane sorption is comparable to oxygen and nitrogen, and the heat of carbon dioxide sorption is much greater than all other gases tested [6].

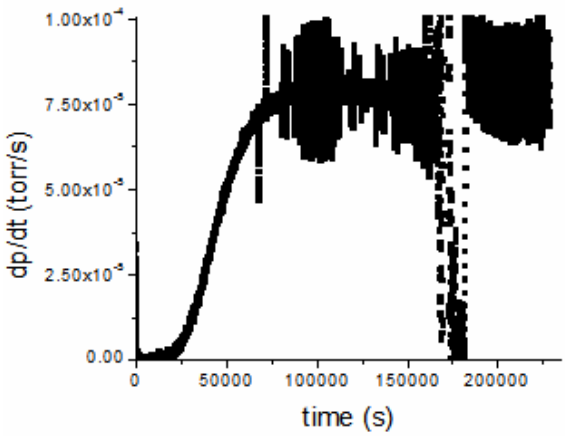

Figure B.4: Derivative of permeate pressure versus time for a 40 psia 90:10::CO_2:CH4 permeation in a 50.0 vol.% zeolite 4A-PVAc MMM.

Figure B.4 shows “normal” derivative behavior, and the steady-state value is maintained over a very long time. The “normal” behavior of the mixed gas case versus the unusual behavior of the pure gas case suggests that a difference in experimental procedure may explain the discrepancy.

As described in Chapter 3, mixed gas permeation experiments require a retentate flow to ensure that feed concentration remains constant throughout the experiment. As it happens, fairly large retentate flow rates were used in the mixed gas experiments in this work. We hypothesize that the convective atmosphere of the feed created by these large retentate flow rates ($\geq$ 0.4 cc_{STP}/s), actually prevent water from accumulating on the upstream face of the samples. Conversely, the dead-end nature of the pure gas permeation tests (i.e. no retentate flow) makes water accumulation on the upstream face of the sample possible. This water would of course slowly diffuse into the sample, and due to the hydrophilicity of zeolite 4A [6], water would preferentially sorb into the zeolites and slowly block access to the pure gases. This, of course, could result in an initially high flux that slowly decays to a minimum value where water has saturated the sieves, rendering them effectively impermeable.

Furthermore, zeolite 4A has high affinity for carbon dioxide sorption, which makes it more difficult for water to totally out-compete carbon dioxide for sorption sites, thereby making the decreasing flux less likely for the mixed gas case even if we are over-emphasizing the convective nature of the mixed gas case. The absence of decreasing fluxes for helium permeation could be due to the comparatively rapid experiment times (i.e. water never gets a chance to block the zeolites), or the fact that zeolite 4A does very little to increase helium permeability in the first place (as shown in Table B.1). More

work is needed to prove this hypothesis. The first test should be to perform pure gas permeation experiments with the same retentate flow as the mixed gas case on fresh samples. If it is shown that a retentate flow fixes the issue, then it may be necessary to revisit low loading zeolite 4A MMMs and allow permeation experiments to occur over the same long time scales to look for previously unseen decreasing fluxes.

B.4 References

[1] Mahajan, R., *Formation, characterization, and modeling of mixed matrix membrane materials*. 2000, The University of Texas at Austin, Ph.D. Thesis.

[2] Moore, T.T. and W.J. Koros, *Non-ideal effects in organic-inorganic materials for gas separation membranes.* Journal of Molecular Structure, 2005. **739**(1-3): p. 87-98.

[3] Rezac, M.E., P.H. Pfromm, L.M. Costello, and W.J. Koros, *Aging of thin polyimide ceramic and polycarbonate ceramic composite membranes.* Industrial & Engineering Chemistry Research, 1993. **32**(9): p. 1921-1926.

[4] Hill, A.J., K. Nagai, and B.D. Freeman, *Free volume dynamics and physical aging of high-permeability membrane polymers.* Abstracts of Papers of the American Chemical Society, 1999. **218**: p. 10-MACR.

[5] Nagai, K., L.G. Toy, B.D. Freeman, M. Teraguchi, and T. Matsuda, *Influence of physical aging and methanol conditioning on gas permeability and hydrocarbon solubility of poly[1-phenyl-2-[p-(triisopropylsilyl)phenyl]acetylene] (ptpsdpa).* Abstracts of Papers of the American Chemical Society, 1999. **218**: p. 13-MACR.

[6] Breck, D.W., *Zeolite molecular sieves*. 1973, New York: Wiley.

[7] Qiu, L.Y., V. Murashov, and M.A. White, *Zeolite 4a: Heat capacity and thermodynamic properties.* Solid State Sciences, 2000. **2**(8): p. 841-846.

APPENDIX C

PURE GAS PERMEABILITY IN CUTPA MMMS

C.1 Introduction

Chapters 5 and 6 discuss the performance of CuTPA MMMs. While the mixed gas results are fully represented (i.e. all values and errors are given) in Chapter 5, such details for pure gas data were omitted for clarity. Section C.2 provides a table that summarizes all data. Values are given ± one standard deviation (when applicable). No errors are provided for permselectivities for the two high loading CuTPA MMMs since they were computed from single samples (albeit from duplicate runs for each gas). Note that the "normalized" values for each loading of MMM are shown directly below the actual values in rows denoted "__ % / PVAc". These "normalized" values are simply the MMM values divided through by the complimentary value for PVAc (as was done throughout this thesis). Note that the diffusivities provided are only apparent diffusivities (because of the filling of sorptive sinks during transient permeation) computed from the permeation time lags with Equation 2.12.

Pure gas permeation data of the high loading CuTPA MMMs were "normal", i.e. the data did not show evidence of contamination effects as seen and discussed in Appendix B for the high loading zeolite 4A MMMs. This discrepancy is presumably caused by CuTPA having lower water sorption affinity and lower water sorption capacity relative to zeolite 4A. The sorption isotherms in Appendix A certainly support this hypothesis as all other penetrants show lower sorption affinities and capacities in CuTPA compared to zeolite 4A.

C.2 CuTPA MMM Pure Gas Permeation Summary

Table C.1: CuTPA-PVAc MMM Transport Data Summary. P [=] Barrers, D [=] cm^2/s (apparent values from permeation time lags). Values ± 1 standard deviation (except where only 1 sample tested).

	P_{He}	P_{CO2}	P_{O2}	P_{N2}	P_{CH4}	D_{CO2}	D_{O2}	D_{N2}	D_{CH4}	$\alpha_{CO2/N2}$	$\alpha_{O2/N2}$	$\alpha_{CO2/CH4}$	$\alpha_{N2/CH4}$	$\alpha_{He/CH4}$
25 vol% CuTPA	19.0 ± 0.5	3.26 ± 0.23	0.624 ± 0.026	0.0918 ± 0.0031	0.0806 ± 0.0035	$5.1 \times 10^{-9} \pm 1.5 \times 10^{-9}$	$2.0 \times 10^{-8} \pm 1.0 \times 10^{-8}$	$4.1 \times 10^{-9} \pm 2.9 \times 10^{-9}$	$5.7 \times 10^{-10} \pm 1.5 \times 10^{-10}$	35.4 ± 1.7	6.79 ± 0.14	40.4 ± 2.5	1.14 ± 0.02	236 ± 11.8
25 % / PVAc	1.28	1.30	1.25	1.21	1.16	0.83	0.45	0.34	0.19	1.04	1.03	1.16	1.05	1.11
44 vol% CuTPA	28.6 ± 0.1	4.91	0.968 ± 0.001	0.140 ± 0.001	0.118 ± 0.004	5.0×10^{-9}	$1.3 \times 10^{-8} \pm 2.5 \times 10^{-10}$	$2.1 \times 10^{-9} \pm 4.1 \times 10^{-11}$	$4.6 \times 10^{-10} \pm 8.0 \times 10^{-11}$	34.9	6.89	41.7	1.19	243
44 % / PVAc	1.94	1.96	1.93	1.84	1.69	0.81	0.29	0.17	0.16	1.03	1.05	1.20	1.10	1.15
65 vol% CuTPA	60.7 ± 0.1	9.95 ± 0.82	2.07 ± 0.03	0.286 ± 0.002	0.209 ± 0.003	$1.6 \times 10^{-8} \pm 1.5 \times 10^{-9}$	$4.7 \times 10^{-8} \pm 3.4 \times 10^{-10}$	$7.7 \times 10^{-9} \pm 4.9 \times 10^{-11}$	$1.5 \times 10^{-9} \pm 2.9 \times 10^{-11}$	34.8	7.26	47.6	1.37	290
65 % / PVAc	4.11	3.97	4.14	3.75	3.00	2.66	1.04	0.63	0.53	1.03	1.10	1.36	1.26	1.37

APPENDIX D

PURE GAS PERMEATION IN PARTIAL K^+A MMMS

D.1 Introduction

Chapter 6 reports and discusses the pure gas permeation data of the two partially K^+ exchanged zeolite 4A MMM samples, but the data were presented in "normalized" form, i.e. values were divided through by their pure PVAc counterparts as done elsewhere in this thesis. Section D.2 simply provides the raw values with errors (where applicable) for these MMMs.

D.2 Pure Gas Permeation Data for Partially K^+ Exchanged MMMs

Table D.1 provides the pure gas permeabilities (in Barrers) for the 13.1 % K^+/Na^+ balance and 6.76 % K^+/Na^+ balance MMMs, denoted as #1 and #2 respectively (as in Chapter 6).

Table D.1: Pure gas permeabilities (in Barrers) of partially K^+ exchanged MMMs.

	P_{He}	P_{CO2}	P_{O2}	P_{N2}	P_{CH4}
Partial K^+ #1	12.8 ± 0.4	2.53	0.470 ± 0.005	0.0708 ± 0.0048	0.0608 ± 0.0007
Partial K^+ #2	13.3 ± 0.3	1.97	0.408 ± 0.013	0.0597 ± 0.0012	0.0505 ± 0.0016

Table D.2 provides the apparent gas diffusivities computed from the permeation time lags with Equation 2.12. Recall that these are only apparent diffusivities due to the filling of sorptive sinks during the transient portion of a permeation experiment.

Table D.2: Apparent diffusivities (in cm^2/s) of partially K^+ exchanged MMMs.

	D_{CO2}	D_{O2}	D_{N2}	D_{CH4}
Partial K^+ #1	1.6×10^{-10}	$5.2 \times 10^{-9} \pm 4.6 \times 10^{-10}$	$6.7 \times 10^{-10} \pm 5.6 \times 10^{-11}$	$2.6 \times 10^{-10} \pm 1.9 \times 10^{-11}$
Partial K^+ #2	1.4×10^{-10}	$4.8 \times 10^{-9} \pm 2.3 \times 10^{-10}$	$7.1 \times 10^{-10} \pm 5.9 \times 10^{-11}$	$2.6 \times 10^{-10} \pm 2.3 \times 10^{-11}$

Finally the permselectivity values are provided in Table D.3. Note that error bars are not provided for the partial K^+ #2 MMM because a limited amount of partially K^+ exchanged material only allowed for one sample. However, each gas (except carbon dioxide) was duplicated for this MMM.

Table D.3: Pure gas permselectivities (unitless) of partially K^+ exchanged MMMs.

	$\alpha_{N2/CH4}$	$\alpha_{O2/N2}$	$\alpha_{CO2/N2}$	$\alpha_{CO2/CH4}$	$\alpha_{He/CH4}$
Partial K^+ #1	1.16 ± 0.07	6.66 ± 0.37	37.6	42.0	210 ± 4.7
Partial K^+ #2	1.18	6.83	33	39.0	263

Note that standard deviations in Tables D.1, D.2, and D.3 are only rough estimates of error since no more than 3 repeat measurements were made (see Section 3.2 for more details).